Thermophysical Properties of Methane

Daniel G. Friend, James F. Ely, and Hepburn Ingham

Thermophysics Division, National Institute of Standards and Technology, Boulder, Colorado 80303

Received April 7, 1988; revised manuscript received November 4, 1988

New correlations for the thermophysical properties of fluid methane are presented. The correlations are based on a critical evaluation of the available experimental data and have been developed to represent these data over a broad range of the state variables. Estimates for the accuracy of the equations and comparisons with measured properties are given. The reasons for this new study of methane include significant new and more accurate data, and improvements in the correlation functions which allow increased accuracy of the correlations especially in the extended critical region. For the thermodynamic properties, a classical equation for the molar Helmholtz energy, which contains terms multiplied by the exponential of the quadratic and quartic powers of the system density, is used. The resulting equation of state is accurate from about 91 to 600 K for pressures < 100 MPa and was developed by considering *PVT*, second virial coefficient, heat capacity, and sound speed data. Tables of coefficients and equations are presented to allow the calculation of these and other thermodynamic quantities. Ancillary equations for properties along the liquid–vapor phase boundary, which are consistent with the equation of state and lowest order scaling theory, are also given. For the viscosity of fluid methane, a low-density contribution based on theory is combined with an empirical representation of the excess contribution. The approximate range of the resulting correlation is 91 to 400 K for pressures < 55 MPa. The correlation for the thermal conductivity includes a theoretically based expression for the critical enhancement; the range for the resulting correlation is about 91 to 700 K for pressures below 100 MPa.

Key words: correlation; density; equation of state; heat capacity; methane; phase boundary; pressure; speed of sound; thermal conductivity; thermophysical properties; transport properties; virial coefficients; viscosity.

Contents

List of Tables

List of Figures

LIST OF SYMBOLS AND UNITS

Symbol	Description	SI Units (used in text)	Reference
A	Molar Helmholtz energy	J mol^{-1} [a]	Eq.(1)
a,b	Exponents in scaled equation	···	Eq.(23),Table 10
B	Second virial coefficient	dm^3 mol^{-1}	Table 7
C	Expansion coefficient in $\rho_{\sigma v}$	···	Eq. (6)
C_i	Coefficients in $\Omega^{(2,2)*}$	···	Eq.(12), Table 8

Symbol	Description	SI Units (used in text)	Reference
C_p	Isobaric specific heat capacity	J mol^{-1} K^{-1}	Table 7
C_v	Isochoric specific heat capacity	J mol^{-1} K^{-1}	Table 7
E	Constant in scaled equation	···	Eq. (24), Table 10
F	Crossover function in λ_{cr}	···	Eq. (20)
F_T, F_A, F_ρ	Coefficients in F	··	Eq. (20), Table 10
f_{int}, f_i	Contribution from internal modes	···	Eqs. (13),(14), Table 8
G	Molar Gibbs energy	J mol^{-1}	Table 7
G_i	Coefficients in $\rho_{\sigma L}$	···	Eq. (4),Table 3
g_i	Coefficients in η_{ex}	···	Eq. (15),Table 9
H	Molar enthalpy	J mol^{-1}	Tables 1,7
H_i	Coefficients in P_σ	···	Eq. (3),Table 3
J_i	Coefficients in $\rho_{\sigma V}$	···	Eq. (5),Table 3
j_i	Coefficients in λ_{ex}	···	Eq. (17),Table 9
k	Boltzmann constant	J K^{-1}	Table 1
M_r	Relative molecular mass	···	Table 1
N_A	Avogadro constant	mol^{-1}	Table 1
n_i	Coefficients in ϕ^r	···	Eq. (2),Table 2
P	Pressure	MPa	···
P^*_σ	Reduced saturation pressure, P_σ/P_c	···	Eq. (5a)
Q	Constant in scaled equation	···	Eq. (23),Table 10
Q_i	Coefficients in ϕ^{id}	···	Eq. (7),Table 4
R	Molar gas constant	J mol^{-1} K^{-1}	Table 1
R	Constant in scaled equation	···	Eq. (23),Table 10
r	Intermolecular separation	nm	Eq. (11)
r_i	Exponent of δ	···	Eqs. (2),(15),(17), Tables 2,9
S	Molar entropy	J mol^{-1} K^{-1}	Eq.(28),Table 7
S	Constant in scaled equation	···	Eq. (24),Table 10
SWEOS	Schmidt–Wagner Equation of State		
s_i	Exponent of τ	···	Eqs. (2),(15),(17), Tables 2,9
t	Reduced temperature, kT/ϵ	···	Eqs. (10),(12)
T	Temperature, IPTS-68	K	···
T^*	Reduced temperature, $(T_c - T)/T_c$	···	Eq. (21)
U	Molar internal energy	J mol^{-1}	Table 7
u	Unified atomic mass unit	kg	Table 1
V	Intermolecular potential	J	Eq. (11)
W	Constant in scaled equation	···	Eq. (25),Table 10
w	Speed of sound	m s^{-1}	Table 7
Z	Compressibility factor, $P/RT\rho$	···	Eq. (5)
Greek			
α	Scaling exponent	···	Ref. 11
β	Scaling exponent in $\rho_{\sigma L}, \rho_{\sigma v}$	···	Eqs. (4),(5), Table 3
Γ	Constant in scaled equation	···	Eq. (26),Table 10
γ	Potential parameter	···	Ref.16
γ	Scaling exponent	···	Eq. (18),Table 10
δ	Reduced density, ρ/ρ_c	···	···
δ^*_σ	Reduced density variable	···	Eq. (16)
ϵ	Scaling exponent in P_σ, 2-α	···	Eq. (3),Table 3
ϵ	Small temperature difference	K	Eq. (28)
ϵ	Energy parameter in $V(r)$	J	See ϵ/k
ϵ/k	Energy parameter in $V(r)$	K	Eq. (11),Table 1
η	Shear viscosity	μPa s	Eq. (8)

Symbol	Description	SI Units (used in text)	Reference
θ	Variable in scaled equation	...	Eqs. (23),(24)
Λ	Coupling constant in λ_{cr}	...	Ref. 11
Λ^*	Constant in λ_{cr}	m^{-1}	Eq. (18),Table 10
λ	Thermal conductivity	$mW\ m^{-1}\ K^{-1}$	Eq (9)
ν	Scaling exponent	...	Eq (18),Table 10
ρ	Molar density	$mol\ dm^{-3}$	...
ρ^*	Reduced density, $(\rho_c - \rho)/\rho_c$	...	Eq. (22)
σ	Distance parameter in $V(r)$	nm	Eqs. (10), (11) Table 1
τ	Reduced inverse temperature, T_c/T	...	...
ϕ	Reduced Helmholtz energy, A/RT	...	Eq. (1)
χ_T^*	Reduced compressibility	...	Eqs. (19),(23),(26)
Ω	Variable in scaled equation	...	Eqs. (23),(25)
$\Omega^{(2,2)*}$	Reduced collision integral	...	Eqs. (10),(12)
Superscripts			
id	Ideal gas contribution		Eq. (1), Table 1
r	Residual contribution		Eq. (1)
Subscripts			
c	Value at critical point		Table 1
cr	Critical contribution		Eqs. (9),(18)
ex	Excess contribution		Eqs. (8),(9),(15),(17)
exp	Value from experiment		Eq. (30)
t	Value at triple point		Table 1
tL,tV	Value at triple point in liquid,vapor		Table 1
σ	Value at saturation boundary		Eq. (3)
σL,σV	Value in saturated liquid, vapor		Eqs. (4),(5),(28)
δ	Partial derivative with respect to δ		Tables 5,6
τ	Partial derivative with respect to τ		Tables 5,6
0	Value at zero density		Eqs. (8)–(10),(13)

[a] Throughout this paper, the mole (mol) quantifies the amount of substance whose elementary entities are the molecular constituents of the methane fluid.

1. Introduction

Because of the industrial importance of methane, we have felt it necessary to examine the newly available thermophysical property data and to re-evaluate the older data to produce more useful and accurate correlations. In this paper we present an empirical equation of state for methane based on extensive multiproperty analysis, as well as correlations for the liquid–vapor phase boundary and for the viscosity and thermal conductivity of methane. Tables of coefficients for these correlating equations and graphical representations of the functions for easy accessibility of estimated values of certain properties are included. Discussions of the accuracy of these correlations and their applicable ranges, and explicit comparisons with experimental data are also given. In an Appendix, we have compiled very brief tables of thermophysical properties in the ideal or dilute gas limit, along the liquid–vapor phase boundary, and in the one-phase region. Extensive tables of properties and comparisons with experimental data will be published separately.[1]

This paper represents one of a new series of National Institute of Standards and Technology (NIST) (formerly National Bureau of Standards) correlations based on critically evaluated thermophysical property data and presented

in a standardized format using similar functional representations. Correlations for ethane, propane, butane, and carbon dioxide are also underway.

1.1. Need for this Correlation

Within the last decade, subsequent to the 1976 publication of the International Union of Pure and Applied Chemstry (IUPAC) monograph on methane,[2] there have been extensive international experimental studies on the properties of methane. Notable among these are the very recent reports by Kleinrahm, Wagner, and Duschek[3,52] on the coexistence surface and the *PVT* relationship in the critical region of methane. We also have considered, to mention some of the recent experiments, the *PVT* measurements of Trappeniers *et al.*,[4] the Burnett data of Mollerup,[5] the sound speed measurements of Baidakov *et al.*[6], the experimentally derived correlation of Morris,[7] the thermal conductivity data of Roder,[8] and the viscosity data of Diller.[9] Some of the older high precision thermophysical property measurements, including some made at NIST, remain useful, and new data will continue to be published. Discussion of the data sets used in our correlations and comparisons with a more extensive group of data sets are presented.

Theoretical advances have placed the concept of the universality of critical behavior on firm footing, and have established certain nonanalytic functional behaviors with specified critical exponents (including corrections to the asymptotic scaling theories).[10,11] However, the problem of using these concepts in the determination of wide ranging engineering correlations is not completely solved. In particular, the problem of switching from the scaled equation of state used in the critical region to the useful and well understood analytic forms, which are widely used for the majority of the phase diagram, remains unsolved. In addition, in the theory of dynamic scaling, the basis for determining the extent of any critical enhancement of transport properties, both in temperature and in density, is not firmly specified. For the present correlations we have decided to retain a completely analytic form for the equation of state. This allows straightforward determination of derived properties and ensures continuity of all properties and their derivatives throughout the phase diagram.

There is a need for improved accuracy of equation of state correlations in the critical region, based partly on the industrial desire for tighter tolerances with their inherent economic benefits and on newly feasible processes in nearly critical fluids. Thus we have used a form for the equation of state, denoted SWEOS, introduced by Schmidt and Wagner[12] and shown by them to approximate the critical region properties of oxygen very well. This SWEOS contains two types of exponential density dependences (as shown below) and seems to represent an improvement in the critical region of methane as compared to the more usual Benedict-Webb-Rubin (BWR)-type equations.[13] For the thermal conductivity, we use a nonanalytic scaling form for the critical region enhancement. For the viscosity, no clear enhancement is seen in the experimental data, so that a nonanalytic enhancement contribution is not included in the correlation. For the transport properties, the present correlations represent distinct advantages over the previously published NIST correlations.[13,14] The new NIST data of Refs. 8 and 9 give us confidence in the accuracy of our correlations. Additionally, the dilute gas terms use the Chapman–Enskog theory directly for viscosity and with an improved treatment of internal degrees of freedom for the thermal conductivity. The necessary collision integral, tabulated in Ref. 16, was fit to a simple function. The excess functions are represented by polynomial or rational polynomial approximations and have been scaled by corresponding states arguments. These represent a conceptual improvement over the functional forms of Ref. 14 which imply divergent first density correction terms. The new form of the equation of state also improves the transport property correlations which are based on temperature and density variables.

The correlations discussed in this paper have not been established just for primary engineering users; they are also intended, together with the correlations for other fluids, to allow testing of various aspects of corresponding states theory. Thus, these equations will allow examination of theories relating the properties of series of nonspherical fluids, where conformality is difficult to achieve. Further, it is hoped that these correlations will permit the development of better approximations for evaluation of fluid mixture properties. The spirit of these correlations, then, is both to capture the accuracy of the best wide-ranging experimental data and to provide a systematic base of equations of state which can be used to develop predictive corresponding states models.

1.2. Range of Correlations

For the equation of state correlation, we have examined *PVT* data in the range $92 < T < 623$ K, $0.1 < P < 1000$ MPa, and $0.03 < \rho < 35$ mol dm^{-3} as well as virial coefficient, heat capacity, and sound speed data. For the broad range of the phase diagram with pressures < 100 MPa, we consider the accuracy of our correlation to be about 0.3% (standard deviation) when evaluating the density given the temperature and pressure, and 1% when evaluating the pressure given the temperature and density. In the neighborhood of the critical point, the accuracy deteriorates to 0.5% for density calculations. Detailed comparisons with experimental data and estimates of the quality of the correlation in different regions of the phase diagram are given in Sec.4. For the derived properties, the accuracy of the correlation is somewhat less, with details given below. In Figures 1(a) and 1(b) we give representations of the phase diagram for methane, together with isochores and isotherms, from which the interested reader can determine a rough approximation to the scope of the *PVT* relation presented here.

To produce an accurate correlation for the equation of state and derived properties of a fluid, especially one that is to be useful for corresponding states calculations, it is necessary to have accurate values for the critical and triple-point parameters and a good correlation or an accurate and dense set of data for the two-phase boundaries. The selected values of the critical and triple-point parameters, with uncertainties, are given in Table 1. For the liquid–vapor two-phase boundary, the new data of Ref. 3 seem to avoid some of the problems with impurity contamination which may have

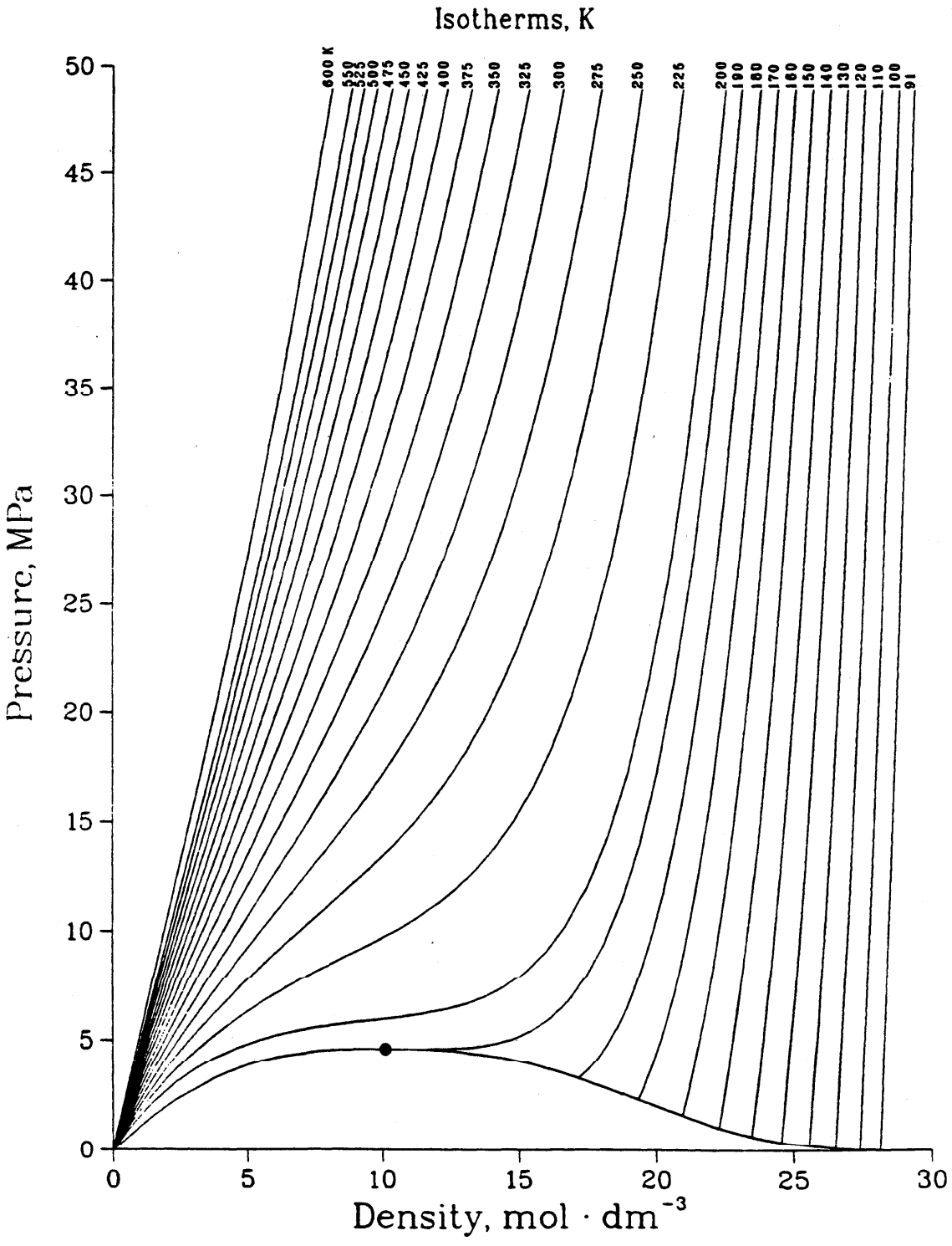

FIG. 1(a). Methane fluid isotherms from the SWEOS. Solid circle denotes the critical point, and two-phase boundary is from ancillary equations.

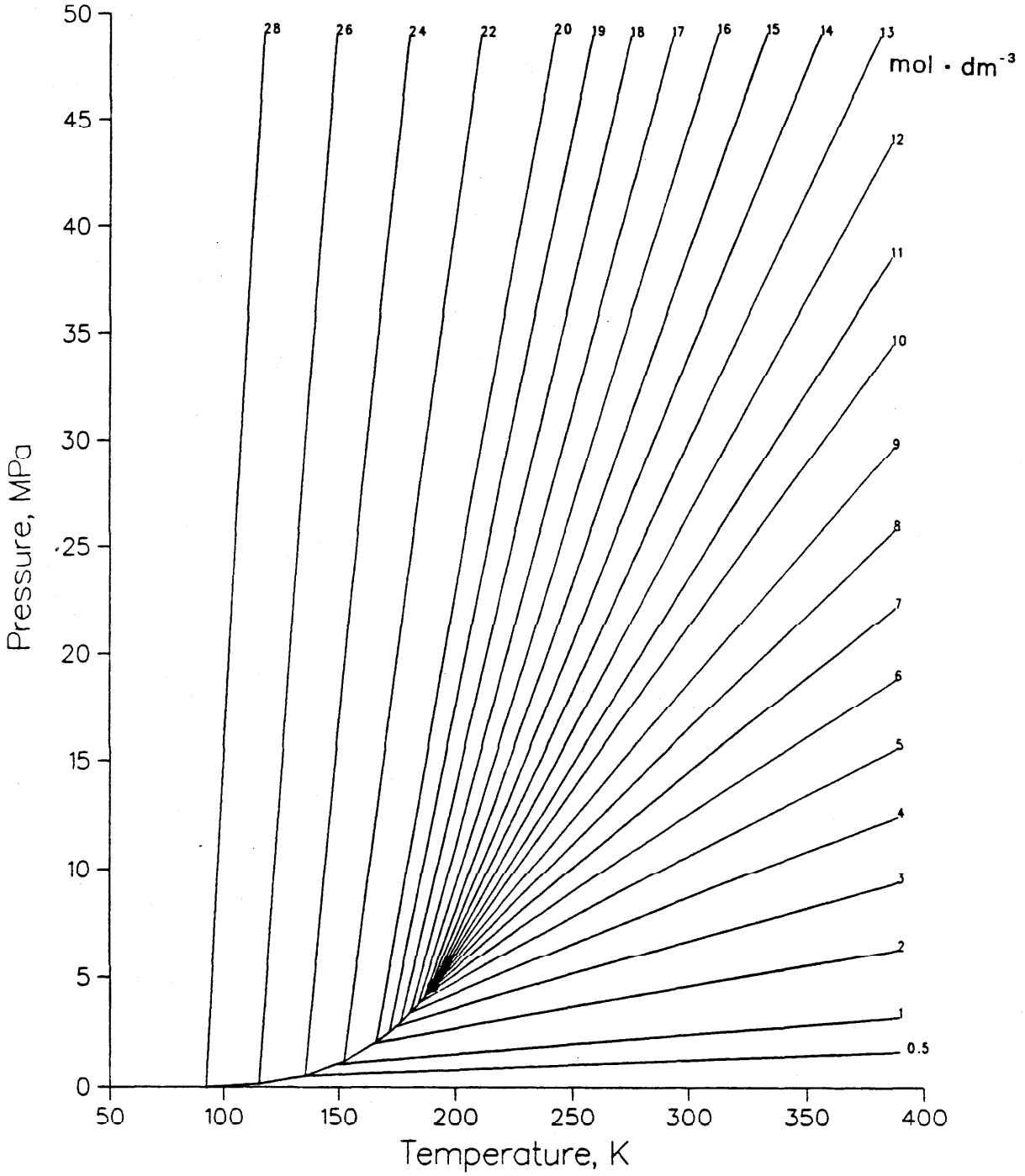

FIG. 1(b). Methane fluid isochores from the SWEOS. Solid circle denotes the critical point, and saturation boundary is from ancillary equation.

TABLE 1

FIXED POINT CONSTANTS AND OTHER PARAMETERS USED IN THE CORRELATIONS

Triple Point:	T_t = 90.6854 ± 0.0003 K P_t = 11.696 ± 0.002 kPa ρ_{tL} = 28.145 ± 0.005 mol•dm^{-3} ρ_{tv} = 15.66 ± 0.05 mol•m^{-3}
Critical Point:	T_c = 190.551 ± 0.01 K P_c = 4.5992 ± 0.003 MPa ρ_c = 10.139 ± 0.01 mol•dm^{-3} Z_c = 0.28631 ± 0.0005
Intermolecular Potential Parameters:	ϵ/k = 174 K σ = 0.36652 nm
Ideal Gas Reference Point Values:	(at 298.15 K and 0.101325 MPa) S^{id} = 186.266 J•K^{-1}•mol^{-1} H^{id} = 10.0177 kJ•mol^{-1}
Miscellaneous:	Relative molecular mass...M_r= 16.043 Universal gas constant...R = 8.314510 J•mol^{-1}•K^{-1} Boltzmann constant....k = 1.380658 x 10^{-23} J•K^{-1} Avogadro constant...N_A = 6.0221367 x 10^{23} mol^{-1} Unified atomic mass unit...u = 1.6605402 x 10^{-27} kg

plagued earlier experiments. Thus, for the phase boundary, and especially for the saturation pressures, we have heavily emphasized the data of Kleinrahm and Wagner[3] in the correlations. The equations determined for the saturation pressures and the saturated liquid and vapor densities are given in Eqs.(3)–(5) and the correlations are illustrated in Figs. 1(a) and 1(b). The estimated accuracies of these correlations are generally 0.06% for the pressure, 0.2% for the liquid density, and 0.5% for the vapor density, but the accuracies deteriorate near the triple-point and critical point temperatures.

The form of the SWEOS, together with values of certain reference point parameters (also given in Table 1) and the ideal gas specific heat capacity, allows easy determination of many of the derived thermodynamic properties. In Table 7 we have collected the explicit algebraic forms, in a manner quite similar to the original tables of Schmidt and Wagner,[12] which will allow one to evaluate several of these quantities. Comparisons with some experimental data and estimates of the accuracy of the derived property correlations are given in Sec. 4.2. The accuracy of the correlation decreases as the order of the derivatives increases and again, the accuracy generally is worst in the critical region. With these provisos one may determine any other thermodynamic properties, throughout the above stated range of the correlations, from the SWEOS by using the usual relationships of thermodynamics.

The available experimental data for the transport prop-

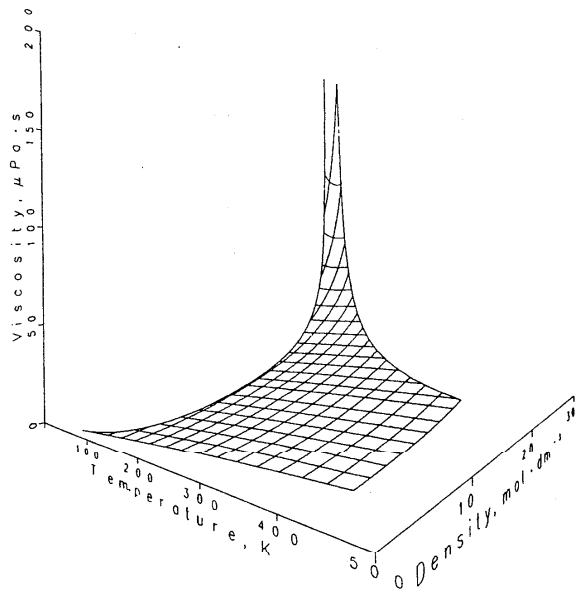

FIG. 2. Three-dimensional representation for the viscosity coefficient surface. The viscosity is in μPa s; the density is in mol dm^{-3}.

erties are not nearly as extensive. The temperature range for the viscosity is 91 to 444 K; the pressure range is 0.1 to 55 MPa; and the density range is 0.04 to 29 mol dm^{-3}. In this region of the phase diagram, the extrema of the viscosity are 8 and 220 μPa s. The viscosity correlation has an associated error of about 1.5%. Figure 2 depicts the relationships among viscosity, temperature, and density and again enables the reader to obtain a crude value for this property without

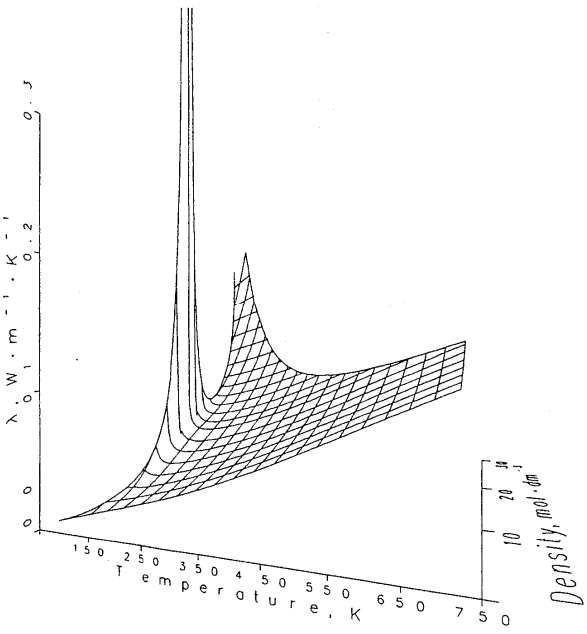

FIG. 3. Three-dimensional representation for the thermal conductivity coefficient surface. The thermal conductivity is in mW m^{-1} K^{-1} and the density is as in Fig.2. Note the divergence near the critical point.

evaluation of the algebraic expressions. The useful experimental data for thermal conductivity are between 99 and 725 K, 0.1 and 125 MPa, and 0.03 and 29 mol dm^{-3}, with resulting range in λ of 0.01 to 0.24 W m^{-1} K^{-1}. The thermal conductivity correlation has an accuracy of about 1.5% and is shown in Fig. 3.

1.3. Historical Context

This report represents the latest contribution in a long history of attempts to correlate the thermophysical properties of methane. The IUPAC monograph of Angus *et al.*[2] contains an excellent bibliography on the available correlations and the experimental work concerning the thermodynamic properties of methane prior to 1976, as well as tables and an excellent BWR-type equation of state. Prior to the IUPAC publication, the NIST report by Goodwin,[17] which summarized and correlated much of the NBS experimental thermodynamic work on methane, was widely accepted as a definitive work on the subject. Subsequently, there have been periodic reports by NIST authors[13,18] which represent improvements based on additional data, re-evaluation of data, and improved methods of correlation. The recent Soviet monograph by Sychev *et al.*[18(a)] also gives tables and correlations for thermodynamic properties and includes bibliographic information for much of the Soviet experimental work on methane.

For the transport properties of fluid methane, the papers of Hanley *et al.*[14,19] have provided a standard for the evaluation and correlation of the data prior to 1975, while Ref. 13 includes more recent data.

1.4. Organization of Paper

We conclude this introduction with a brief overview of the organization of the paper. In Sec. 2, we present the precise forms of the correlating equations for the SWEOS, two-phase boundary, ideal gas state and transport property correlations and, for ease of use, tables of the fitted coefficients. In Sec. 3, we discuss the various data sets which were considered and used in the correlations. Section 3 also contains a brief description of the techniques used in developing the multiproperty correlations, while Sec. 4 presents the results including comparisons with the data and discussion of the accuracy of the correlations; our brief conclusions are presented in Sec. 5. Finally, in the Appendix, we include very brief tables of thermophysical properties.

2. Correlating Equations

2.1. Equation of State

We have chosen the equation of state form presented by Schmidt and Wagner in Ref. 12. This SWEOS was introduced as an improvement over the BWR equation, especially to represent data in the extended critical region. The general form includes terms multiplied by $\exp[-(\rho/\rho_c)^4]$ in addition to terms with $\exp[-(\rho/\rho_c)^2]$ as occur in the BWR equation. The critical density ρ_c and critical temperature T_c are used as reduction parameters. The form of the polynomial in reduced temperature and density (and the

exponential terms) were determined by Schmidt and Wagner.[12] They used a selection algorithm with a set of 336 terms which were optimized to best fit the wide ranging data for oxygen. We have retained this choice of polynomial, because it seems also to improve the fit for fluid methane.

As in Ref. 12, we consider the molar Helmholtz energy A as the sum of ideal and residual terms and write

$$A(\rho,T) = A^{\mathrm{id}} + A^{r} = RT\phi = RT(\phi^{\mathrm{id}} + \phi^{r}) . \quad (1)$$

With the definitions $\delta = \rho/\rho_c$ and $\tau = T_c/T$, the dimensionless residual term becomes

$$\phi^{r} = \sum_{i=1}^{13} n_i \delta^{r_i}\tau^{s_i} + e^{-\delta^2} \sum_{i=14}^{24} n_i \delta^{r_i}\tau^{s_i} + e^{-\delta^4} \sum_{i=25}^{32} n_i \delta^{r_i}\tau^{s_i} . \quad (2)$$

The coefficients n_i, determined by fitting the data, and the exponents r_i and s_i are given in Table 2. Equation (2) and Table 2 are essentially the same as Eq. (11) in the Schmidt and Wagner paper.[12]

Using Eq. (2) and Table 2, together with the associated equation for the ideal gas free energy [see Eq. (7)] and the constants in Table 1, all of the thermodynamic properties of methane can be evaluated using standard thermodynamic relationships. Equations for several of the important properties in terms of ϕ and its derivatives are given in Table 7. In addition, for ease of use, Table 6 gives the coefficients and exponents needed to evaluate the first and second density, temperature, and mixed derivative of ϕ^{r}

2.2. Liquid–Vapor Saturation Boundary

Although the SWEOS allows calculation of saturation properties by a Maxwell construction technique within the two-phase region, it is useful to have separate correlations of the two-phase boundary. For this reason, we present new correlating equations for the saturation pressure P_σ, the density of the saturated vapor $\rho_{\sigma v}$, and the density of the saturated liquid $\rho_{\sigma L}$, all as functions of temperature. These saturation boundary correlations were also used as input in the development of the equation of state.

There have been numerous equations proposed in the literature to correlate the vapor pressure as a function of temperature. For example, Chap. 6 in the book by Reid *et al.*[20] and Table 5 in a study by Wagner[21] give many possibilities. Quite recently, Kleinrahm and Wagner[3] presented a slightly revised form which was optimized to correlate their excellent new data on methane. We have chosen to use a formula which explicitly reproduces the nonanalytic scaling theory results in the critical region, and thus we use an extension of the equation introduced by Verbeke.[22] The extension involves additional powers of temperature within the exponential for increased flexibility. Additionally, we have written the equation in terms of $T^* = (T_c - T)/T_c$ so that the critical behavior may be easily discerned by expansion of the exponential about $T^* = 0$. Thus we write

$$P_\sigma(T) = P_c \exp[H_1 T^*/(1 - T^*) + H_2 T^* + H_3 T^{*\epsilon} + H_4 T^{*2} + H_5 T^{*3},] \quad (3)$$

where the dimensionless fitted coefficients H_i and the exponent ϵ are given in Table 3.

In Eq. (3), the saturation pressure P_σ precisely equals critical pressure at the critical temperature, and the exponent ϵ was forced to have its scaling theory value (that is $\alpha = 2 - \epsilon = 0.1$ as in, for example, studies by Levelt Sengers *et al.*[23] and Rainwater and Moldover[24]). Although our values for the critical parameters differ slightly from those used in Ref. 24 for a critical region analysis, the expansion of Eq. (3) in the critical region gives a coefficient of T^* which differs by $<1\%$ from that obtained in Ref. 24. The higher order terms in the expansion, including the term multiplied by $T^{*\epsilon}$, differ substantially as expected since Eq. (3) correlates the saturation pressure from the triple point to the critical point, whereas Rainwater and Moldover[24] examined only the critical region.

There are also many formulas to describe and correlate the densities of both liquid and vapor on the two-phase boundary. For the liquid, we have chosen an equation in T^* which reduces to the known (lowest order) scaling result in the limit $T^* \to 0$. The equation, which has the added flexibility available with a ratio of terms in T^*, is

TABLE 2

EXPONENTS AND COEFFICIENTS FOR THE RESIDUAL FREE ENERGY ϕ^r (Eq. (2))

	i	r_i	s_i	n_i
$\delta^{r_i}\tau^{s_i}$	1	1	0	0.38443609966
	2	1	1.5	-0.17969259880 x 10
	3	1	2.5	0.32944494737
	4	2	-0.5	0.22631272844 x 10^{-1}
	5	2	1.5	0.75923676880 x 10^{-1}
	6	2	2	0.69375844726 x 10^{-1}
	7	3	0	0.24116326395 x 10^{-1}
	8	3	1	0.10700992085 x 10^{-1}
	9	3	2.5	-0.38093327516 x 10^{-1}
	10	6	0	0.47153756114 x 10^{-3}
	11	7	2	0.55660767881 x 10^{-3}
	12	7	5	0.54875934653 x 10^{-6}
	13	8	2	-0.99963269997 x 10^{-4}
$e^{-\delta^2}\delta^{r_i}\tau^{s_i}$	14	1	5	-0.12808797928
	15	1	6	0.38019887338 x 10^{-1}
	16	2	3.5	0.13922665055
	17	2	5.5	-0.87499634886 x 10^{-1}
	18	3	3	-0.33489416576 x 10^{-2}
	19	3	7	-0.51757629712 x 10^{-1}
	20	5	6	0.25283517912 x 10^{-1}
	21	6	8.5	0.51870320595 x 10^{-3}
	22	7	4	-0.16677059452 x 10^{-2}
	23	8	6.5	-0.60740192739 x 10^{-3}
	24	10	5.5	-0.97291535999 x 10^{-4}
$e^{-\delta^4}\delta^{r_i}\tau^{s_i}$	25	2	22	-0.29884401046 x 10^{-4}
	26	3	11	-0.13094011124 x 10^{-1}
	27	3	18	0.19817583380 x 10^{-1}
	28	4	11	0.20846576233 x 10^{-1}
	29	4	23	-0.35802505263 x 10^{-1}
	30	5	17	-0.20348685174
	31	5	18	0.21596475509
	32	5	23	-0.42934062825 x 10^{-2}

TABLE 3

COEFFICIENTS NEEDED FOR LIQUID-VAPOR BOUNDARY CORRELATIONS

Saturated Vapor Pressure Eq. (3)	Saturated Liquid Density Eq. (4)	Saturated Vapor Density Eq. (5) or (5a)
ϵ = 1.90	β = 0.355	β = 0.355
H_1 = -6.589879	G_1 = 1.838982	J_0 = -0.7377483
H_2^1 = 0.6355175	G_2^1 = -0.7727452	J_1^0 = -1.241532
H_3 = 11.31028	G_3^2 = 0.5592446	J_2^1 = -1.649972
H_4^4 = -10.38720	G_4^3 = -0.3807793	J_3^2 = 2.281949
H_5 = 3.393075		J_4^3 = 1.439570

$$\rho_{\sigma L}(T) = \rho_c\left[1 + \frac{G_1 T^{*\beta} + G_2 T^{*2} + G_3 T^{*3}}{1 + G_4 T^{*(1-\beta)}}\right], \quad (4)$$

where the coefficients G_i and exponent β appear in Table 3. The critical exponent β was assumed to have the effective universal value[23] of 0.355 which is identical to the value used for the enhancement of the thermal conductivity. (See Table 10.)

The expansion of Eq.(4) about $T^* = 0$ yields coefficients of $T^{*\beta}$ and T^* which differ from those obtained in Ref. 24 by about 3% and 1.5%, respectively. Additionally, these coefficients are within the ranges quoted by Kleinrahm and Wagner[3] for their critical region analysis, although the saturated liquid density correlation of Ref. 3 does not reproduce these coefficients when expanded in the critical region. (A comparison between Eq. (4) and other correlations is given below.)

For the density of the saturated vapor, it is desirable to use an equation which has the theoretically predicted behavior in both the low density (ideal gas) limit and in the neighborhood of the critical point. While these limits may not be simultaneously discernable at a glance, the equation

$$\rho_{\sigma v}(T) = \frac{P_\sigma(T)}{RT}\left\{1 + P_\sigma(T)\tau^8 \frac{Z_c - 1}{P_c}\left[1 + \frac{J_0 T^{*\beta} + J_1 T^{*2\beta} + J_2(T^* + T^{*4}) + J_3 T^{*2}}{1 + J_4 T^*}\right]\right\}^{-1}, \quad (5)$$

with $Z_c = P_c/(RT_c\rho_c)$, the critical compressibility factor, has the ideal gas behavior at the lowest pressures and can be rewritten as

$$\rho_{\sigma v}(T) = \rho_c(1 - T^*)^7\left\{1 - \frac{1}{Z_c}\left[1 - \frac{(1-T^*)^8}{P^*_\sigma}\right] + (1 - Z_c^{-1})\frac{J_0 T^{*\beta} + J_1 T^{*2\beta} + J_2(T^* + T^{*4}) + J_3 T^{*2}}{1 + J_4 T^*}\right\}^{-1}. \quad (5a)$$

This last equation, with $P^*_\sigma = P_\sigma(T)/P_c$, reduces to the lowest order scaling result in the limit $T^* \to 0$, namely

$$\rho_{\sigma v} \propto \rho_c(1 - CT^{*\beta} + \cdots). \quad (6)$$

The value of β for the vapor density correlations remains at the value of 0.355, and $C[= J_0(1\text{-}Z_c^{-1})]$ is forced to have the same value as G_1 in the saturated liquid density correlation of Eq. (4). Because of the presence of the exponent 2β in Eq. (5), higher order terms in the critical region expansion, Eq. (6), are not directly comparable. The equality of C and G_1 reproduces the observed and theoretically predicted symmetry of the two-phase boundary around the critical point. Despite the presence of the $T^{*2\beta}$ term in Eq. (5), the rectilinear diameter [defined as $\frac{1}{2}(\rho_{\sigma L} + \rho_{\sigma v})$] determined by Eqs.(4) and (5) is very nearly linear in the critical region. The coefficients for Eqs. (5) and (5a) are given in Table 3. The data and estimates of the reliability for all three two-phase boundary correlations are given in Sec. 4.1.

2.3. Ideal Gas Reference State Equation

Thermodynamic functions may be derived for the ideal gas by using statistical mechanical models with spectroscopic data for methane. Because these functions tend to be more accurate than the corresponding values obtained by direct evaluation using thermodynamic experiments, it is customary to consider the results obtained from the spectroscopic data at the standard pressure of 0.101 325 MPa (1 atm) as a reference state with which the wide ranging correlations must agree. We have chosen to use Goodwin's fit[25] of the spectroscopically derived data of McDowell and Kruse.[26] The constants for Eq.(7) include the conversion to currently accepted values for the fundamental constants. The corresponding values of the entropy and enthalpy at standard conditions (298.15 K and 0.101 325 MPa) are given in Table 1. These values exclude any contributions from nuclear spin, and thus all values for the entropy and for the thermodynamic potentials (internal energy, Helmholtz energy, Gibbs energy, and enthalpy) are relative to an assumed zero of the appropriate quantity. Our resulting ideal gas properties agree well with those adopted by Angus *et al.*[2] (although we note the apparent typographical error in the entry for the entropy in their Sec. 3.1) who used the same spectroscopic model and data.[26]

To conform with the notation of Schmidt and Wagner[12] and our Eq. (1), we have rewritten the ideal gas equations of Goodwin[25] as a single equation for the ideal gas Helmholtz energy in terms of the temperature and density. As in Eq. (2), the temperature and density terms were reduced by the critical values of Table 1. Thus we write, in dimensionless form,

$$\phi^{id}(\delta,\tau) = A^{id}/RT = Q_1 + \ln\delta + Q_2 \ln\tau + Q_3\tau^{-1/3} + Q_4\tau^{-2/3} + Q_5\tau^{-1} + Q_6 \ln(1 - e^{Q_7\tau}) \quad (7)$$

with the coefficients Q_i, calculated directly from Ref. 25, given in Table 4. Equation (7) must be evaluated at the experimental density and temperature, although for most of the properties in Table 7, there is no density (or pressure) dependence in the required derivatives. The ideal gas thermodynamic quantities correlated by Goodwin[25] and tabulated by McDowell and Kruse[26] were for the ideal gas at 0.101 325 MPa (1 atm); in this limit, using the ideal gas equation of state, Eq. (7) can be written as

TABLE 4

COEFFICIENTS NEEDED FOR IDEAL GAS FREE ENERGY, EQ.(7)

Q_0 = -15.479844	Q_4 = 1.6900979
Q_1 = -10.413865	Q_5 = -0.3911541
Q_2 = 2.5998324	Q_6 = 4.7206715
Q_3 = -3.3854083	Q_7 = -10.543907

TABLE 5

IDEAL GAS FREE ENERGY AND ITS DERIVATIVES

	ϕ^{id} Eq. (7)	$\delta\phi_\delta^{id}$ (=1)	$\tau\phi_\tau^{id}$	$\delta^2\phi_{\delta\delta}^{id}$ (=-1)	$\tau^2\phi_{\tau\tau}^{id}$	$\delta\tau\phi_{\delta\tau}^{id}$ (=0)
1	Q_1	1	Q_2	-1	$-Q_2$	0
$\ln\delta$	1	0	0	0	0	0
$\ln\tau$	Q_2	0	0	0	0	0
$\tau^{-1/3}$	Q_3	0	$-Q_3/3$	0	$4Q_3/9$	0
$\tau^{-2/3}$	Q_4	0	$-2Q_4/3$	0	$10Q_4/9$	0
τ^{-1}	Q_5	0	$-Q_5$	0	$2Q_5$	0
$\ln(1-e^{Q_7\tau})$	Q_6	0	0	0	0	0
$(e^{-Q_7\tau}-1)^{-1}$	0	0	$-Q_6Q_7\tau$	0	0	0
$e^{Q_7\tau}(e^{Q_7\tau}-1)^{-2}$	0	0	0	0	$-Q_6Q_7^2\tau^2$	0

$$\phi^{id}(\tau) = Q_0 + (Q_2+1)\ln\tau + Q_3\tau^{-1/3} + Q_4\tau^{-2/3} + Q_5\tau^{-1} + Q_6\ln(1-e^{Q_7\tau}) .$$

In Table 4, values of both Q_0 and Q_1 are given, although in practice the former is not needed for the evaluation of any property.

2.4. Derived Property Equations

In Tables 5 and 6, whose use is described in the next paragraph, we have collected the coefficients necessary to calculate the six lowest order derivatives for the ideal gas and residual contributions to the free energy. These are the first two density derivatives along isotherms, the temperature derivatives along isochores, and the mixed derivatives. As in the paper by Schmidt and Wagner,[12] we consider the reduced density and the inverse reduced temperature as independent variables, and we denote the derivatives as subscripts to the appropriate free energy quantity. For example

$$\phi_\delta^r = \left.\frac{\partial\phi^r(\delta,\tau)}{\partial\delta}\right|_\tau = \frac{\rho_c}{RT}\left.\frac{\partial A^r(\rho,T)}{\partial\rho}\right|_T ,$$

is the isothermal (reduced) density derivative of the (reduced) residual free energy. Second derivatives are analogously defined, but have two subscripts to indicate the parameters with respect to which the derivatives are taken.

To calculate derivatives of the ideal gas contribution to the free energy, one is guided by the form of Eq. (7). The left-most column of Table 5 lists the terms necessary for the various derivatives, and the remaining columns give the coefficients of these terms directly beneath the heading which indicates the quantity to be calculated. The resulting terms are to be added as in Eq. (7). As indicated in the table, the density derivatives of the ideal gas free energy are particularly simple: $\delta\phi_\delta^{id} = 1$, $\delta^2\phi_{\delta\delta}^{id} = -1$, and $\delta\tau\phi_{\delta\tau}^{id} = 0$. The values of the Q_i parameters are obtained from Table 4. For derivatives of the residual free energy, Eq. (2) and Tables 2 and 6 can be used. As in Eq. (2), the derivatives are obtained by summing 32 terms of three general types. Each of the terms has factors consisting of powers of the reduced density and temperature with the explicit exponents r_i and s_i and coefficients n_i given for each value of i in Table 2. The additional

TABLE 6

RESIDUAL FREE ENERGY AND ITS DERIVATIVES

	$n_i\delta^{r_i}\tau^{s_i}$ (i = 1 to 13)	$e^{-\delta^2}n_i\delta^{r_i}\tau^{s_i}$ (i = 14 to 24)	$e^{-\delta^4}n_i\delta^{r_i}\tau^{s_i}$ (i = 25 to 32)
ϕ^r	1	1	1
$\delta\phi_\delta^r$	r_i	$r_i - 2\delta^2$	$r_i - 4\delta^4$
$\tau\phi_\tau^r$	s_i	s_i	s_i
$\delta^2\phi_{\delta\delta}^r$	$r_i(r_i-1)$	$[r_i(r_i-1) -2(2r_i+1)\delta^2 +4\delta^4]$	$[r_i(r_i-1) -4(2r_i+3)\delta^4 +16\delta^8]$
$\tau^2\phi_{\tau\tau}^r$	$s_i(s_i-1)$	$s_i(s_i-1)$	$s_i(s_i-1)$
$\delta\tau\phi_{\delta\tau}^r$	r_is_i	$s_i(r_i-2\delta^2)$	$s_i(r_i-4\delta^4)$

exponential factor, with its argument either the second or fourth power of the density, is indicated in the column heading of Table 6 where appropriate. The remaining coefficients relevant to the derivative being calculated are given in the appropriate row in that table.

In Table 7, the most common thermodynamic quantities of interest have been expressed in terms of the reduced derivatives of the molar Helmholtz energy. As in Ref. 12, all extensive quantities (that is, the various thermodynamic potentials and heat capacities) are given on a per mole basis. The density derivatives of the ideal gas contribution to the free energy have been explicitly evaluated and included in the table where appropriate.

2.5. Transport Property Correlations

For both the viscosity and thermal conductivity, the present correlations reduce to the theoretically rigorous Chapman–Enskog theory[15] at the lowest densities. Added to these zero-density terms are empirical functions which represent the excess portion of the transport coefficient. For the methane thermal conductivity, which clearly displays a critical enhancement in the experimental results, we also add a term based on the theoretical description of the critical enhancement given by Sengers *et al.*[11] The viscosity is given by

$$\eta(\rho,T) = \eta_0(T) + \eta_{ex}(\rho,T) \tag{8}$$

TABLE 7

THERMODYNAMIC PROPERTY EQUATIONS

Pressure:	$P(\rho,T) = \rho RT\,(\,1 + \delta\phi^r_\delta)$
Internal Energy:	$U(\rho,T) - RT\,(\,\tau\phi^{id}_\tau + \tau\phi^r_\tau\,)$
Enthalpy:	$H(\rho,T) = RT\,(\,1 + \tau\phi^{id}_\tau + \tau\phi^r_\tau + \delta\phi^r_\delta\,)$
Gibbs Energy:	$G(\rho,T) = RT\,(\,1 + \phi^{id} + \phi^r + \delta\phi^r_\delta\,)$
Helmholtz Energy:	$A(\rho,T) = RT\,(\,\phi^{id} + \phi^r\,)$
Entropy:	$S(\rho,T) = -R\,(\,\phi^{id} + \phi^r - \tau\phi^{id}_\tau - \tau\phi^r_\tau\,)$
Isochoric Heat Capacity:	$C_v(\rho,T) = -R\,(\,\tau^2\phi^{id}_{\tau\tau} + \tau^2\phi^r_{\tau\tau}\,)$
Isobaric Heat Capacity:	$C_p(\rho,T) = C_v(\rho,T) + R\,\dfrac{(\,1 + \delta\phi^r_\delta - \delta\tau\phi^r_{\delta\tau}\,)^2}{1 + 2\delta\phi^r_\delta + \delta^2\phi^r_{\delta\delta}}$
Saturated Liquid Heat Capacity:	$C_{\sigma L}(T) = C_v(\rho_{\sigma L},T) - R\,(\,1 + \delta\phi^r_\delta - \delta\tau\phi^r_{\delta\tau}\,)\,\dfrac{T}{\rho_{\sigma L}}\,\dfrac{d\rho_{\sigma L}}{dT}$
Speed of Sound:	$w^2(\rho,T) = \dfrac{RT}{uN_A M_r}\,\dfrac{C_p(\rho,T)}{C_v(\rho,T)}(1+2\delta\phi^r_\delta+\delta^2\phi^r_{\delta\delta})$
Second Virial Coefficient:	$B(T) = \dfrac{1}{\rho_c}\lim_{\delta\to 0}\phi^r_\delta$

and the expression for thermal conductivity is

$$\lambda(\rho,T) = \lambda_0(T) + \lambda_{ex}(\rho,T) + \lambda_{cr}(\rho,T) . \quad (9)$$

These terms are described in this section.

2.5.1. Dilute Gas Correlation

The Chapman–Enskog theory for the dilute gas viscosity gives, to lowest order in the Sonine polynomial expansion,

$$\eta_0(T) = \frac{5\sqrt{\pi u M_r kT}}{16\pi\sigma^2\Omega^{(2,2)*}(t)} \quad (10)$$

$$= 10.50\sqrt{t}/\Omega^{(2,2)*}(t)\ \mu\text{Pa s} . \quad (10a)$$

Equation (10) is identical to Eq. (8.2)–(10) in Ref. 15, whereas in Eq. (10a) the constants have been evaluated for methane. The reduced collision integral $\Omega^{(2,2)*}$ is a function only of the reduced temperature $t = kT/\epsilon$ and the intermolecular potential function. For evaluation of Eq. (10), we have used the 11-6-8, $\gamma = 3$ potential function

$$V(r) = \epsilon[(12/5)(r_m/r)^{11} - (2/5)(r_m/r)^6 - 3(r_m/r)^8] , \quad (11)$$

where $r_m = 1.1145\sigma$. The parameters ϵ and σ, which are defined by $V(r_m) = -\epsilon$ and $V(\sigma) = 0$, were chosen to give the best fit to the low density transport data and are given in Table 1. The additional constants of Eq. (10), the relative molecular mass M_r, the unified atomic mass unit u, and the Boltzmann constant k, are also given in Table 1. A discussion of the utility of the 11-6-8, $\gamma = 3$ potential in correlating transport property data has been given by Hanley and Klein.[27] This potential, with the present values of ϵ and σ, has not been optimized for thermodynamic property evaluation. Rather than directly evaluate the collision integral, we fit the tabulated results of Klein *et al.*[16] to the form

$$\Omega^{(2,2)*} = \left[\sum_{i=1}^{9} C_i t^{[(i-1)/3-1]}\right]^{-1} . \quad (12)$$

The coefficients C_i for Eq. (12) are listed in Table 8. The fit agrees with the tabulated integration results[16] within about 0.1% in the (reduced) temperature range $0.5 < t < 200$.[1]

For the thermal conductivity λ_0 of the dilute gas, a completely rigorous theory is not available for polyatomic molecules, due to the complexities of exchanging energy between internal and external (kinetic) degrees of freedom. We have chosen a modified Eucken model[28] of the form

$$\lambda_0(T) = \frac{\eta_0(T)}{M_r u N_A}\left[\frac{15R}{4} + f_{int}\left(C_p^{id} - \frac{5R}{2}\right)\right] \quad (13)$$

$$= 0.518\,26\ \eta_0(T)\,[3.75 - f_{int}(\tau^2\phi_{\tau\tau}^{id} + 1.5)]$$

$$\text{mW m}^{-1}\text{K}^{-1} , \quad (13a)$$

where C_p^{id} is the (temperature dependent) ideal gas contribution to the isobaric specific heat capacity and f_{int} is a dimensionless function which describes the energy exchange mentioned above. When using Eq. (13a), the viscosity should be expressed in μPa s, as in Eq. (10a). The specific heat contribution, having been written in terms of a derivative of the ideal gas free energy, can be evaluated using Tables 4 and 5. The form for f_{int} is chosen empirically as

$$f_{int} = f_1 + (f_2/t) , \quad (14)$$

with the fitted coefficients f also given in Table 8.

2.5.2. Excess Property Correlation

For the excess viscosity, we use a rational polynomial in the reduced density δ and inverse reduced temperature τ, and scaled by dimensional analysis and critical point values. (Note that the parameter $t = Tk/\epsilon$, used above, is the temperature reduced by the interparticle potential energy scale, while $\tau = T_c/T$ is the inverse temperature reduced by the critical temperature.) Thus, we write

$$\eta_{ex}(\rho,T) = \frac{P_c^{2/3}(M_r u)^{1/2}}{(T_c k)^{1/6}}\left[\sum_{i=1}^{9} g_i\delta^{r_i}\tau^{s_i}\right] \times\left[1 + \sum_{i=10}^{11} g_i\delta^{r_i}\tau^{s_i}\right]^{-1} \quad (15)$$

$$= 12.149\left[\sum_{i=1}^{9} g_i\delta^{r_i}\tau^{s_i}\right] \times\left[1 + \sum_{i=10}^{11} g_i\delta^{r_i}\tau^{s_i}\right]^{-1}\ \mu\text{Pa s} , \quad (15a)$$

where the exponents r_i and s_i and the dimensionless fitted coefficients g_i are given in Table 9. Alternatively, the triple-point density of the liquid could be incorporated into Eq. (15).[29]

The excess thermal conductivity λ_{ex} has been correlated to a polynomial in δ and τ with a factor in the final term of δ_σ^*, defined by

TABLE 8

COEFFICIENTS FOR FIT OF DILUTE GAS TRANSPORT PROPERTIES

$\Omega^{(2,2)*}$, Eq. (12)		f_{int}, Eq. (14)	
C_1	-3.0328138281		
C_2	16.918880086	f_1	1.458850
C_3	-37.189364917		
C_4	41.288861858	f_2	-0.4377162
C_5	-24.615921140		
C_6	8.9488430959		
C_7	-1.8739245042		
C_8	0.20966101390		
C_9	$-9.6570437074 \times 10^{-3}$		

TABLE 9

COEFFICIENTS FOR EXCESS TRANSPORT PROPERTY CORRELATIONS

	η_{ex}, Eq. (15)			λ_{ex}, Eq. (17)		
i	r_i	s_i	g_i	r_i	s_i	j_i
1	1	0	0.41250137	1	0	2.4149207
2	1	1	-0.14390912	3	0	0.55166331
3	2	0	0.10366993	4	0	-0.52837734
4	2	1	0.40287464	4	1	0.073809553
5	2	1.5	-0.24903524	5	0	0.24465507
6	3	0	-0.12953131	5	1	-0.047613626
7	3	2	0.06575776	* 2	0	1.5554612
8	4	0	0.02566628			
9	4	1	-0.03716526	* Term divided by δ_σ^*		
10	1	0	-0.38798341			
11	1	1	0.03533815			

$$\delta_\sigma^*(T) = \begin{cases} \rho_{\sigma v}(T)/\rho_c\,, & \text{if } T<T_c \text{ and } \rho<\rho_c\,, \\ 11\,, & \text{otherwise}\,. \end{cases} \quad (16)$$

In Eq. (16), $\rho_{\sigma v}$ is the density of the saturated vapor; the term is included to account for the behavior of the vapor near the two-phase boundary. The function, with all dimensions contained in the initial factor, is

$$\lambda_{ex}(\rho,T) = \frac{P_c^{2/3}k^{5/6}}{T_c^{1/6}(M_r u)^{1/2}}\left[\sum_{i=1}^{6} j_i \delta^{r_i}\tau^{s_i} + j_7\delta^2/\delta_\sigma^*\right] \quad (17)$$

$$= 6.296\,38\left[\sum_{i=1}^{6} j_i \delta^{r_i}\tau^{s_i} + j_7\delta^2/\delta_\sigma^*\right] \text{mW m}^{-1}\,\text{K}^{-1}\,. \quad (17a)$$

The exponents and dimensionless fitting coefficients for Eq. (17) are given in Table 9. In both excess functions, Eqs. (15) and (17), there are strong density dependences and weak temperature dependences.

2.5.3. Critical Enhancement Correlation

While both the viscosity and the thermal conductivity exhibit an increase or divergence near the liquid–vapor critical point, presumably due to dynamic interactions among clusters formed because of large-scale density fluctuations,[11] it is only in the thermal conductivity that the divergence is strong and the enhancement is easily observed in a broad region around the critical point. For this reason, the present transport property correlations include an enhancement contribution only for the thermal conductivity. Although the theoretical description is not completely rigorous, the algorithm developed by Sengers *et al.*[11] is both sufficiently accurate and flexible to correlate the present thermal conductivity data. We rewrite Eq. (3.15) in Ref. 11 as

$$\lambda_{cr}(\rho,T) = \frac{\Lambda^* k\rho_c^2}{6\pi\eta(\rho,T)P_c}\left[\frac{T}{\rho}\frac{\partial P}{\partial T}\right]_\rho^2 \chi_T^{*(\gamma-\nu)/\gamma} F(T^*,\rho^*) \quad (18)$$

$$= \frac{91.855}{\eta(\rho,T)\tau^2}[1+\delta\phi_\delta^r - \delta\tau\phi_{\delta\tau}^r]^2 \times \chi_T^{*0.4681} F(T^*,\rho^*)\,\frac{\text{mW}}{\text{m K}}\,, \quad (18a)$$

where the viscosity is expressed in μPa s in Eq. (18a).

In Eq. (18), Λ^* is a fitted parameter which reflects the dynamic couplings which occur during energy transport, the amplitude of the critical correlation length divergence, and the amplitude of the critical compressibility divergence. (It thus differs from Λ, a dimensionless constant in Ref. 11, which has a theoretical value near 1. Using the values of the amplitudes from Ref. 11, we find $\Lambda \approx 1.4$ from the present empirical fit.) The exponents γ and ν are the critical exponents associated with the divergences of the thermodynamic compressibility and correlation length, respectively. They are taken directly from Sengers *et al.*[11] The dimensionless temperature dependent and density dependent function χ_T^* is a reduced and symmetrized compressibility defined by

$$\chi_T^* = \delta\frac{P_c}{\rho_c}\frac{\partial\rho}{\partial P}\bigg|_T \quad (19)$$

$$= 0.286\,31\;\delta\tau[1+2\delta\phi_\delta^r + \delta^2\phi_{\delta\delta}^r]^{-1}\,. \quad (19a)$$

Finally, F is a dimensionless empirical crossover or damping function,

$$F(T^*,\rho^*) = \exp\{-[F_T|T^*|^{1/2} + F_\rho\rho^{*2} + F_A\rho^*]\}\,, \quad (20)$$

where F_T, F_A, and F_ρ are constants to be fitted and T^* and ρ^* measure deviations from the critical point according to

$$T^* = (T_c - T)/T_c \quad (= 1 - 1/\tau) \quad (21)$$

and

$$\rho^* = (\rho_c - \rho)/\rho_c \quad (= 1-\delta)\,. \quad (22)$$

The values of the fitted parameters and necessary constants are given in Table 10 (with the critical constants given in Table 1).

Although the isochoric derivative in Eq. (18) remains finite and well behaved near the critical point, the isothermal density derivative in Eq. (19) can give problems in this region. Therefore, when evaluating the thermal conductivity enhancement in the range $|T^*|<0.03$ and $|\rho^*|<0.25$ (that is, 185 K$\leqslant T\leqslant$196 K and 7.6 mol dm$^{-3}\leqslant\rho\leqslant$12.7 mol dm^{-3}), we use a scaled equation of state rather than the analytic SWEOS discussed above. Following Sengers *et al.*,[11] we use the MLSG scaled equation of state introduced by Vicentini-Missoni, Levelt Sengers, and Green.[30a] Using the new temperature dependent and density dependent variables θ (not to be confused with the Schofield parameter in Ref. 11) and Ω, we rewrite Eq. (2.11) in Ref. 11 as

$$\chi_T^*(\rho,T) = Q\,|\rho^*|^{-a}\theta^b[\theta + \Omega(\theta+R)]^{-1}\,. \quad (23)$$

The variables are defined as

$$\theta = \begin{cases} 1 + E(1 + ST^*|\rho^*|^{-1/\beta})^{2\beta} & \text{if } T^* < -|\rho^*|^{1/\beta}/S \\ 1 & \text{if } T^* > -|\rho^*|^{1/\beta}/S \end{cases} \quad (24)$$

and

$$\Omega = WT^*|\rho^*|^{-1/\beta}\,, \quad (25)$$

TABLE 10

CONSTANTS NEEDED TO EVALUATE λ_{cr}, EQ. (18)
(and using Eq. (23) if $|T^*|<0.03$ and $|\rho^*|<0.25$
or Eq. (26) if $|T^*|<0.03$ and $\rho^*=0$)

Fitted coefficients:	$\Lambda^* = 2.235 \times 10^9$ m^{-1} $F_T = 2.646$ $F_\rho = 2.678$ $F_A = -0.637$
Critical exponents:	$\gamma = 1.190$ $\nu = 0.633$ $\beta = 0.355$
Universal constants:	a = 3.352 b = 0.732 E = 0.287 R = 0.535
Fluid dependent constants derived from Ref. [11] :	Q = 0.1133 S = -6.098 W = -1.401 Γ = 0.0801

while, the universal constants a, b, β, R and E, and fluid dependent constants, Q, S, and W, are given in Table 10. The second equality in Eq. (24) is only used in a narrow region near the saturation boundary for temperatures between about 189.8 K and T_c. It is needed as an adjustment to the MLSG equation because the saturation boundary given in Ref. 11 is not precisely identical to that defined by our ancillary Eqs. (3)–(5) or by the SWEOS itself. Thus, the second equality of Eq. (24) prevents a spurious singularity in the critical enhancement calculation; the resultant behavior of the calculated thermal conductivity in this small region does not follow the theoretical enhancement model. Along the critical isochore (that is, when $\rho^* = 0$), factors within Eq. (23) diverge; however the limit is well defined as

$$\chi_T^*(\rho = \rho_c, T) = \Gamma |T^*|^{-\gamma}, \tag{26}$$

with Γ also given in Table 10. Thus, along this isochore, and within the restricted temperature range mentioned above, Eq. (26) should be used to avoid spurious infinities. The algebraic relationships among the constants introduced above and the more fundamental constants discussed in Ref. 11 are given in Table 11.

In summary, Eq. (18) is used to evaluate the critical enhancement of the thermal conductivity; the value of χ_T^* comes from Eq. (19) in general, from Eq. (23) in the restricted critical region mentioned above, or from Eq. (26) when along the critical isochore if $|T^*| < 0.03$. The constants in Table 10 complete the necessary information to evaluate λ_{cr}. (Note: Very recent theoretical advances have led to an improved crossover formalism for the transport propery enhancements. Application to methane will be discussed in a forthcoming publication by Olchowy and Sengers.[72].

TABLE 11

RELATIONSHIPS AMONG PARAMETERS DEFINED IN EQS.(18) - (26) AND PARAMETERS FOUND IN REF. [11]

$$\Lambda^* = \Lambda\, \Gamma^{\nu/\gamma}\, \xi_o^{-1}$$

$$a = \gamma / \beta$$

$$b = (1 + 2\beta - \gamma) / 2\beta$$

$$R = \delta - \beta^{-1} - 1$$

$$Q = (1 + E)^{(\gamma-1)/2\beta} / D\, \delta$$

$$S = -x_o^{-1}$$

$$W = -x_o^{-1}\, \delta^{-1}$$

3. Development of the Correlations

3.1. Fundamental Constants, Fixed Points, and Ideal Gas Properties

The fundamental constants which were used are given in Table 1 and agree with the values recently recommended by the Committee on Data for Science and Technology (CODATA).[30,31] The relative molecular mass for methane was derived from the atomic values of the recent IUPAC tables[32] and agrees with the value used by Angus *et al.*[2] and by Goodwin.[17] Uncertainties associated with these quantities can be found in the original references.

The values of the fixed point constants at the triple point of methane were not needed for the present correlations. However, they determine the range of validity of many of the equations of Sec. 2 and may be of interest in their own right; therefore, they are presented in Table 1. The triple-point temperature of methane is a Secondary Reference Point adjunctive to IPTS-68; its recommended value[33] is given. This value agrees (within combined uncertainties) with the value adopted by Angus *et al.*[2] and the experimental determination of Kleinrahm and Wagner.[3] For the pressure at the triple point, we recommend the value established by Pavese[34] using triple-point cells. This value agrees very well with the measured result of Ref. 3, and it differs by only 0.4% and 0.2% from the values adopted by Goodwin[17] and Angus *et al.*,[2] respectively. Using either our Eq. (3) for the saturated vapor pressure and the value of T_t in Table 1 or the present equation of state [Eqs. (2) and (7)], Maxwell relations, and the same T_t, we obtain values for P_t which are within 0.02% of the recommended value (that is, nearly within the uncertainty stated by Pavese[34]).

The fluid densities at the triple point were obtained from the present equation of state using the stated value of T_t and Maxwell relations, and their uncertainties were estimated by comparing to other references. The liquid density is 0.002 mol dm^{-3} below that used in Ref. 17 or calculated from Eq. (4), 0.004 mol dm^{-3} above that calculated in Ref. 3, and 0.019 mol dm^{-3} (0.07%) above the value calculated in Ref. 2. The density of the vapor at the triple point as given in Table 1 is about 10^{-5} mol dm^{-3} below that given in Refs. 2 and 17, 2×10^{-5} mol dm^{-3} above that obtained using Eq. (5), and 3×10^{-5} mol dm^{-3} (0.2%) above the value calculated in Ref. 3.

The state variables at the critical point of methane are of great import for the present correlations, as they enter directly into many of the equations of Sec. 2. During the development of the present correlations, we attempted to improve the overall fit by allowing the critical parameters to vary. Since we did not find an alternative set of values which significantly improved the quality of the fit, we chose to use the critical values of Kleinrahm and Wagner,[3] which they obtained from very careful analysis of their near-critical *PVT* data. The critical temperature agrees, within the uncertainties, with the temperatures used by Angus *et al.*[2] and by Goodwin,[17] that is, 190.555 K. For the critical pressure and density, we have assigned more conservative estimates of uncertainty than those quoted in Ref. 3, which we obtained

by using the present correlations and evaluating the pressure and mean of the coexisting densities at a temperature 20 mK below T_c. For comparison, the critical pressures and densities are given as 4.595 MPa and 10.1095 $\pm$ 0.12 mol dm^{-3} in Ref. 2, and 4.5988 MPa and 10.0 mol dm^{-3} in Ref. 17. The IUPAC monograph gives a list of references to both experimentally determined critical parameters and to those chosen by various compilers, while Ref. 3 provides great detail concerning the determination of the values which we have used. The values of T_c, P_c, and ρ_c of Table 1, including all the quoted digits and disregarding the associated uncertainties, should be used when evaluating the correlations of Sec. 2.

The intermolecular potential parameters σ and ϵ in Table 1 were obtained by fitting low-density transport data. Our value for ϵ is 3.6% above that reported by Hanley *et al.*[14] using earlier data, while that for σ differs only very slightly (0.4%). The same potential function, Eq. (11), was used in both cases. Maitland *et al.*[35] have very recently determined the scaling parameters in the interparticle potential using a fit to low-density viscosity data and a corresponding states assumption. They obtained $\epsilon/k = 163.558$ K (6% below our value) and $\sigma = 0.3709$ nm (1% above the present value). This discrepancy is not surprising since the parameters are sensitive to the form of the model potential which is assumed, the particular properties being fitted, and the temperature range of the input data. We emphasize that the intermolecular potential parameters of Table 1 are not appropriate when using the Lennard-Jones (12-6) potential instead of the 11-6-8, $\gamma = 3$ potential of Eq. (11). Good results cannot be expected when calculating equilibrium thermodynamic properties (such as the second virial coefficient) using Eq. (11) with the given parameters.

The remaining entries in Table 1, those concerning the values of the entropy and enthalpy at standard conditions, were evaluated using Eq. (7). These and all quantities evaluated using either the ideal gas Helmholtz energy, Eq. (7), itself or its first temperature derivative are relative values. Contributions from the nuclear spin have been excluded; the value of the ideal gas enthalpy is zero at zero temperature. The values in Table 1 agree with the values in Refs. 2, 25, and 26 to, at worst, one part in ten thousand. The study by McDowell and Kruse[26] is the source of these quantities, and additional references are given by Angus *et al.*[2] A comparison with Wagman *et al.*,[36] shows a discrepancy of 0.27% in the enthalpy and 0.06% in the entropy (adjusted to atmospheric pressure).

The development of the ideal gas correlations was discussed in Sec. 2.3. Equation (7) is equivalent to the correlation developed by Goodwin[25] but it has been adjusted to use the current values of R and T_c and extended to arbitrary values of the pressure. It yields nearly identical results for the (dimensional) ideal gas properties at atmospheric pressure. Discussions of the quality of this correlation, the statistical mechanical approximations, and the data used are given in Refs. 2, 25, and 26. When Eq. (7) is used at the upper temperature limit of the present PVT correlation, at 600 K, the error in the ideal gas heat capacity C_p is about 1.3%. In the range $T_t \leqslant T \leqslant 360$ K, the errors in any ideal gas property are thought to be less than a few hundredths of a percent.

3.2. Residual Molar Helmholtz Energy

The coefficients associated with Eq.(2) were determined by multiproperty linear least-squares fitting, with the exponents used, r_i and s_i, identical to those determined by Schmidt and Wagner.[12] The critical parameters of Table 1 were introduced into the fitting routine as constraints on the pressure and its first two isothermal density derivatives at the critical point. Thus we required

$$P(\rho_c,T_c) = P_c$$

and

$$\left.\frac{\partial P(\rho_c,T_c)}{\partial \rho}\right|_T = \left.\frac{\partial^2 P(\rho_c,T_c)}{\partial \rho^2}\right|_T = 0 .$$

The densities and pressures along the two-phase boundary, second virial coefficient data, PVT data, specific heat capacities at isochoric and isobaric conditions and along the saturated liquid boundary, and speed of sound in the single phase and along the liquid phase boundary were used in the determination. The sources of the data and the details concerning the use of different types of thermodynamic data in our fitting scheme are discussed in this section.

The relative weights of data within the fitting routine were obtained from a determination of the type of thermodynamic data, the source of the experimental data, the region of the phase diagram, and the Gaussian error propagation formula. A complete discussion of the calculation of the weight for each of the $\sim$4000 points used is not feasible in this paper, but some indication will be given here and below. The overall multiplier used to weight a particular property was determined by a selection process which sought to simultaneously obtain reasonable agreement for all data types, with particular emphasis paid to reproducing the two-phase boundary. It was found to be impossible to fit all data within the stated experimental accuracy since data were frequently incompatible within the stated accuracies. Further it is sometimes impossble to fit certain highly accurate data to within experimental error even though they may be compatible with other data of lesser accuracy. This is often the case when combining data such as speed of sound with other types of data. When data were incompatible in a particular region of the phase diagram, determination of emphasis and de-emphasis, reflected in the relative weight given to the data, was made by considering the intrinsic merits of the experimental methods used, as well as examination of the agreement with additional data both within and outside the region of interest. Further details concerning the weights are given below, and explicit values are in Ref. 1.

Figure 4 illustrates the regions of the P-T phase space which were used during the fitting process, and we have indicated which properties and which references were most heavily weighted to achieve the final correlation of Eq. (2) and Table 2. Additional experimental data were used with limited weighting, and these references and further discussion of the fitting routine are given for each property in this section; see also Ref. 1. While the actual determination of the weights is somewhat *ad hoc*, we thought it was preferable to the alternative of averaging among inconsistent data. The Gaussian error formula was invoked by assuming fixed relative or ab-

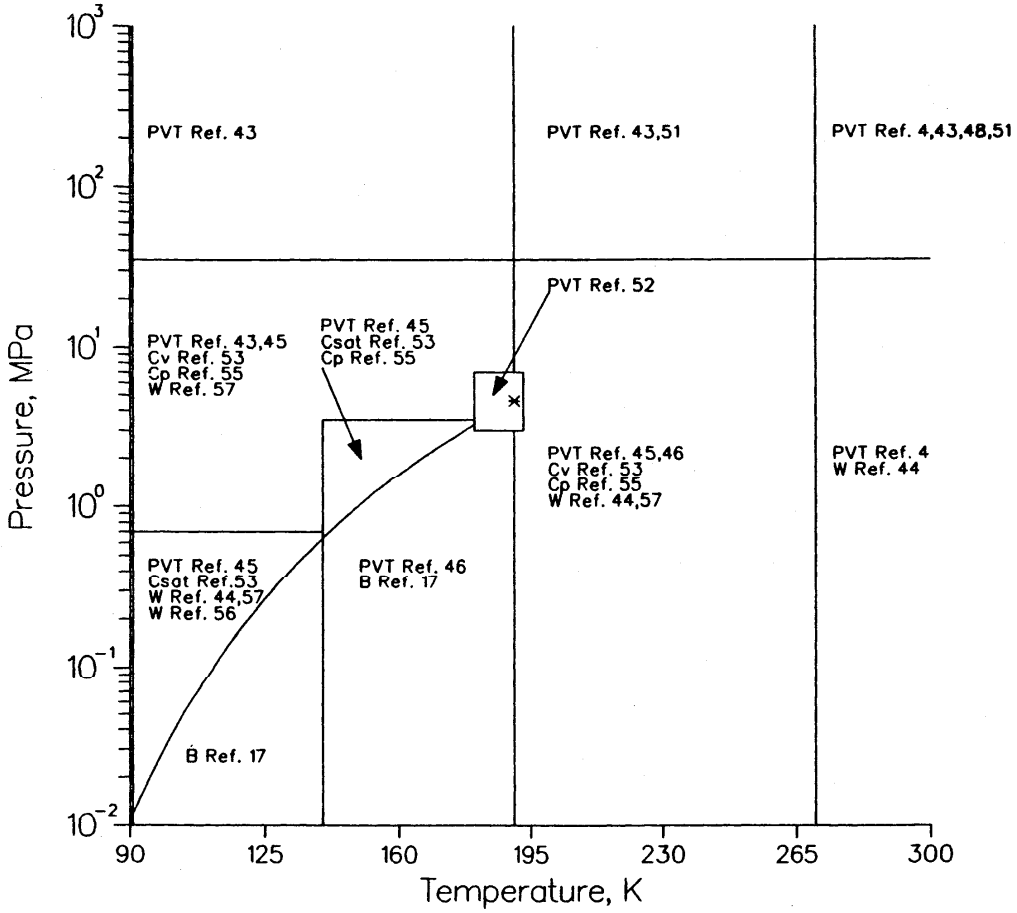

FIG. 4. Regions of P-T space and references for the primary data used in each region.

solute accuracies for the various dependent and independent quantities involved in each type of data. Thus, if $z = z(x,y)$ with absolute accuracies σ_x, σ_y, and σ_z (or relative accuracies σ_z/z, etc.) the relative weight is given by

$$Wt \propto \left[\sigma_z^2 + \left(\sigma_x \left.\frac{\partial z}{\partial x}\right|_y\right)^2 + \left(\sigma_y \left.\frac{\partial z}{\partial y}\right|_x\right)^2\right]^{-1/2}. \quad (27)$$

In a few instances individual data were omitted from the final determination of the fitted coefficients. These data were excluded when the deviations from a preliminary version of the correlation were well beyond deviations for similar points or differed greatly from trends determined from similar points.

The fitting of the saturation boundary *PVT* data was unique in that the data input to the least-squares routine consisted of values of $P_\sigma, \rho_{\sigma V}$, and $\rho_{\sigma L}$ at 20 temperatures evenly spaced between 91 and 186 K. These data were evaluated from the ancillary equations described in Sec. 2.2 and discussed further in Sec. 3.3. This was done to ensure that the saturation properties determined from the equation of state are as accurate as possible; the two-phase boundary determined from the Helmholtz energy correlation is completely compatible with the ancillary equations. Three distinct minimization conditions $[P_\sigma(T) - P(\rho_{\sigma V},T)$, $P_\sigma(T) - P(\rho_{\sigma L},T)$, and the Gibb's condition, $A(\rho_{\sigma L},T) + P_\sigma/\rho_{\sigma L} - A(\rho_{\sigma V},T) - P_\sigma/\rho_{\sigma V}]$ associated with the saturation boundary were incorporated within the fitting routine. In these expressions, the ideal gas contributions to the pressure and thermodynamic potentials were subtracted, since only the residual molar Helmholtz energy was determined from the fitting procedure. The functions of density and temperature were evaluated as indicated in Table 7. Heavy emphasis, through additional weighting, was placed on the liquid density and Gibb's condition, especially above 165 K; also the density of the saturated vapor was heavily weighted above 145 K. The data for the second virial coefficient which were used in this correlation are identical to those used by Goodwin[17]; the original sources are Refs. 37–41. An additional six points from Douslin *et al.*,[37] not used by Goodwin, have been added to the data. The zero-density limit indicated in the expression for the second virial coefficient in Table 7 implies that only the parameters n_i with $i = 1,2,3,14$, and 15 are directly affected by these data. The weighting for the virial data tended to be high, especially for $T < 250$ K and for the data of Douslin *et al.*,[37] Byrne *et al.*,[39] and Levelt Sengers *et al.*[41] The last data set, from Ref. 41, consists of smoothed data evaluated from other sources. No data above 625 K, the upper limit of the present correlation, were used in the fit. Experimentally determined third

TABLE 12
SOURCES OF PVT DATA

FIRST AUTHOR	REF.	NO.PTS.	TEMPERATURE RANGE, K	PRESSURE RANGE, MPa	DENSITY RANGE mol•dm^{-3}	PRESSURE AAD-%[c]	DENSITY AAD-%[d]
Achtermann	42	35	323	1.1-29	0.4-11	0.04	0.04
Achtermann[a]	42a	139	273-293	0.1-9	0.04-5	0.04	0.04
Cheng	43	66	111-309	22-110	14-29	1.8	0.20
Douslin	37	201	273-623	1.6-40	0.8-13	0.05	0.05
Gammon[e]	44	217	113-323	0.1-25	0.1-26	0.96	0.53
Goodwin	45	554	92-300	0.3-35	3-29	0.72	0.12
Goodwin[b]	46	46	150-270	1-4	1-2	0.09	0.11
Kleinrahm	52	187	180-193	3.3-6.7	3.7-16	0.03	0.35
Kvalnes	47	158	203-473	0.1-101	0.03-25	0.71	0.38
Mollerup[b]	5	23	310	0.15-74	0.06-19	0.12	0.07
Morris[b]	7	105	250-409	123-682	20-32	1.9	0.40
Robertson	48	53	308-473	150-1000	21-35	7.0	1.4
Sivaraman[a,f]	49	104	193-423	1.5-28	1-14	0.16	0.34
Trappeniers	4	472	273-423	1.8-260	0.8-26	0.12	0.07
Van Itterbeek	50	163	114-188	0.8-31	17-28	7.2	0.32
Vennix	51	254	172-274	2.5-69	3-22	0.68	0.55

[a] These data arrived too late to be included in the correlations.

[b] Some of these data are from correlations of experimental measurements.

[c] Average absolute percent deviation when pressure is calculated from experimental temperature and density.

[d] Average absolute percent deviation when density is calculated from experimental temperature and pressure.

[e] Some tabulated densities near the two-phase boundary were determined from alternative correlations.

[f] For temperatures above 250 K, densities were from alternative correlations.

virial coefficient data were not used in the present correlation. These data are difficult to obtain and consequently suffer from inaccuracies.

The largest body of thermodynamic data for methane consists of *PVT* measurements, and more than 2500 points were considered in this correlation. In Table 12 we have summarized the approximate ranges of the data for each reference, and Fig.4 indicates those data which were given the most emphasis. Some data in Table 12, as indicated, were not included in the fit because they were only recently acquired, but they are cited for the sake of completeness. The other data in Table 12 were given only minor weight in any region of Fig.4 in which they are not explicitly mentioned. The actual weight for each datum can be found in Ref. 1. While most of the data used consisted of unaltered, primary measurements as tabulated in the original references, changes of temperature scale (to IPTS-68) and conversion of units were sometimes necessary. Certain references, as indicated in Table 12, provide correlations only or provide tabulated results which have been obtained from correlations of experimental data. In the former case, we have calculated the *PVT* points, within the suggested range of the correlation, to include in the data base for the current fitting routine. The *PVT* data entered the fitting routine through minimization of the expression $P(\rho,T) - \rho RT - \rho RT\delta\phi^r_\delta(\delta,\tau)$. A discussion of the comparison between the present correlation and the experimental data is deferred to the next section.

The isochoric heat capacity data which we have used in developing the correlation include 332 experimental points from Younglove,[53] adjusted as discussed by Roder,[54] and the additional points reported in Ref. 54. The experimental densities which were reported were established from an older equation of state[54] as well as absolute calibration of certain volumes. The resultant uncertainty in the tabulated experimental densities seemed to have no significant effect on the present correlation. The ideal gas contribution to the heat capacity was subtracted from the data, and the second temperature derivative of the residual Helmholtz function, as indicated in Table 7, was fit to the resultant residual isochoric heat capacity. These data were most heavily emphasized in the region of moderate supercritical temperatures and pressures and in the liquid, especially below 150 K but only between P_C and 35 MPa.

The source of the isobaric heat capacity data used in our fit was the paper by Jones *et al.*[55] We converted their smoothed tabulated results to SI units. Because C_p is nonlinear in the residual free energy and its derivatives, as seen in Table 7, and the experimental variables are pressure and temperature (whereas, the independent variables in the free energy are density and temperature), the experimental data could not be input directly into the linear least-squares fitting routine. The input density was calculated from the experimental *PT* state point using a previous iteration of the SWEOS. The fit was linearized by subtracting two terms from the experimental heat capacity: the ideal gas isochoric heat capacity at the same temperature and the term $T(\partial P/\partial T|_\rho)^2\,(\partial\rho/\partial P|_T)/\rho^2$ evaluated from the previous SWEOS. The remainder is the residual isochoric heat capacity, linear in $\phi^r_{\tau\tau}$, and was fit as such. The regions of major emphasis for the C_p data, as illustrated in Fig.4, were the moderately dense liquid and the region of moderate supercritical temperatures and pressures below 35 MPa.

The specific heat capacity while maintaining the liquid at saturation $C_{\sigma L}$ was also measured by Younglove[53] and Roder.[54] The data were reduced[54] by using the equation of state of Goodwin.[17] These data were used in the routine which fit the residual Helmholtz energy, after a linearization process. The required orthobaric derivative (that is, the derivative along the saturation boundary) was approximated by differences according to

$$C^r_{\sigma L}(T) = T\left.\frac{\partial S^r(\rho_{\sigma L},T)}{\partial T}\right|_\sigma \approx T\frac{S[\rho_{\sigma L}(T+\epsilon)] - S[\rho_{\sigma L}(T-\epsilon)]}{2\epsilon}, \tag{28}$$

where the function $\rho_{\sigma L}(T)$ was evaluated using the ancillary Eq. (4), and ϵ was chosen to be 0.01 K. The corresponding expression for the ideal gas contribution to $C_{\sigma L}$, which was subtracted from the experimental data, is

$$C^{\rm id}_{\sigma L}(T) \approx T\frac{\Delta S^{\rm id}}{\Delta T} - \frac{RT}{\rho_{\sigma L}T}\frac{\Delta(\rho_{\sigma L}T)}{\Delta T}. \tag{29}$$

Here the deltas indicate differences as in Eq. (28) and the temperature difference was taken to be 0.01 K, consistent with Eq. (28). Alternative linearization schemes, such as that implied by the $C_{\sigma L}$ entry in Table 7, could also be used. Such schemes could make use of the analytically known derivative properties of the ancillary equation [Eq. (4)] instead of calculating the difference as in Eq. (28). The saturated liquid heat capacities were entered into the linear fit for the free energy, and they were heavily emphasized.

The final type of thermodynamic data which we considered was the speed of sound, both in the single phase region and along the saturation boundary. Again, as indicated in Table 7, these data are not linearly related to the free energy. The mechanism by which these data entered the fit was iterative, in that a preliminary version of the SWEOS was used to calculate $\partial P/\partial\rho|_T$ from the sound speed data according to

$$\left.\frac{\partial P}{\partial\rho}\right|_T = uN_AM_rw^2_{\rm exp}\frac{C_V(\rho,T)}{C_P(\rho,T)} \tag{30}$$

where the heat capacities and the densities are calculated from the experimental $P-T$ state point. For the data on the saturation boundary, the Maxwell construction, using the preliminary SWEOS, was used to find the density. The values of the density derivative, with the corresponding density and experimental temperature, were then used as input into the next iteration of the fitting process. The residual portion of this derivative, as seen in Table 7, can be expressed as a linear combination of ϕ^r_δ and $\phi^r_{\delta\delta}$. More than 500 sound speed data from Refs. 6,44 and 56–59 were used in this manner with conversion of units and temperature scale sometimes necessary. The major emphasis was on the data of Straty,[57] Gammon and Douslin,[44] and Blagoi *et al.*[56] (near the triple point only) as indicated in Fig.4. The critical re-

gion data of Ref. 44, which assumed a slightly different critical density in the experimental analysis, were given very little weight in the fitting scheme. Because the value of $\partial P/\partial\rho|_T$ is very small near the critical point, and, therefore, subject to a large relative uncertainty, it was very difficult to use sound speed data near the critical point in our correlation. As an alternative to Eq. (30) a different linearization scheme which emphasizes the dominant $(\partial P/\partial T|_\rho)/\sqrt{c_v}$ contribution to the sound speed in the general critical region, could have been used.

The coefficients, n_i of Eq. (2), as listed in Table 2, represent the best least-squares fit of the residual molar Helmholtz energy for methane within the constraints discussed above. We defer to Sec. 4 a discussion of the comparison between the correlation and the experimental data.

3.3. Ancillary Equations for the Two-Phase Boundary

In the ancillary equations, Eqs. (3)–(5), for the saturated vapor pressure and the densities of the coexisting liquid and vapor, the critical constants were considered fixed at the values given in Table 1. In addition, the exponents β and ϵ were given their effective scaling law values, as discussed in Sec. 2. During the course of establishing these correlations, we varied the exponents and the critical parameters; as there was no significant improvement with an alternate set of parameters, the above mentioned choices were retained. Additionally, alternate values for the integer exponents of T^* and alternate forms of the equations were explored, with the resulting Eqs. (3)–(5) giving the best agreement with the experimental data.

The experimental measurements of Kleinrahm and Wagner[3] were our sole source of data for determining the coefficients in Eqs. (3)–(5) for the liquid–vapor boundary; these coefficients appear in Table 3. (Comparisons with other data are given in the following section.) As in Ref. 3 we have concluded that the reported impurities in the methane sample used by Prydz and Goodwin[60] were sufficient to cause the discrepancy between the experimental vapor pressures reported in Ref. 60 and those of Ref. 3. These differences are especially troubling near the triple point where the difference approaches 0.5%. Unpublished data by Haynes[61], in the region 95–140 K, indicate vapor pressures smaller than those of Ref. 60 and in good agreement with the values of Kleinrahm and Wagner.[3] Discussions of other experimental sources of saturated vapor pressure data are given by Angus *et al.*[2] as well as by Kleinrahm and Wagner.[3] To obtain the coefficients H_i, Eq. (3) was linearized by taking the logarithm of both sides, and a linear least-squares fitting routine was used. The input data for the saturated vapor pressure were the 38 points obtained from Ref. 3 after averaging the multiple points at a single temperature. Equal weighting from the triple point to the critical temperature was used in the fitting routine.

The correlation for the density of the liquid along the two-phase boundary, Eq. (4), was obtained in an analogous manner. While alternative experimental data for this property exist, again the data of Kleinrahm and Wagner[3] were chosen to give a single, consistent, accurate set of measurements for all three coexistence properties along the entire liquid–vapor phase boundary. The data of Haynes and Hiza,[62] obtained with a magnetic suspension densimeter, are systematically higher than those of Ref. 3 (see Fig. 7 in the following section), but cover a smaller range in temperature. The two sets of data agree within their stated uncertainties. Additional discussions of available saturated liquid density data are given in Angus *et al.*,[2] Kleinrahm and Wagner,[3] and Haynes and Hiza.[62] Equation (4) was linearized, and 38 points from Ref. 3 were used to calculate the coefficients G_i using a linear least-squares algorithm.

Equation (5) for the density of the saturated vapor required expressions for both the vapor pressure and the density of the saturated liquid in order to ascertain values for the coefficients J_i. As mentioned above, the value of J_0 was completely determined from the fit for Eq. (4). The value 8 for the exponent of τ was chosen to optimize the fit. The expression was then linearized and the coefficients determined by a least-squares routine. The data again consisted of 38 points from Kleinrahm and Wagner,[3] wherein a discussion of other sources of saturated vapor density data is given. For this property, the data were again equally weighted from the triple point to the critical point temperatures. We think that by using only the accurate and consistent data of Kleinrahm and Wagner for all the phase boundary equations we obtained an excellent description of the phase behavior. This, coupled with the forms of the correlating equations which describe, at least to lowest order, the theoretically predicted behavior of the fluid near the critical point, has resulted in a set of ancillary equations which are accurate, self-consistent, and descriptive of the physical system.

3.4. Transport Property Correlations

3.4.1. Viscosity

The dilute gas viscosity is completely specified by the Chapman–Enskog expression, Eq. (10), with only the form of the potential and its parameters unknown. The flexibility of the m-6-8 family of potentials, its theoretically-based justification, and the utility of the specific 11-6-8, $\gamma = 3$ form for spherical or nearly spherical molecules have been established by Hanley and Klein.[27] Thus, we have chosen this potential, Eq. (11), and fit the associated dimensionless collision integral, $\Omega^{(2,2)^*}$, as tabulated by Klein *et al.*,[16] to the series in $(kT/\epsilon)^{1/3}$ described by Eq. (12). The accurate low-density viscosity measurements of Hellemans, Kestin, and Ro[63] in the range 300 K $< T <$ 470 K were used to establish the distance and energy parameters of the potential function. These data were adjusted to zero density, from the low pressures at which the measurements were made, by subtracting the excess viscosity calculated from a preliminary version of the correlation. These adjustments in no case exceeded 0.15%. Values of ϵ/k in the approximate range 160 to 180 K were considered and the corresponding values of σ were established by means of a least-squares fitting of the data. The tabulated values (Table 1) minimized the root-mean-square (rms) deviations for the data, although there are alternative pairs of ϵ and σ whose fit is only slightly inferior. Compari-

sons with other low-density viscosity data and correlations are given in the following section.

The form of Eq. (15) for the excess viscosity and the exponents of δ and τ, r_i and s_i, were optimized from a limited set of proposed terms by a study of a variety of pure fluids in addition to methane. The dimensionless coefficients g_i for methane were established by using a least-squares algorithm with four sets of input experimental data[9,64–66] after considering several other data sets as listed in the following section on comparisons between the correlations and experimental measurements. The data of Giddings *et al.*[64] were obtained with an absolute capillary-tube viscometer and consist of 100 tabulated points which had been adjusted to nominal pressures. These data, in the range 283–410 K and 0.1–55 MPa, were most heavily weighted. The oscillating quartz-crystal viscometer at NIST was used by Haynes[65] to measure methane viscosity along the saturated liquid boundary and was used by Diller[9] in the range 100–300 K and to 33 MPa. In the former case, the data were adjusted to conform to the saturation densities calculated from Eq. (4) at the experimental temperatures. These densities and the adjusted data were input into the excess viscosity fitting program with moderate weight. The data of Ref. 9 were weighted only in the region $\rho > 18$ mol dm^{-3}. Finally, the paper by Carmichael *et al.*[66] contains experimental data from 278 to 478 K and to 36 MPa which were obtained with a rotating cylinder viscometer. In all cases, a value of the zero density viscosity obtained from Eq. (10) was subtracted from the experimental data to establish the "experimental" excess viscosity. With the exception noted above, the experimental pressure and temperature were used to calculate the density from the present equation of state for input into the least-squares algorithm. Explicit comparisons between the total viscosity correlation and both the primary and other data are given in Sec. 4.

3.4.2. Thermal Conductivity

Only the coefficients in Eq. (14) must be established in order to complete the correlation for the zero density thermal conductivity. Data from the transient hot-wire measurements of Roder[8] and the concentric cylinder experiments of Le Neindre *et al.*[67] were used for this purpose. The tabulated extrapolations to zero density in Ref. 8, consisting of 13 points in the range 133–310 K, were used directly. For the higher temperature regime, 368–621 K, the lowest density point for each of 8 measured isotherms in Ref. 67 was adjusted to zero density by using a preliminary version of the excess thermal conductivity correlation. In all cases, the experimental density was <0.05 mol dm^{-3}, and the adjustment amounted to no more than 0.2% of the measured value of the conductivity. Equation (13) was solved for f_{int} using the above correlations for η_0 and C_p^{id} and the experimental values of λ_0 from Refs. 8 and 67. A least-squares algorithm was then used to calculate the two coefficients of Eq. (14) with equal weight assigned to each datum and with the tabulated value of ϵ/k used. The resulting values are reported in Table 8; comparisons with experimental data are given in the following section.

Because it is difficult to unambiguously separate the excess thermal conductivity [Eq. (17)] from the critical enhancement [Eq. (18)], the method of determining the relevant coefficients is more complicated than the analogous determination of coefficients relevant to the excess viscosity as discussed above. The form of Eq. (17), including the values of the exponents, was determined, as in the case of η_{ex}, by examining several prospects and several fluids. The correlation for the critical enhancement was determined as follows. A preliminary determination of the seven coefficients in Eq. (17) for the excess conductivity was made with limited data well outside the critical region using a least-squares method. These data consisted of the measurements of Roder[8] and the lower two isotherms of Mardolcar and de Castro,[68] all restricted to a temperature-dependent density range of approximately $2 > \rho > 15$ mol dm^{-3}. This range was determined by noting the regions of Fig. 1 of Ref. 8 which do not display any critical enhancement and resulted in about 550 points being used in the preliminary correlation. This preliminary correlation was used to produce an experimental critical enhancement by subtracting from the data both the zero density and excess values calculated from the correlations. Only the 6 supercritical isotherms, including some 500 points in the range 197 K $\leqslant T \leqslant$ 295 K, from Roder[8] were used in the determination of the enhancement correlation.

The expression for the critical enhancement in Eq. (18) is completely determined from thermodynamic properties, viscosity, and universal critical behavior except for the form and coefficients in the damping function, Eq. (20), and the value of the parameter Λ^*. The type of damping function that we have chosen is similar to that introduced by Hanley *et al.*[69] and discussed by Sengers *et al.*[11]; however we have added a term in density, which is not symmetrical about the critical point, into the exponential and removed a similar term as a multiplicative factor in F. The powers of the symmetric temperature and density deviations within the exponential differ from the choices in Refs. 11 and 69. These powers and the asymmetry were empirically observed to provide the best description of the methane experimental critical enhancement data discussed above. They were chosen from a set of trial values by examining this critical data from both isochoric and isothermal viewpoints.

The four coefficients, Λ^*, F_T,F_ρ, and F_A, were determined from a least-squares algorithm after linearizing the problem by taking the logarithm of the experimental enhancement multiplied by the appropriate viscosity and divided by the thermodynamic derivatives indicated in Eqs. (18) and (19), all determined from the previously presented correlations. The weighting scheme in this procedure generally emphasized those data closest to the critical point, except for those points on the 197 K isotherm which seem to display anomalous dispersion. The final values of the coefficients presented in Table 10 were determined iteratively, by repeatedly determining the excess thermal conductivity correlation using a version of the enhancement correlation and then calculating new critical enhancement data which were fit to Eq. (18). The additional fluid-dependent quantities for the scaled equation of state, used very close to the critical point, that is in the range $|T^*| < 0.03$ and $|\rho^*| < 0.25$, in Eqs. (23)–(26), were not considered in the present study. Rath-

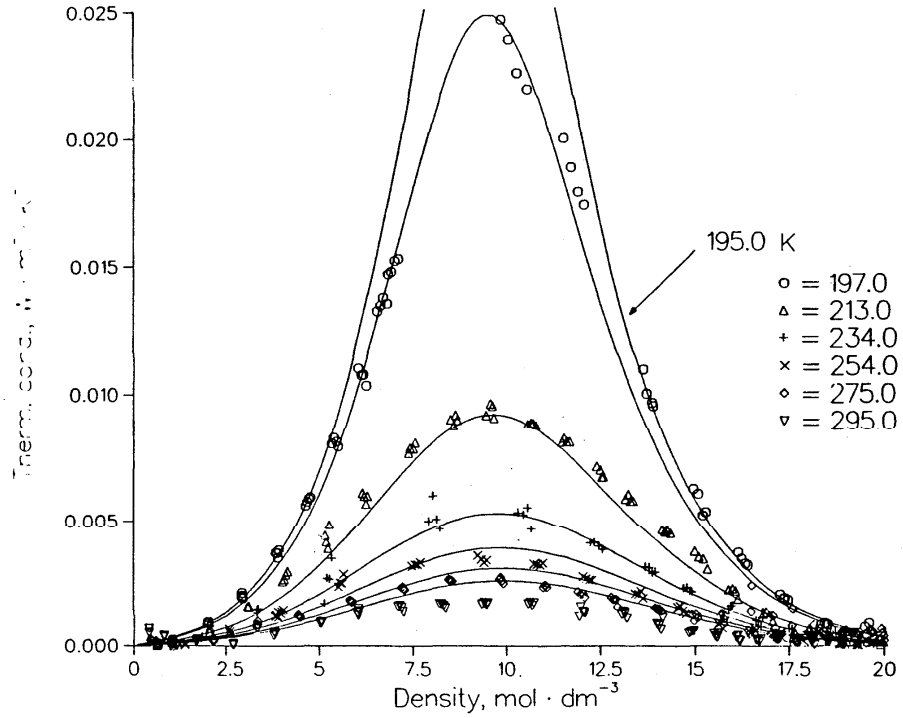

FIG. 5. Critical enhancement of the thermal conductivity. The data shown are from Roder (Ref. 8) (after subtracting contributions from the background and adjusting to lie along isotherms). The curves are from the present enhancement correlation at the same temperatures. A curve at 195 K is included; note that the use of the scaled equation leads to no discontinuities (on this scale) in this curve.

er, since Roder[8] does not include data in this "asymptotically" critical region, we have simply tabulated in Table 10 the results of Sengers *et al.*[11] for methane. In Fig.5, we illustrate the experimental critical enhancement for the primary supercritical data from Ref. 8. For the purposes of this figure, we adjusted the data, according to the final thermal conductivity correlation, so that they are along true isotherms and we plotted the correlation for the critical enhancement along these isotherms.

We complete our discussion of the thermal conductivity correlations by considering the excess contribution, Eq. (17). To obtain data for the excess thermal conductivity correlation, values of λ_0 and λ_{cr} obtained from the correlations were subtracted from the experimental measurements of Roder[8] and of Mardolcar and de Castro.[68] These data spanned the region from 110 to 310 K and 0.2 to 70 MPa and consisted of about 930 points. Equation (17) is linear in the seven j coefficients so these were determined with a least-squares approach with heaviest emphasis at the lower densities for each isotherm. Several points in the critical region in Ref. 8 were not included in the fit because they indicated large experimental uncertainty by their increased dispersion. As indicated above, the fitting routine was processed several times and converged toward a consistent set of critical enhancement and excess thermal conductivity coefficients. The final values of these coefficients are given in Table 10. Comparisons of the entire thermal conductivity correlation with both primary and other data are considered in the following section.

4. Comparisons of Derived and Experimental Properties

In this section we compare the correlations discussed above with experimental data. These data consist of both primary data, which were explicitly used to develop the correlations, and other data, which were not used for any of several reasons including lack of adequate discussion of experimental details, unusually poor precision or accuracy, disagreement with better known results, or simply overly abundant data for a particular property within some region of the phase diagram. To avoid exceptionally long discussion, overly complicated figures, and too many figures, the comparisons given below are representative rather than exhaustive; more complete tabular comparisons are provided in Ref. 1. References to other, especially earlier, sources of experimental data can be found within the papers cited in our reference list.

In all the deviation plots, the zero-line represents the appropriate correlation using the equations of Sec. 2 and the associated tables. The percentage deviations are computed as 100(cor-exp)/exp where "exp" represents the experimental value of a property and "cor" is the value computed from the correlation and the experimental value(s) of the independent variable(s). The precision of a quantity measures its reproducibility; for the correlations of this paper the precision concerns the round-off error and is not of primary interest. The accuracy is a measure of the deviation of a quantity from its true value; the estimates of the accuracies

of our correlations represent our best assesment of the maximum difference between a quantity computed from the correlation given the independent variable(s) and the true physical quantity at the same value(s) of the independent variable(s). The accuracies of the correlations depend on the quantity to be calculated and the range of the independent variable(s) as discussed below. When an uncertainty band is quoted, we believe that the true value lies within the band. Our error estimates represent the maximum deviation between a predicted value and the true value; these estimates are equivalent to the accuracy assesments. Additional statistical quantities concerning the comparison of the correlations with experimental data are given below and in the tables.

4.1. Two-Phase Boundary

In Fig.6, we show the deviation of experimental orthobaric pressure data from the correlation of Eq. (3). The agreement between this correlation and the primary data of Kleinrahm and Wagner[3] is quite good, with an average absolute percent deviation (AAD-%) of 0.011%. As illustrated in Fig.6, either Eq. (3) or the Maxwell construction, using the present SWEOS, reproduces the saturation pressure data of Ref. 3 within the quoted accuracy of the data which ranges from 0.26% near the triple point to 0.012% above 180 K. Statistics concerning a comparison of the Maxwell construction and the ancillary equation are given in Table 13. In addition to the AAD-%, the BIAS (average deviation) and rms deviation are given. All statistics in Table 13 are presented on both a percentage and dimensional basis. As mentioned above, the measurements of Prydz and Goodwin[60] and the associated correlation of Goodwin,[17] also shown in Fig. 6, disagree substantially from the results of Ref. 3. This disagreement is attributed to the presence of impurities in the methane sample used in the earlier work and is illustrated in Fig .6. Additional sources of data are discussed in Angus *et al.*[2] and in Kleinrahm and Wagner.[3] Upon considering the uncertainties of both the triple-point and critical point pressures (Table 1), the quality of the measurements of Ref. 3, and the disconcerting disagreement between the earlier benchmark data, we make the subjective judgment that either the ancillary Eq. (3) or the SWEOS will provide values of the saturation pressures accurate within 0.06% above $T = 120$ K and accurate within 0.3% below this temperature.

For the density of the saturated liquid, Fig. 7 illustrates the deviations between the correlation of Eq. (4) and experimental data from Refs. 3,62,70, and 71. For the primary data of Kleinrahm and Wagner[3] the AAD-% is 0.025% with a maximum deviation of 0.135% near the critical point, and for the 76 points in Fig. 7 the AAD-% deteriorates to 0.05%. Again, either the ancillary equation or the value of the density from the SWEOS can be used with an estimated accuracy well within 0.2% throughout the range from the triple point to just below the critical point.

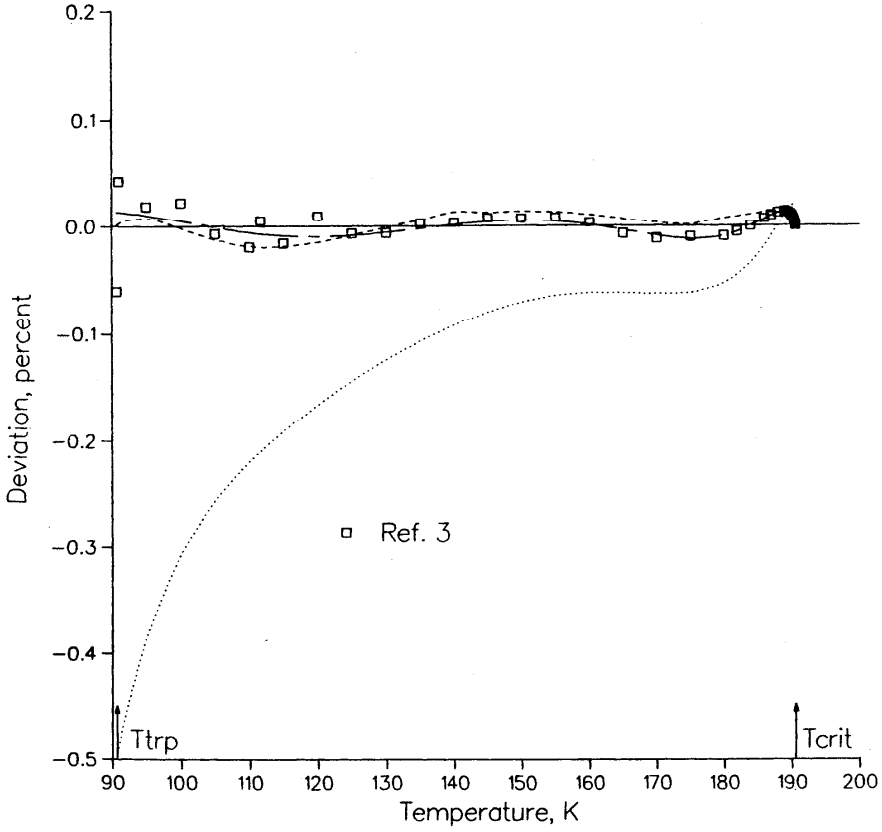

FIG. 6. Saturation pressures compared to Eq.(3). Dotted line is the Goodwin correlation (Ref. 17); dashed line is the from the Maxwell construction using the SWEOS; broken line is the correlation of Kleinrahm and Wagner (Ref. 3); open squares are the data from Ref. 3.

TABLE 13

STATISTICS FOR THERMODYNAMIC PROPERTY DATA VERSUS SWEOS CORRELATION

TYPE	NO.PTS.	SOURCE	AAD-% (percent)	BIAS-% (percent)	RMS-% (percent)	AAD	BIAS	RMS	
P_σ	20	Eq.(3)[a]	0.010	-0.002	0.011	0.096	-0.086	0.132	kPa
$\rho_{\sigma L}$	20	Eq.(4)[a]	0.026	0.023	0.031	0.006	0.005	0.006	$mol \cdot dm^{-3}$
$\rho_{\sigma v}$	20	Eq.(5)[a]	0.041	0.030	0.043	0.35	-0.06	0.71	$mol \cdot m^{-3}$
B	57	[37-41]	0.667	0.188	1.086	0.001	-0.001	0.002	$dm^3 \cdot mol^{-1}$
PVT[b]	2574[d]	Table 12	0.232	-0.088	0.683	0.026	-0.011	0.073	$mol \cdot dm^{-3}$
PVT[c]	2574[d]	Table 12	0.871	0.690	3.856	0.116	0.053	0.381	MPa
C_v	337	[53,54]	0.462	0.165	0.571	0.142	0.047	0.176	$J \cdot mol^{-1} \cdot K^{-1}$
C_p	400	[55]	0.821	0.162	1.514	0.772	0.165	3.345	$J \cdot mol^{-1} \cdot K^{-1}$
$C_{\sigma L}$	69	[53,54]	0.626	0.444	0.716	0.496	0.354	0.791	$J \cdot mol^{-1} \cdot K^{-1}$
W	603	Table 14	0.516	0.006	1.108	2.980	-1.259	4.142	$m \cdot s^{-1}$

[a] These data were generated from the ancillary equations at equally spaced temperatures from 91 to 186 K.

[b] Statistics based on calculation of density from experimental temperature and pressure.

[c] Statistics based on calculation of pressure from experimental temperature and density.

[d] Only points with pressures less than 100 MPa are included in this comparison.

At temperatures very close to the critical point, the oscillations of the deviations shown in Fig. 7 (and Fig. 8) illustrate how difficult it is to produce the shape of the coexistence dome. The classical SWEOS cannot give the correct nonanalytical curvature. The ancillary equation, as indicated in Sec. 2, expresses the theoretically described behavior and, in the critical region, fits the primary experimental data[3] within its reported uncertainty.[3] The maximum deviation between Eq. (4) and the correlation in Kleinrahm and Wagner[3] is 0.18% (near 190.55 K) and the maximum deviation for the classical SWEOS is − 0.9%. The experimental uncertainties are also large in this region; Ref. 3 reports a 1.7% accuracy in $\rho_{\sigma L}$ at 190.53 K. Considering these factors, we estimate that between 190.5 K and T_c, the uncertainty in the saturated liquid density associated with these equations may exceed 1%. Equation (4), the SWEOS, and the correlation in Ref. 3 all give the same critical density at the same T_c, and this density is accurate to about 0.1%. Table 13 gives the statistics associated with the comparison between the SWEOS calculation and the ancillary equation for the 20 points used in the SWEOS fit. Other experimental data are discussed in Refs. 2, 3, 17, and 62.

Figure 8 shows the analogous deviation plot for the density of the saturated vapor; again the primary data is that of Kleinrahm and Wagner.[3] The AAD-% for these data is 0.055% and the maximum deviation is 0.140% near the critical temperature. Other data are discussed in Refs. 2, 3, and 17. The correlating equations from Angus *et al.*[2] and

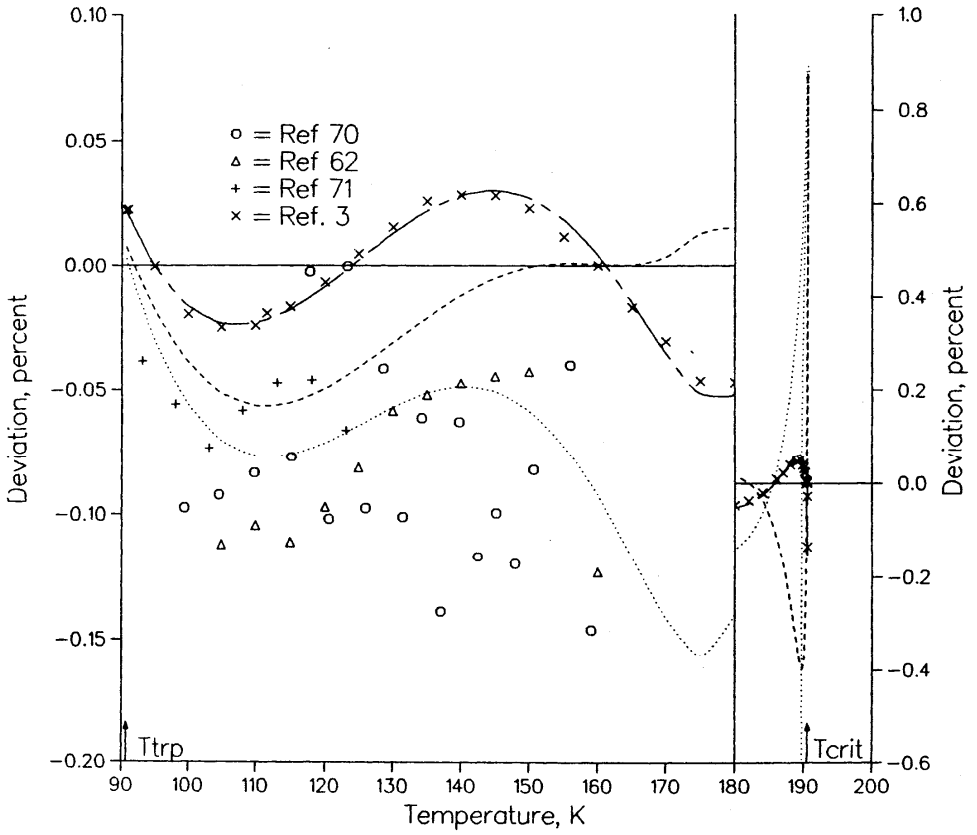

FIG. 7. Saturated liquid densities compared to Eq.(4). Curves are as in Fig. (6). Abbreviated references for experimental data are: 3, Kleinrahm (1986); 70, Orrit (1978); 62, Haynes (1977); and 71, McClune (1976). For temperatures above 180 K the right-hand scale is used.

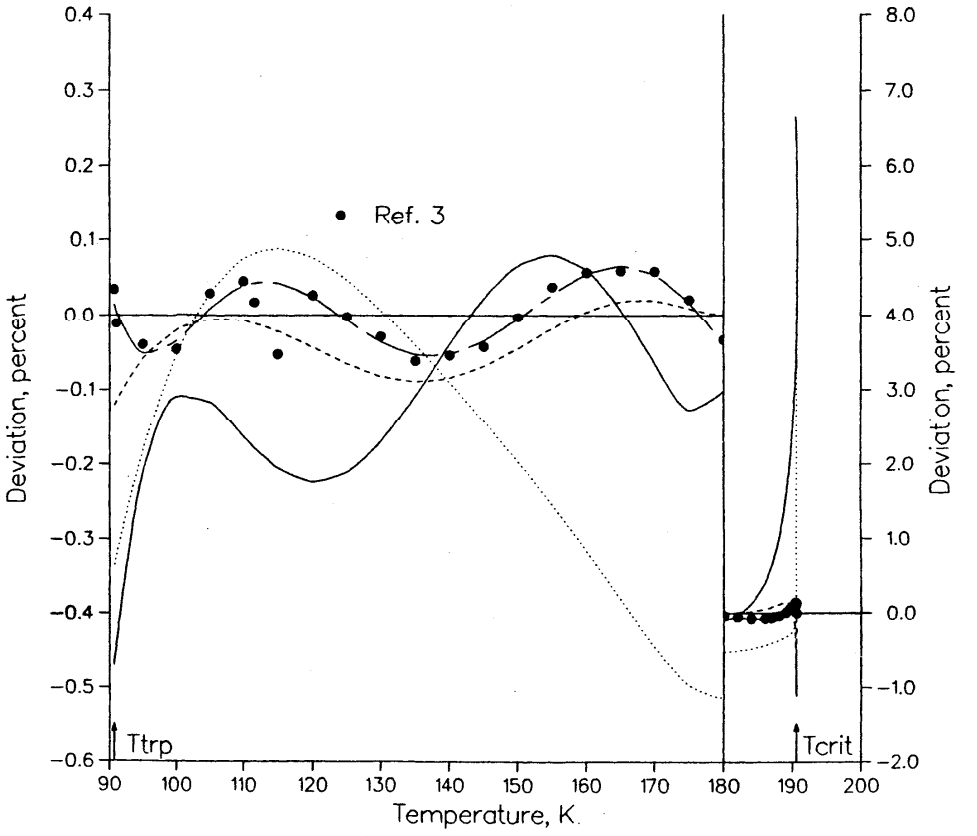

FIG. 8. Saturated vapor densities compared to Eq.(5). Curves and data are as in Fig. 6 with the additional solid curve from IUPAC (Ref. 2). For temperatures above 180 K the right-hand scale is used.

from Goodwin,[17] illustrated in Fig. 8, indicate the behavior as interpreted by those authors. The experimental accuracies in Ref. 3 are worst near both fixed points, that is 0.8% at the triple point and almost 2% near the critical point. Considering these data as well the data and conclusions of Refs. 2 and 17, we estimate that the error associated with either Eq. (5) or the SWEOS for the density of the saturated vapor does not exceed 1% from the triple-point temperature to 91 K, 2% above $T = 190.5$ K, and is well under 0.5% for the remainder of the two-phase boundary. The statistical comparison between Eq. (5) and the Maxwell construction using the SWEOS is given in Table 13.

4.2. Thermodynamic Properties from the SWEOS

In this section we discuss the comparisons between experimental measurements and the correlations for several of the thermodynamic properties calculable from the Helmholtz energy using the algebraic expressions in Table 7. In the first subsection, 4.2.1, we discuss the extensive *PVT* comparisons. In Sec. 4.2.2, comparisons for the second virial coefficient, heat capacities, and speed of sound are presented.

4.2.1. PVT Data

For the *PVT* data, there are two types of evaluations which can be informative. One can calculate the pressure using the SWEOS directly from the experimental temperature and density, or one can, with a root-finding technique, calculate the density using the experimental temperature and pressure. To implement the second type of comparison, we used a standard Newton–Raphson algorithm. A third possibility, using pressure and density as independent variables, is not often required and is not considered here. For each of 16 references, Table 12 summarizes the data and certain statistics regarding the fit to the present SWEOS correlation. The pressure AAD-% gives the average absolute percent deviation when pressure is calculated from the SWEOS. The last column in Table 12, the density AAD-%, gives the analogous statistic when the density is calculated. Some of the experimental measurements very near the saturation line were calculated, using the ancillary equations, Eqs. (3)–(5), as residing inside the two-phase envelope. These points, from Gammon and Douslin[44] and from Kleinrahm *et al.*,[52] were ignored both in developing the SWEOS and in the calculation of statistics.

In Table 13, we present several overall statistics for the 2574 data summarized in Table 12 which have pressures < 100 MPa. For the entire set of 2777 points, the major difference occurs in the absolute statistics when calculating pressure from the SWEOS. The very high pressure data are not fit particularly well by the SWEOS (see below) and these points contribute inordinately to the absolute statistics. For instance, the AAD for the 2777 points is nearly 1.5 MPa. In addition to the average absolute deviation, we present the average deviation (or BIAS), and the rms deviation. Each of these three statistics is given on both a percentage and dimensional basis. Of course, the quality of the fit and the quality of the data depend strongly on the region of the phase diagram being considered. For this reason deviation plots are useful and we have several comments on Figs. 9–12.

The steepness of the isotherms is of primary importance when calculating the system pressure from the temperature and density. In the compressed liquid at low temperatures the slope, $\partial P/\partial \rho|_T$, is extremely large, so that small (experimental) uncertainties in the density can lead to very large errors in the calculated pressure. For instance, at 122 K, the slope of about 14 MPa mol^{-1} dm^3 near the two-phase boundary means that an error of 0.1% in the density, typical of many experimental measurements, leads to an error of about 75% in the pressure. This explains the large percent deviations seen in Fig. 9(a) at the lowest pressures. The most severe problems of this sort are seen in the liquid data of Gammon and Douslin,[44] Goodwin,[45] and Van Itterbeek *et al.*[50] for temperatures below about 150 K and for pressures < 1 MPa. However, while these percentage deviations can exceed 60%, the error in computed pressure is still $\lesssim 0.1$ MPa for the data of Refs. 44 and 45. In addition to the problems very near the saturation curve, Fig. 9(a) also indicates that the measurements of Ref. 50 often disagree substantially and systematically with the bulk of the data (most of which are from the more recent publication of Goodwin[45]). The isotherm from Ref. 50 near 166 K exhibits deviations near 10% and those near 171 and 173 K indicate deviations near 5%, even at the highest pressures measured, about 30 MPa. These 3 isotherms are clearly discernable in Fig. 9(a). Finally, the important high pressure measurments of Cheng[43] show some systematic deviations from the correlation, and the 111 K isotherm stands out in the approximate range of 30–70 MPa.

Although we have not reconciled the experimental differences indicated in Fig. 9(a), we offer the following guidelines when calculating pressures from the SWEOS when given densities and temperatures between the triple point and 185 K. For the vapor phase, the errors should not exceed 0.2%. For the liquid below 150 K and below 1 MPa, the percentage uncertainty is extremely large, but the actual pressure should not be off by > 0.1 MPa. Most of the remaining points in Fig. 9(a) indicate that the error should be $< 5\%$. An exception occurs below 120 K or very close to the saturation line, where the uncertainty approaches 10%. Most of the primary *PVT* data (from Goodwin[45]) in this temperature region and below about 30 MPa and 28.5 mol dm^{-3} exhibit deviations from the correlation of well below 1%.

Calculation of an accurate density from a given temperature and pressure is a much easier task in the region below 185 K, as indicated in Fig. 9(b). This figure contains the same experimental data as Fig. 9(a), but the scale is quite different and indicates general uncertainty well below 1%. In the vapor phase, below the break in the data of Fig. 9(b), all points at temperatures below 180 K or pressures below 3.5 MPa show absolute deviations below 0.5%. The few vapor points closer to the critical point in both temperature and pressure show higher deviations because our critical behavior is based primarily on the data of Kleinrahm *et al.*[52] For the important liquid data of Goodwin,[45] the deviations are well under 0.1% for the majority of the points, but deteriorate to 0.2% for densities below 20 mol dm.$^{-3}$ For

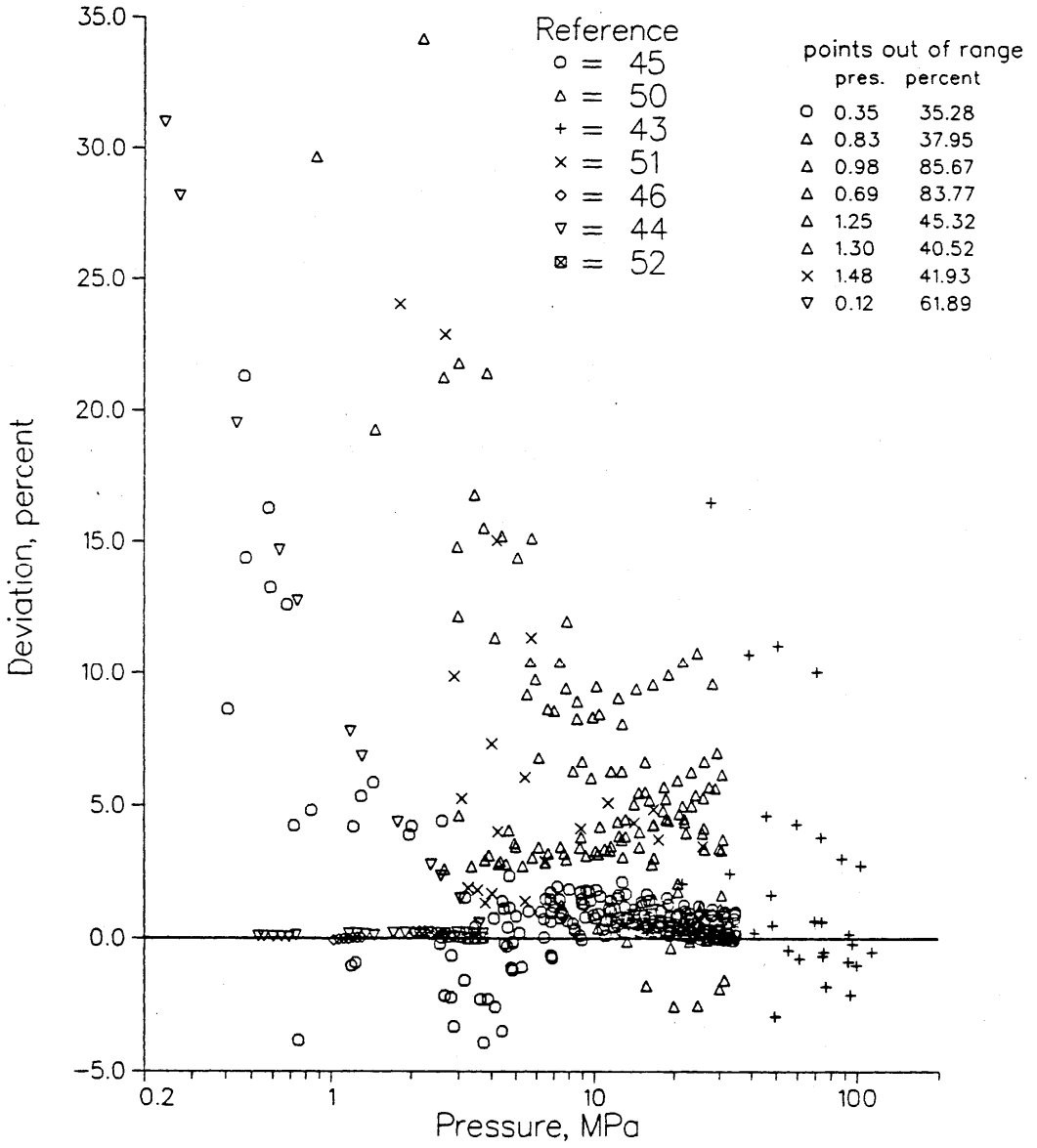

FIG. 9(a). Pressure deviations versus experimental pressure for temperatures at or below 185 K. Abbreviated references, with primary references denoted by asterisk, are: 45*, Goodwin (1974); 50, Van Itterbeek (1963); 43*, Cheng (1972); 51, Vennix (1966); 46* Goodwin (1974); 44, Gammon (1976); and 52*, Kleinrahm (1987). Some of the data from Ref.44 were derived from correlations.

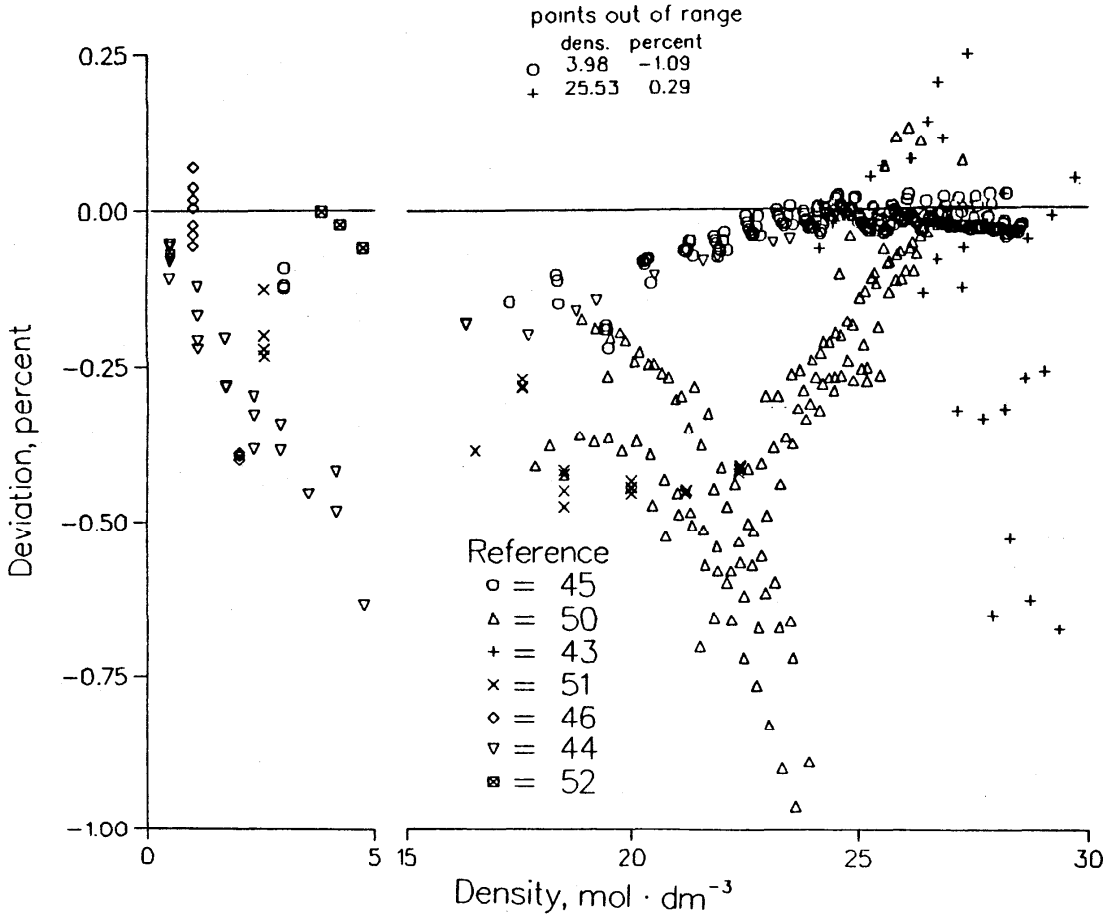

FIG. 9(b). Density deviations versus experimental densities for temperatures at or below 185 K. References are as in Fig. 9(a).

Cheng's[43] data, the 111 K isotherm again exhibits an absolute deviation $>0.5\%$, while the liquid data from Van Itterbeek *et al.*,[50] as in Fig. 9(a), show systematic differences from this correlation, especially above 150 K. In our judgment, the more recent data of Ref. 45 should be the most accurate. We estimate that for the liquid in this range, a 0.2% accuracy in the determination of the density from the SWEOS is expected.

Figures 10(a) and 10(b), covering the temperature range 185–195 K, illustrate the behavior of the SWEOS in the general region of the critical point. For the pressure deviations below about 8 MPa, Fig. 10(a) indicates that agreement among the data from different sources is good and deviations from the correlation are small. These low pressure deviations are typically $<0.1\%$, and the primary critical data of Kleinrahm *et al.*[52] are fit to better than 0.05%. There are a few exceptions, notably in the liquid state, where the deviations are worse. At higher pressures, the pressures calculated for Van Itterbeek *et al.*[50] are significantly greater (up to 4%) than the reported experimental values, and the difference between these data and the data of Goodwin[45] shows a similar discrepancy. Although the higher pressure data of Vennix[51] may seem to confirm those of Van Itterbeek *et al.*,[50] the data of Ref. 51 show considerable scatter relative to the correlation. Moreover, at more moderate pressures, the later data of Ref. 45 conform more closely to the recent accurate measurements of Kleinrahm *et al.*[52] Thus, at the higher pressures, we again prefer the data of Goodwin.[45] In summary, we suggest that in calculating the pressure using the SWEOS in this temperature range, accuracies of better than 0.1% are expected at up to 6 MPa. The accuracy is expected to deteriorate to about 2% at higher pressures.

Because the derivative $\partial P/\partial\rho|_T$ is 0 at the critical point, this point poses no special problems when calculating the pressure from the density and temperature. However, as indicated in Fig. 10(b), the calculation of the density in the near-critical region presents a significant challenge. The experimental difficulties at near-critical conditions, for example the importance of gravitationally induced density gradients, the long time necessary for equilibration of an experimental cell, and the difficulty of accurate temperature measurement, are also well known. For the data in Fig.

10(b) well outside the critical region, that is if $\rho < 3$ mol dm^{-3} or $\rho > 13$ mol dm^{-3}, the deviations are $< 0.5\%$; for the most part the deviations are smaller than 0.1% for the lower densities. The density measurements of Gammon and coworkers[44,49] are effectively relative measurements based on earlier work and different fixed points. The large deviations seen for these datat very nearly critical conditions are not surprising. Since the critical pressure which Vennix deduced in 1966 from his data[51] differs by $> 0.5\%$ from the value which we have accepted (Table 1), the large deviations seen for that data in Fig. 10(b) are also not unexpected. The data of Goodwin exhibit 1% deviations from our correlation near 5 mol dm^{-3} and near the critcal pressure. While this seems anomalous, these data also showed relatively large deviations from the correlation of Ref. 45. The primary critical region data, from Kleinrahm *et al.*,[52] are fit quite well by the present SWEOS. In general the deviations are much better than 0.4%, although in the region 190.450 K $< T <$ 190.555 K (reduced temperature $-0.000\,021 < T^* < 0.000\,53$), deviations of near 1% and up to an extreme of 4.3% occur when 4.58 MPa $< P <$ 4.61 MPa. An additional point in Table 2 of Ref. 52 exhibits a 7.5% deviation from the present correlation, but appears to be a misprint. Our study suggests that in this temperature range the SWEOS should return a density well within 0.5% accuracy. The exception is quite close to the critical point, 190.4 K $< T <$ 190.6 K and 4.4 MPa $< P <$ 4.8 MPa, where errors of nearly 5% are possible.

Figures 11(a) and 11(b) represent the temperature range 195 to 300 K and display the largest quantity of *PVT* data with a very large range in pressures. The illustration of the pressure deviations, Fig. 11(a), shows both the sparsity of data and the systematic trends in the SWEOS in the very high pressure region above about 100 MPa. We have several observations concerning this figure. Below about 10 MPa the general agreement among data sets and with the SWEOS is good, as most deviations are well under 0.5%. There is some uncertainty in the lower isotherms, up to 205 K. However, even here 1% deviations are rare. Above 10 MPa both the agreement among the data and the quality of the SWEOS are much worse. The data of Trappeniers *et al.*,[4] Morris,[7] Cheng,[43] Kvalnes and Gaddy,[47] and Vennix[51] show strong

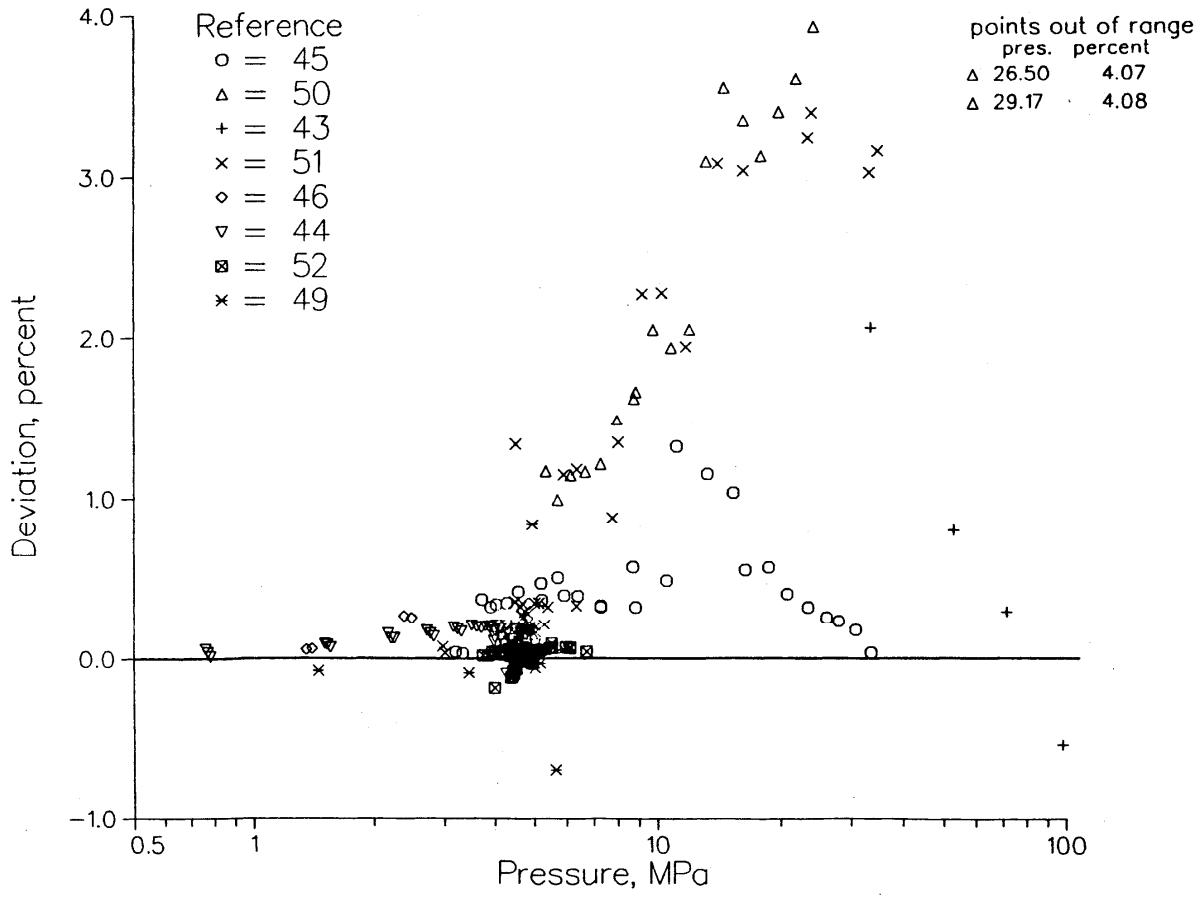

FIG. 10(a). Pressure deviations versus experimental pressures for temperatures between 185 and 195 K. Abbreviated references, with primary references denoted by asterisk, are: 45*, Goodwin (1974); 50, Van Itterbeek (1963); 43*, Cheng (1972); 51*, Vennix (1966); 46*, Goodwin (1974); 44, Gammon (1976); 52*, Kleinrahm (1987); and 49, Sivaraman (1986).

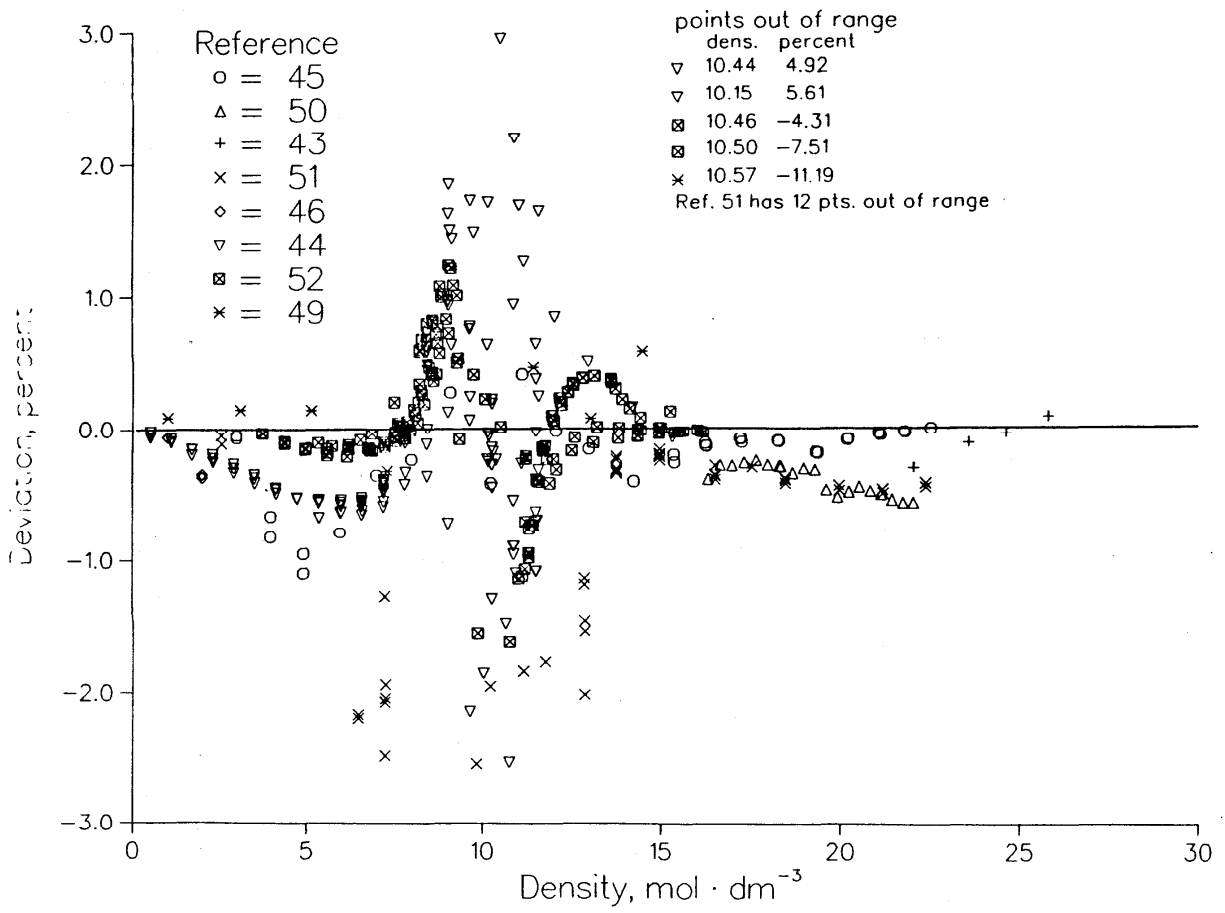

FIG. 10(b). Density deviations versus experimental densities for temperatures between 185 and 195 K. References are as in Fig. 10(a).

systematic departures from the equation of state, up to 4% at the lowest temperatures or highest pressures. They also show discrepancies of more than 4% for nearly identical state points measured at different laboratories. The largest deviations seen in Fig. 11(a) occur, as in Fig. 9(a), when the slope $\partial P/\partial \rho|_T$ is relatively large. Our conclusions concerning pressure predictions from the present SWEOS in this temperature region follow directly from these observations. Below 10 MPa an accuracy of 0.5% is expected, while above these pressures 5% errors are possible. A plot of the pressure prediction with density on the abcissa shows that 15 mol dm^{-3} is an approximate limit below which small errors are anticipated and above which the 5% range is possible.

In the temperature region 195–300 K, Fig. 11(b) again shows both systematic trends in the SWEOS and inconsistency among the data in the prediction of densities from given pressures and temperatures. In general the deviations are small, typically below 0.1%. At the higher densities, above 20 mol dm^{-3}, the deviations increase to about 0.4%. Additionally, a few points from Kvalnes and Gaddy,[47] Sivaraman and Gammon,[49] and Vennix[51] show extreme deviations. These are typically at the lowest temperatures of this range, up to 210 K, and in the density range of about 6–14 mol dm^{-3}. There seem to be problems associated with the proximity to the methane critical point. In our judgment, 0.2% is the general accuracy associated with the SWEOS for most of this region, except for a deterioration to 0.5% above 20 mol dm^{-3} and below 210 K.

For temperatures above 300 K, Figs. 12(a) and 12(b) show deficiencies in the SWEOS at very high pressures or densities. The pressure deviations of Fig. 12(a) are quite small, typically $<0.1\%$, for pressures <40 MPa (or densities <20 mol dm^{-3}). Even in this pressure range, there are a few outliers and larger deviations especially above 400 K. The extreme and systematic problems are seen at pressures above 100 MPa. They are most severe at the highest isotherm in this pressure domain (423 K) and at the highest pressure (1000 MPa) or at densities above 32 mol dm^{-3}. The steepness of isotherms, as measured by $\partial P/\partial \rho|_T$, which approaches 150 MPa $mol^{-1}dm^3$, again causes difficulties in the calculation of pressures. Figure 12(b) shows that this is not the only problem. The experimental data in this region are from Morris[7] and from Robertson and Babb.[48] Both sets have been obtained by relative methods and have been

smoothed by the authors of those papers. Nonetheless, it is apparent that the present correlation does not represent the data well and will give large errors in this region. The correlation of Morris[7] or that of Angus *et al.*[2] conforms much more closely to these very high pressure data than does the current correlation. These high pressure data would give a significant contribution to the overall statistics for pressure predictions so that all points with pressures exceeding 100 MPa are excluded from the statistics of Table 13. We summarize our observations of the data and the SWEOS for predicting pressures at temperatures above 300 K as follows. For pressures below 40 MPa and temperatures to 600 K, the expected accuracy is 0.2%. In the pressure range 40–200 MPa the accuracy is near 1%, and for higher pressures a 20% accuracy must be anticipated. In the highest pressure range, above 800 MPa, it is also prudent to restrict the temperature to 450 K because there are no data at significantly higher temperatures.

For the calculation of densities at the higher temperatures, Fig. 12(b) indicates reasonable deviations below about 20 mol dm^{-3} and systematic problems above this density. For the low-density region deviations $<0.1\%$ are typical, with the exception of certain points from Trappeniers *et al.*,[4] Mollerup,[5] Kvalnes and Gaddy,[47] and Sivaraman and Gammon.[49] Other than a single extreme point, these points are still within about 0.3% of the correlation and are mostly above 360 K. In the high density range, the problems discussed above for the pressure predictions are reflected in Fig. 12(b) as well. The data of Morris[7] and Robertson and Babb[48] are consistent but differ from the SWEOS. Again the worst high-density deviations, approaching 4%, occur along the highest measured isotherm, 473 K. In our subjective judgment, for temperatures below 350 K and densities below 15 mol dm^{-3}, an accuracy of 0.2% should be associated with the SWEOS. For temperatures up to 600 K or densities to 20 mol dm^{-3}, the error increases to 0.5%. The error in-

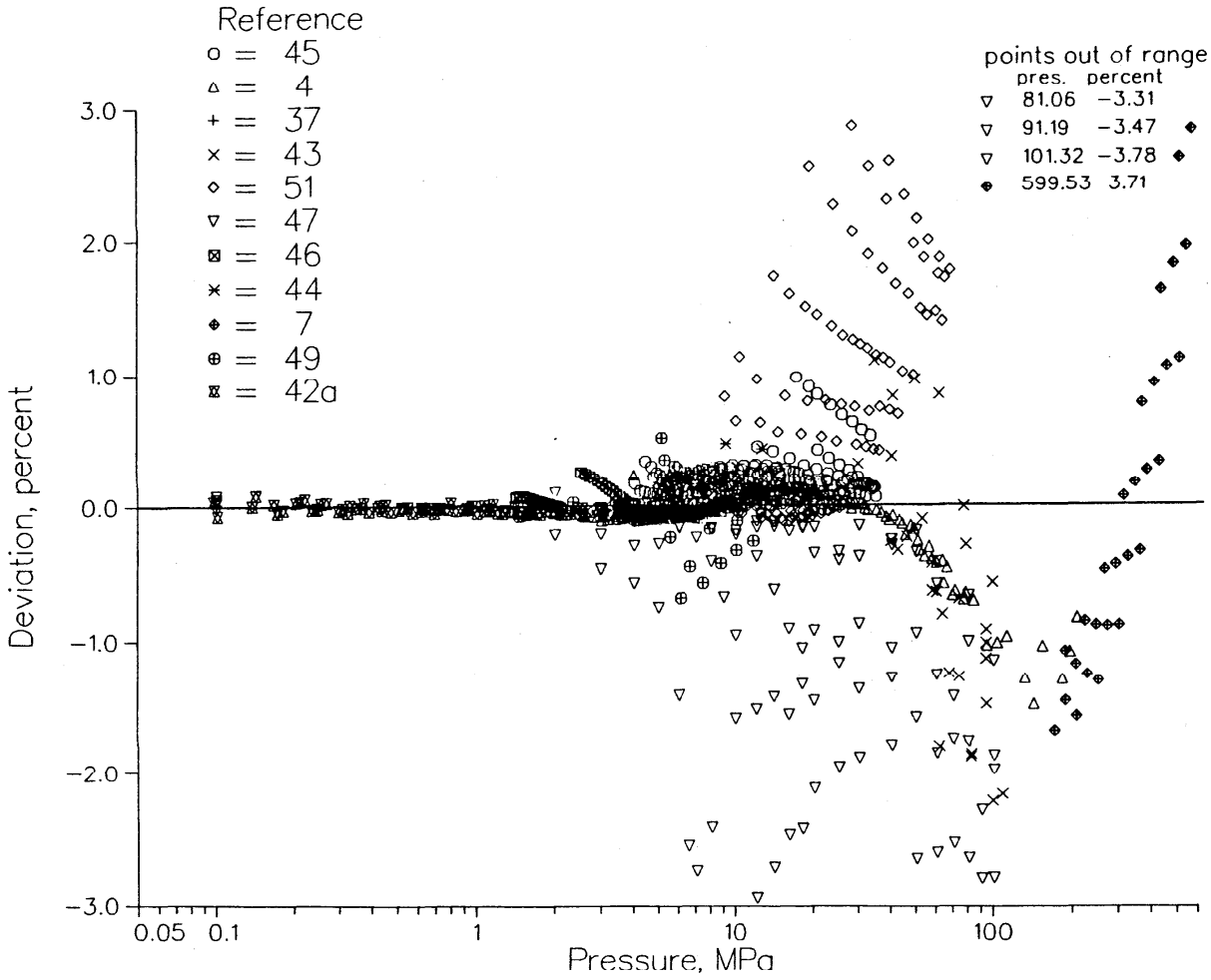

FIG. 11(a). Pressure deviations versus experimental pressures for temperatures between 195 and 300 K. Abbreviated references, with primary references denoted by asterisk, are: 45*, Goodwin (1974); 4*, Trappeniers (1979); 37 Douslin (1964); 43*, Cheng (1972); 51*, Vennix (1966); 47, Kvalnes (1931); 46*, Goodwin (1974); 44, Gammon (1976); 7, Morris (1984); 49, Sivaraman (1986); and 42(a), Achtermann. Some of the data from Ref.49 were derived from correlations.

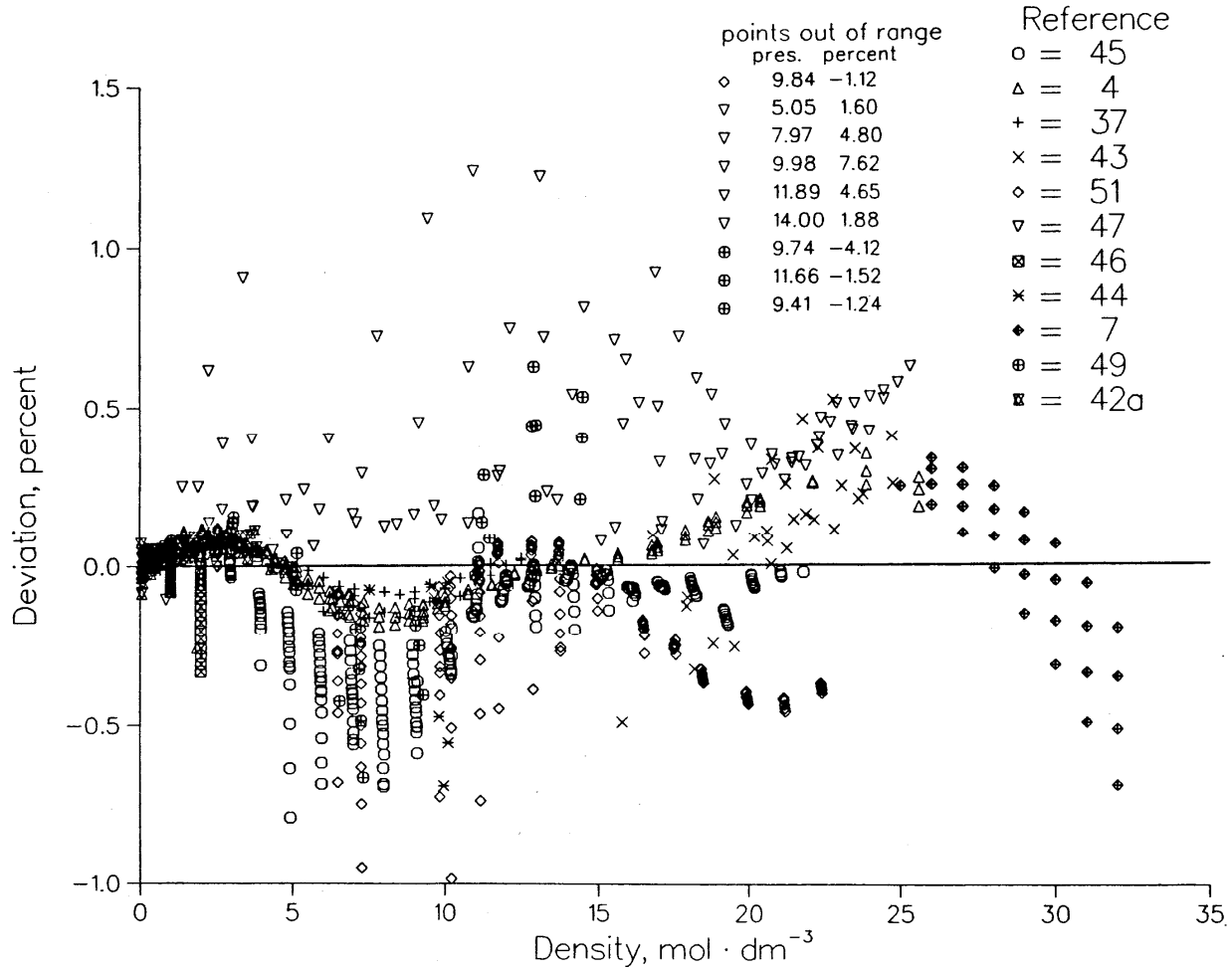

FIG. 11(b). Density deviations versus experimental densities for temperatures between 195 and 300 K. References are as in Fig. 11(a).

creases to 1% up to 25 mol dm^{-3} and 5% at higher densities. Extrapolation of the SWEOS to state points above 450 K for the density range above 20 mol dm^{-3} is not advised.

4.2.2. Other Thermodynamic Data

The deviation plot for the second virial coefficient is shown in Fig. 13 for the data of Douslin *et al.*,[37] Hoover *et al.*,[38] Byrne *et al.*,[39] Pope[40] and the correlation of Levelt Sengers *et al.*[41] Among the 57 points considered, 3 points are out of range: the lowest two temperatures from Ref. 40 and the lowest temperature from Ref. 38. Including all the data, the AAD-% for the second virial coefficient is 0.667%, corresponding to an absolute average deviation (AAD) of about 0.001 dm^3 mol^{-1}. A complete set of statistics is given in Table 13. Throughout the range, from the triple point to 625 K, the estimated accuracy in the correlation for the second virial coefficient is about 1%.

For the isochoric heat capacity data of Younglove[53] and Roder,[54] the 337 points have an AAD-% of $<0.5\%$; additional statistics are given in Table 13. These statistics concern the comparison between the experimental heat capacities and those calculated from the SWEOS at the experimental (corrected) densities and temperatures. Since the densities were established from sparse pressure measurements and an earlier methane equation of state,[54] these data, as used to construct the present SWEOS, are not on an equal footing with primary PVT measurements. However, the problem is not severe as indicated by the AAD of <0.02 mol dm^{-3} between the experimental densities and those calculated from the SWEOS using the tabulated (corrected) experimental pressures; additionally, the AAD-% is 0.02% between the heat capacities calculated from experimental pressures and those calculated from the experimental densities.

Figure 14 shows the deviations for the computed isochoric heat capacities from the experimental values. The independent variables in the computation of the heat capacities were, again, the experimental temperature and corrected experimental density; the reported pressures were not used. The measurements were made along approximate isochores and these are indicated in the figure. Most of the larger de-

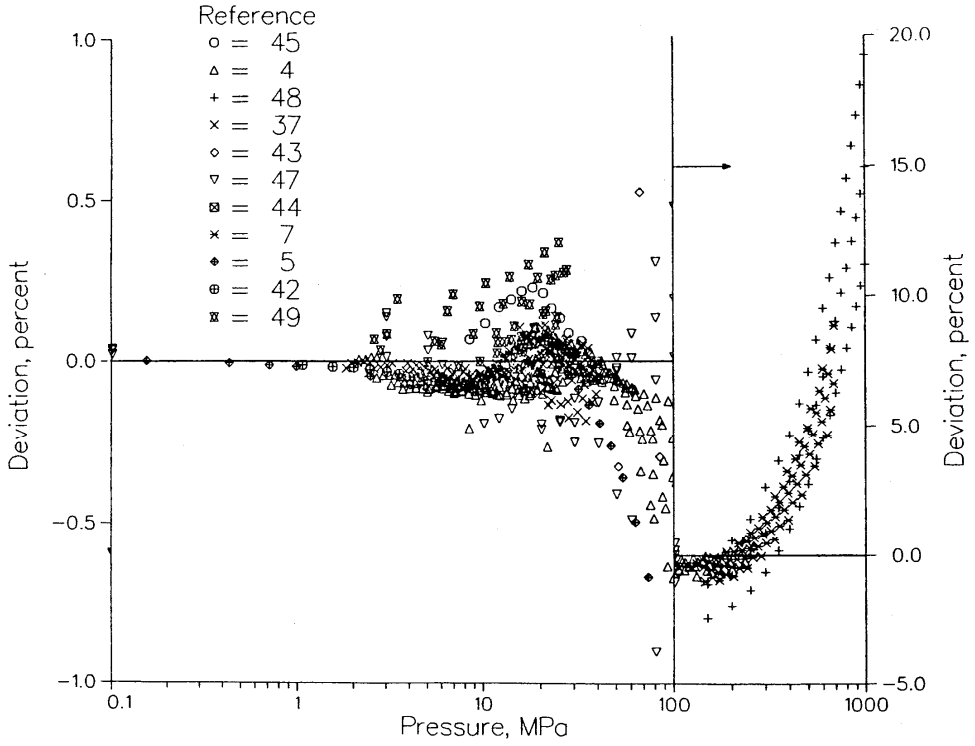

FIG. 12(a). Pressure deviations versus experimental pressures for temperatures above 300 K. For pressures greater than 100 MPa use the right-hand scale. Abbreviated references, with primary references denoted by asterisk, are: 45*, Goodwin (1974); 4*, Trappeniers (1979); 48, Robertson (1969); 37, Douslin (1964); 43*, Cheng (1972); 47, Kvalnes (1931); 44, Gammon (1976); 7, Morris (1984); 5, Mollerup (1985); 42, Achtermann (1986); and 49, Sivaraman (1986).

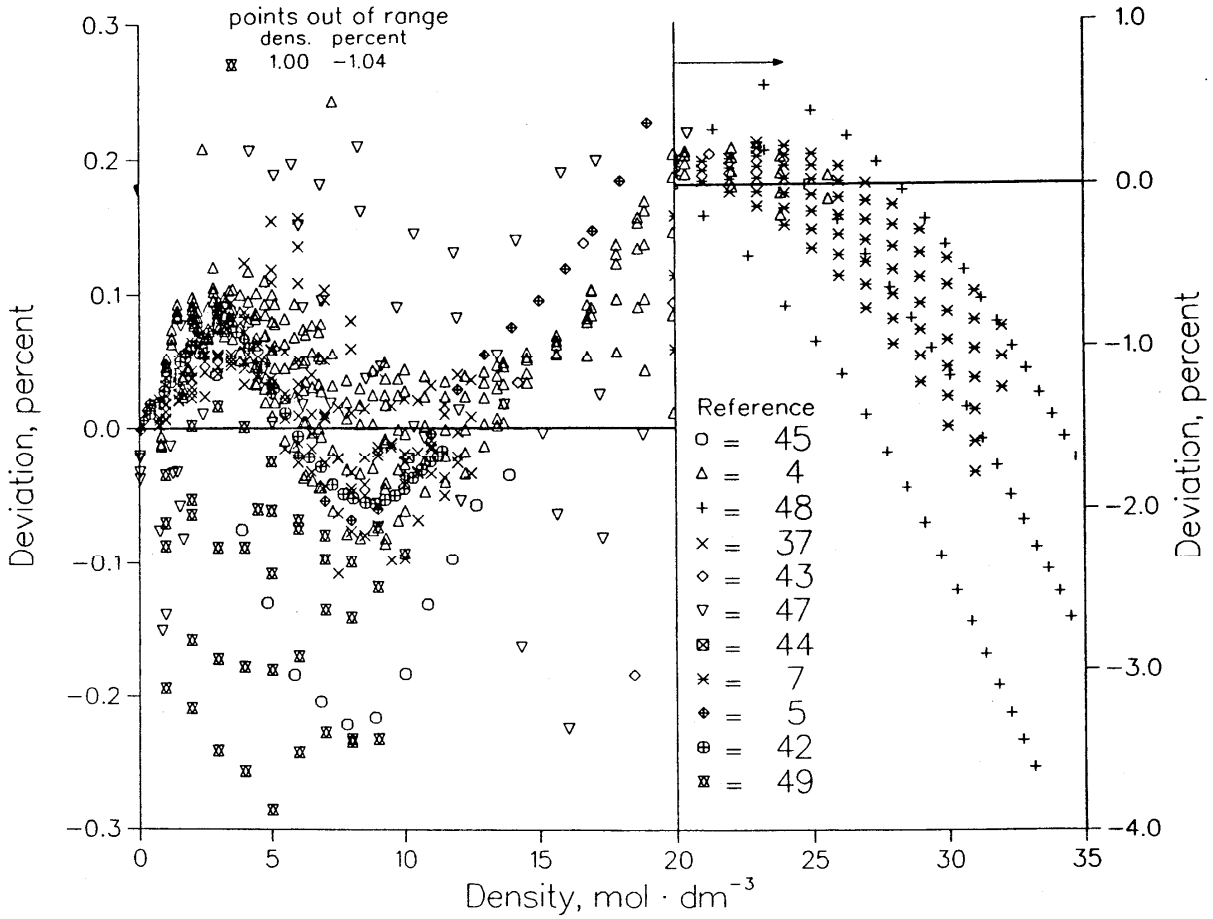

FIG. 12(b). Density deviations versus experimental densities for temperatures above 300 K. For densities greater than 20 mol dm^{-3} use the right-hand scale. References are as in Fig. 12(a).

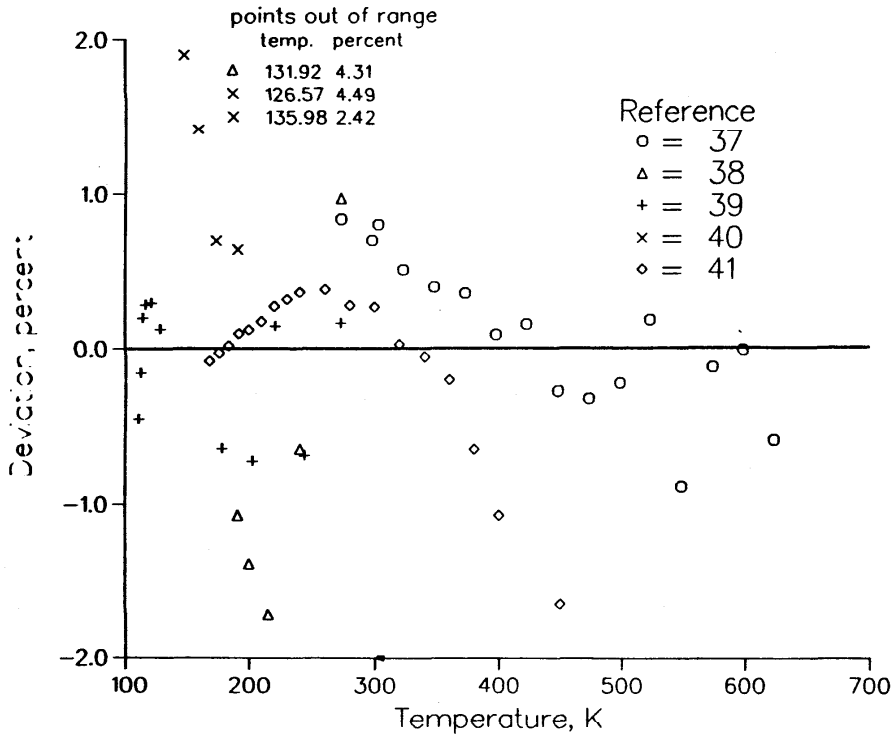

FIG. 13. Second virial coefficient deviations versus temperature. Abbreviated references are: 37, Douslin (1964); 38, Hoover (1968); 39, Byrne (1968); 40, Pope (1971); and 41, Levelt-Sengers (1972).

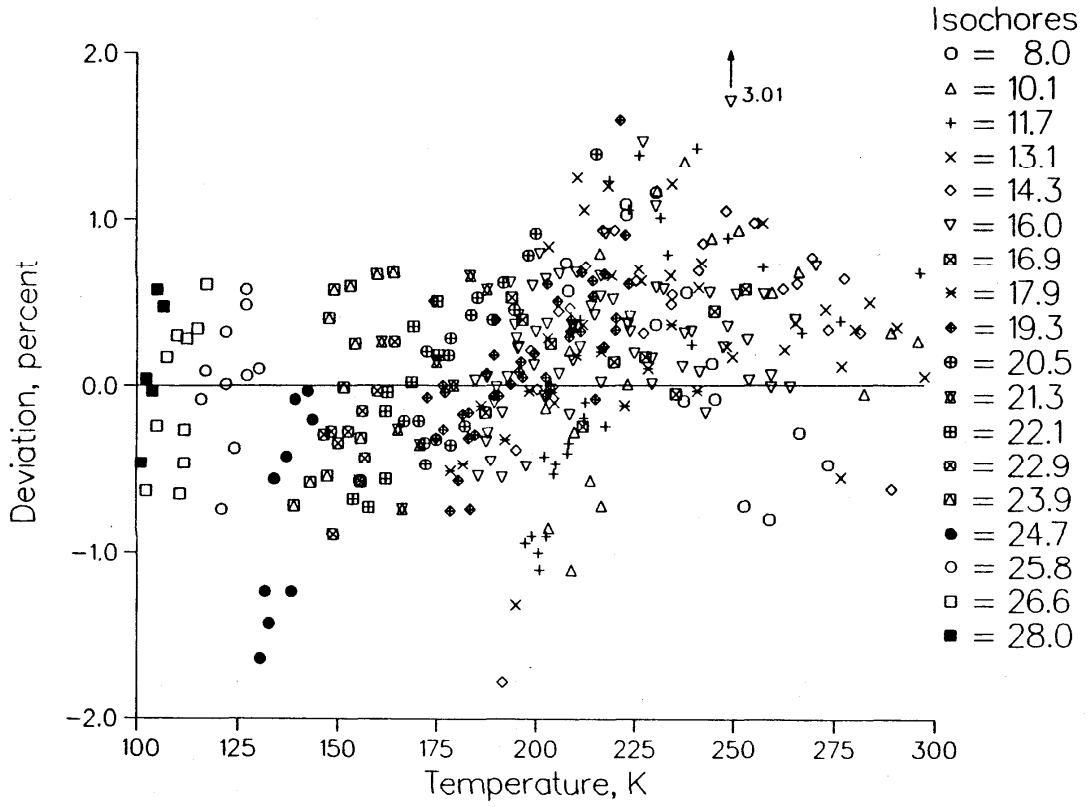

FIG. 14. Isochoric heat capacity (C_v) deviations versus temperature. Combined data of Younglove (Ref. 53) and Roder (Ref. 54). Isochores are in mol dm^{-3}.

viations occur for isochores below about 14 mol dm^{-3}, especially near the critical temperature, and for some of the low temperature liquid isochores. While both the statistics and the appearance of Fig. 14 indicate exceptional agreement with these data, it must be noted that these data were used to establish the SWEOS and the experimental uncertainty approaches 2%[54] even outside the critical region. In our judgment, then, a 2% accuracy should be expected when calculating C_V from the SWEOS outside the critical region, and the accuracy approaches 5% for temperatures between 180 and 200 K for densities up to 14 mol dm^{-3}. The asymptotically critical behavior of C_V is not well described by this (or any) classical equation of state.

The 1963 paper by Jones *et al.*[55] provides the major source of isobaric heat capacity data for methane used in the construction of the SWEOS. The data are compared to the SWEOS in Fig. 15, and Table 13 summarizes the statistics of the comparison. The deviations are generally better than 1% although several data with much larger deviations (to 16%) contribute substantially to the statistics. Among the regions of the phase diagram which show larger than usual deviations are the lowest temperature isotherm (116 K), the lowest pressure isobar (1 MPa) for most temperatures below the critical value, and the highest pressure isobars (about 10 and 14 MPa) at intermediate temperatures. However, the most prominent deviations are in the general region of the critical point (170 to 222 K and 3 MPa to 6 MPa), where the heat capacity is most sensitive to temperature. These deviations cast some doubt about the shape of the SWEOS Helmholtz energy surface in the vicinity of the critical point (since C_P probes the three second derivatives of ϕ). We note however that the tabulated data have already been smoothed by Jones *et al.*,[55] (necessitating certain assumptions on their part concerning the shape of the surface), the purity of the methane was reported as 99.45 mol% (which may affect critical region measurements), and the temperature rise measured for the individual datum, (a crucial parameter in critical region measurements), was not reported.

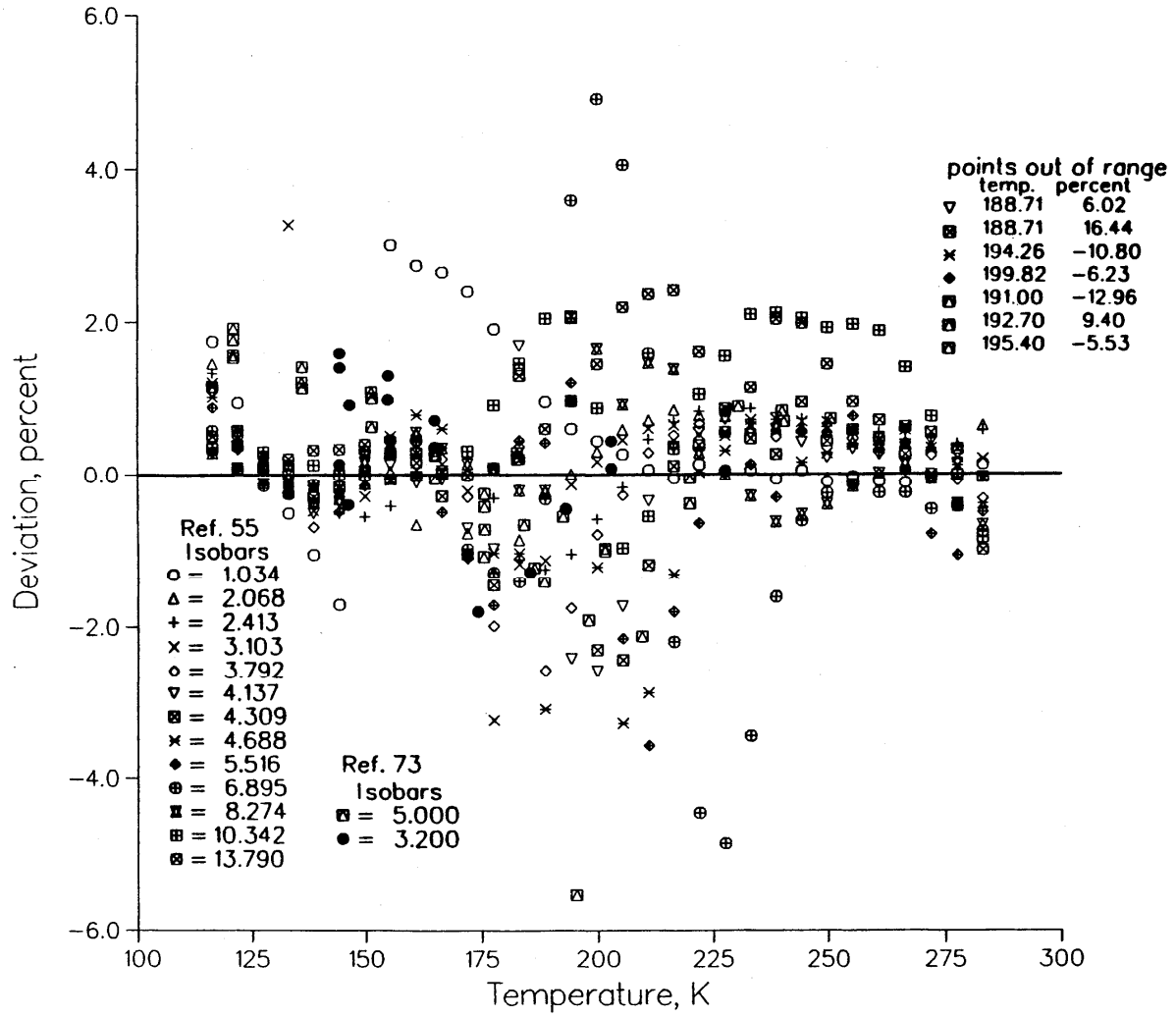

FIG. 15. Isobaric heat capacity (C_P) deviations versus temperature. Abbreviated references are: 55, Jones (1963); and 73, Van Kasteren (1979). Isobars are in MPa.

Van Kasteren and Zeldenrust[73] provide an additional 2 isobars of C_P measurements, and the deviations for their data are included in Fig. 15. The trends are similar to those for the primary data, with most points within the 1% or 2% band of deviations. The data on the 5 MPa isobar and within the range 191 to 198 K, near the critical point, show deviations up to 13%. On the 3.2 MPa isobar, data in the range 178 to 181 K show extreme deviations, up to 92%. The temperature rises for these 4 data seem to take the system across the two-phase boundary, and the points may have been tabulated without taking the latent heat into consideration. These data are not illustrated in Fig. 15, and after the elimination of these 4 points, the AAD-% for the van Kasteren and Zeldenrust data is 1.4%. We estimate, from these observations, that the SWEOS will give isobaric heat capacities to within about 2% for the liquid and supercritical fluid from 115 to about 300 K for pressures to about 15 MPa. The uncertainty is assumed to be worse outside these ranges, and in the general critical region defined above, 20% errors may be possible. Very close to the critical point, the behavior of this classical SWEOS will not describe the heat capacities accurately.

The heat capacity of the saturated liquid was also measured by Younglove[53] and Roder.[54] These data, which were used in the development of the SWEOS, are compared with the correlation in Fig. 16, and the associated statistics are included in Table 13. Most of the deviations are well under 1%, and the AAD-% is about 0.6%. The largest deviation is 3.7% and occurs near the critical point. The data reduction necessary to arrive at experimental values of $C_{\sigma L}$ requires the use of an equation of state,[54] including knowledge of the two-phase boundary, so that the measurements are not absolute. In Ref. 54, the quoted experimental accuracy is 2% and deteriorates to 5% near the critical point. The accuracy of the SWEOS in predicting saturated liquid heat capacities is 2% from the triple point to 186 K and 5% for temperatures approaching the critical point.

There are several sources for sound speed measurements, and Table 14 includes all of those used to construct the SWEOS. For our comparisons, data which were reported as lying along the liquid saturation boundary have been treated identically to those in the single-phase region; the pressure and density were determined from the experimental temperature by using the Maxwell construction with the present SWEOS. The major discrepancies between the experimental measurements and the SWEOS calculations, do-

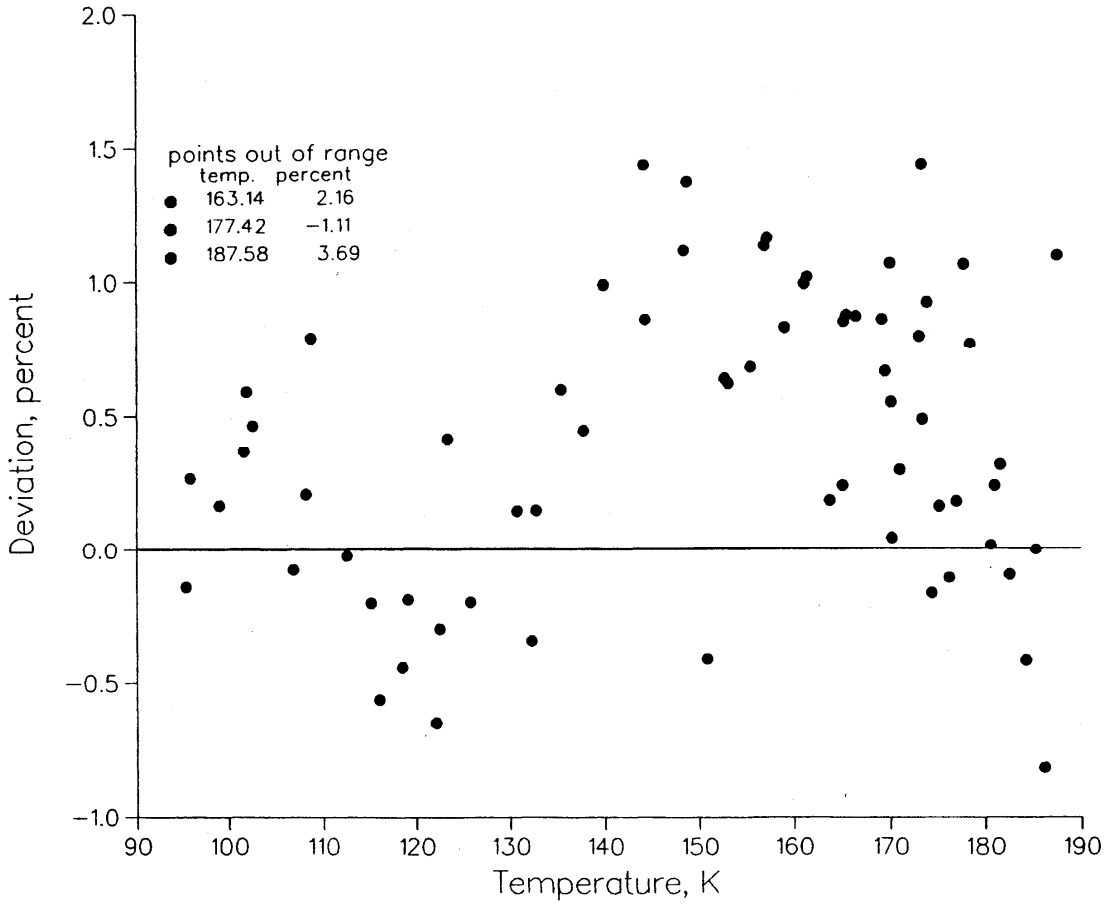

FIG. 16. Saturated liquid heat capacity ($C_{\sigma L}$) deviations versus temperature. Combined data of Younglove (Ref. 53) and Roder (Ref. 54).

TABLE 14

SOURCES OF SOUND SPEED DATA

FIRST AUTHOR	REF.	NO.PTS.	TEMPERATURE RANGE, K	PRESSURE RANGE,MPa	SOUND SPEED DEVIATIONS FROM SWEOS AAD,%	BIAS,%	RMS,%
Baidakov[a,b]	6	119	150 - 183	1 - 4	0.475	-0.425	0.267
Blagoi[a]	56	26	91 - 178	0.01- 3	0.461	-0.134	0.572
Gammon[a,c]	44	138	113 - 323	0.1 - 25	0.844	0.584	1.752
Sivaramin[d]	49	104	193 - 423	1.5 - 28	0.164	0.005	0.272
Straty[a]	57	91	91 - 300	0.01- 35	0.424	-0.264	0.522
Van Dael[a]	58	28	94 - 190	0.02-4.6	0.820	0.037	1.342
Van Itterbeek[b]	59	97	111 - 190	0.1 - 20	0.492	-0.007	1.205

[a] Some of these data were along or near the two-phase boundary.

[b] Data inside the metastable or two-phase region were eliminated.

[c] Data very close to the critical point have been excluded; see text.

[d] These data arrived too late to be included in the correlations.

minating the statistics for the data of Gammon and Douslin,[44] occur in the critical region. Data from Ref. 44 obtained at state points between 189.5 and 191.5 K and between 4.5 and 4.7 MPa have been excluded from the statistical comparisons in Tables 13 and 14. These 58 points have corresponding reduced temperatures, $(T^* = [T_c - T]/T_c)$, from -0.0050 to 0.0055 and reduced pressures, $(P^* = [P_c - P]/P_c)$, from -0.02 to 0.02.

We anticipate, at state points very close to the critical point, that experimental sound speed measurements will be exceedingly difficult to obtain and interpret. We are also aware that our classical equation of state cannot give accurate results for derivative properties in the asymptotically critical limit. In particular, theory indicates that the speed of sound should vanish at the critical point; in our formulation this speed is about 231 m s^{-1}. This discrepancy between theory and our correlation occurs principally because the very small divergence of the isochoric heat capacity ($\sim |T\text{-}T_c|^{-\alpha}$ where α is about 0.1) is not predicted by a classical equation of state; in our formulation the value of C_v at the critical point is about 45 J mol^{-1} K^{-1}. In addition, because of truncation error, the nominally zero value of $\partial P/\partial\rho|_T$ is equal to about 10^{-8} J mol^{-1} and the related C_P which should diverge strongly, is found to be about 10^{13} J mol^{-1} K^{-1} at the critical point.

Gammon and Douslin[44] emphasized the critical region in their methane sound speed measurements, and therefore some of their data had to be excluded to generate a useful comparison with the present classical equation of state. These data are included, however, in Fig. 17 and we will now discuss them briefly. The largest deviation for the excluded data exceeds 25% and occurs at 190.56 K ($T^* \approx -5\times10^{-5}$) and 4.6 MPa ($P^* \approx -3\times10^{-4}$). If we include the temperature range 189.5 to 191.5 K with pressures from 4.5 to 4.7 MPa, the entire set of 196 points from Ref. 44 has an AAD-% of 3.4% compared with the 0.8% figure shown in Table 14. The overall value for the sound speed's AAD-%, including all the sources in Table 14 and incorporating the data from Ref. 44 which were previously excluded, for a total of 661 data, is 1.3%.

In Fig.17, we illustrate the deviations between the experimental data and the SWEOS; we have several additional comments concerning the comparison. Measurements along or near the saturated liquid boundary were made by Baidakov *et al.*,[6] Gammon and Douslin,[44] Blagoi *et al.*,[56] Straty[57] and Van Dael *et al.*[58] These generally show excellent agree-

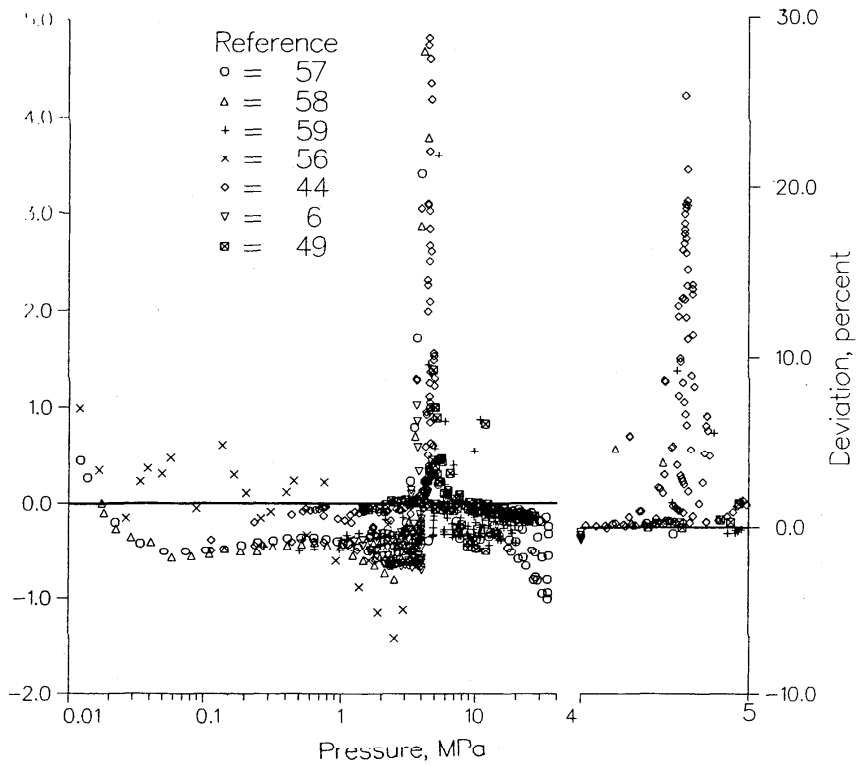

FIG. 17. Sound speed (W and $W_{\sigma L}$) deviations versus pressure. Inset at right shows the large deviations near the critical point. Abbreviated references, with primary references denoted by asterisk, are: 44*, Gammon (1976); 6, Baidakov (1982); 57*, Straty (1974); 59, Van Itterbeek (1967); 58, Van Dael (1965); 56, Blagoi (1967); and 49, Sivaraman (1986).

ment but are consistently about 0.5% percent higher than values calculated from the SWEOS. Above about 180 K, the deviations change sign, and above 188 K, the deviations for the Gammon and Douslin[44] data exceed 5%. In the vapor near the phase boundary, the data of Ref. 44 also typically show 0.5% deviations below 180 K with large critical-region deviations occurring above about 188 K. We again emphasize that our classical SWEOS cannot give the nonanalytic behavior of the sound speed in the critical region. Further from the phase boundary, the vapor deviations of Ref. 44 are typically 0.1% except as the critical region is approached. For the compressed liquid, the deviations from Baidakov *et al.*,[6] Straty,[57] and Van Itterbeek *et al.*[59] remain better than about 0.5%, but deteriorate to 1% above about 20 MPa. For temperatures above the critical value, Refs. 44, 49, and 57 provide data up to 423 K. With the exception of the critical region, deviations for these sound speed data are typically 0.5%. For pressures above 20 MPa, the deviations are higher. The very recent higher temperature results of Sivaraman and Gammon,[49] which were not used to construct the correlation, exhibit deviations mostly in the 0.1% range.

We can summarize these observations by the following subjective guidelines for the use of the SWEOS in predicting the speed of sound in methane. Below 180 K or above 195 K, with pressures below about 20 MPa, for the saturated liquid, compressed liquid, vapor phase, and supercritical fluid, accuracies of 0.6% can be anticipated. Between 180 and 188 K, or above 20 MPa (to about 35 MPa), the accuracy decreases to 1.5%. In the asymptotically critical region, the SWEOS cannot be used for sound speed predictions; in the general region of the critical point, 188 to 195 K and 4.5 to 4.7 MPa, the uncertainties can exceed 5%.

These comparisons with experimental data (and the process of determining the coefficients of the SWEOS, as described in Sec. 3), only probe four derivatives of the dimensionless, residual Helmholtz energy, namely $\phi^r_\delta, \phi^r_{\delta\delta}, \phi^r_{\tau\tau}$, and $\phi^r_{\delta\tau}$. While this should describe the actual surface quite well, additional uncertainties will enter any calculation which requires other derivatives of ϕ^r or integrals of the Helmholtz function. We hesitate to make any quantitative predictions of the errors involved in calculating any thermodynamic quantities not discussed in this section, but we do conjecture that these errors will be comparable to those found with any other precision equation of state for methane.

4.3. Transport Property Comparisons

4.3.1. Viscosity

The viscosity of the dilute methane gas, as described by Eq. (10), is compared with experimental data in the deviation plot of Fig. 18. The primary data of Hellemans *et al.*[63] are described quite well by the correlation and have an AAD-% of 0.19%. Data from Refs. 63, 64, 66, and 74–81 are shown in the figure, and additional data sources are discussed in these references. Where appropriate, the data have been adjusted to zero density by subtracting the (small) value of the excess viscosity calculated from the correlation of Eq. (15) at the experimental pressure, which was usually near 0.1 MPa. For the 78 points illustrated, in the range from

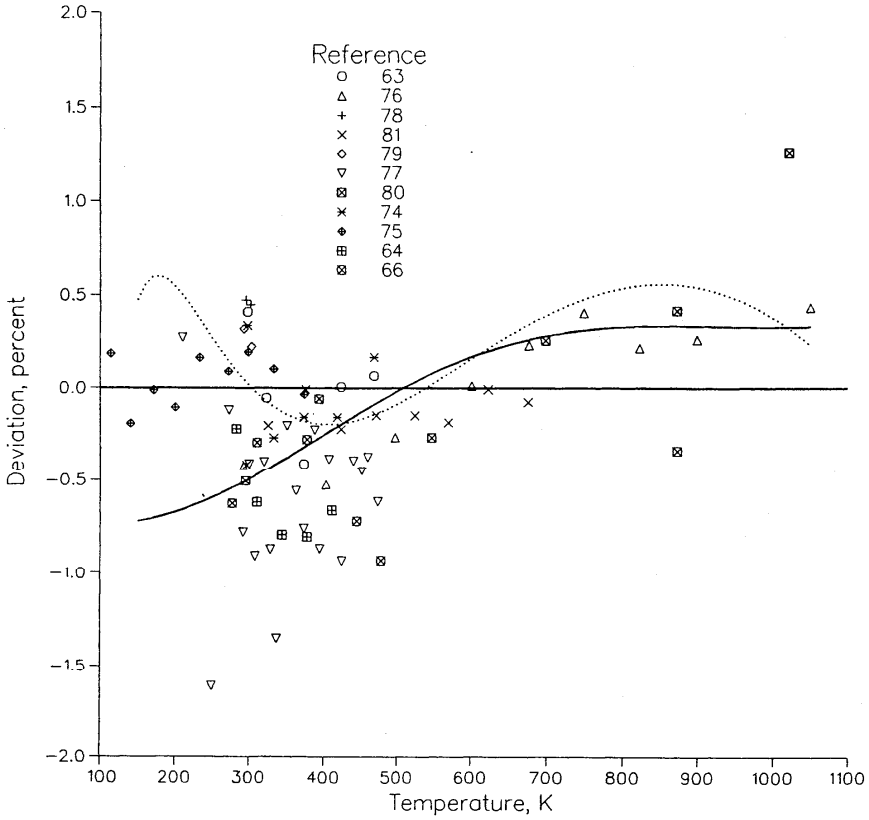

FIG. 18. Dilute-gas viscosity coeffcient deviations versus temperature. Solid line is the correlation of Hanley *et al.* (Ref. 14); dotted line is the correlation from Maitland *et al.* (Ref. 35). Abbreviated references are: 63, Hellemans (1973); 76, Dawe (1970); 78, Kestin (1971); 81, Timrot (1975); 79, Kestin (1968); 77, De Rocco (1958); 80, Maitland (1973); 74, Abe (1978); 75, Clarke (1969); 66, Carmichael (1965); and 64, Giddings (1966).

210 to 1050 K, the comparison of the data to Eq. (10) gives an AAD-% of 0.39%, a BIAS-% of −0.21%, and an rms-% of 0.46%. The sources are in good agreement, with the largest deviations in the oldest (1958) measurements of De Rocco and Halford[77] and in some of the zero density extrapolations from Giddings *et al.*[64] and Carmichael *et al.*[66] The two additional correlations shown, from Hanley *et al.*[14] and from Maitland *et al.*,[35] also agree well with the current correlation; there is a maximum deviation of about 1.5% near the triple-point temperature.

From the dispersion of the data and correlations, the quoted experimental accuracies associated with the data, and a study of the use of the 11-6-8 intermolecular potential in the Chapman–Enskog dilute gas theory, we estimate that the correlation of Eqs. (10) and (12) will give dilute gas viscosities for methane with associated accuracies of 0.5% from 270 to 600 K and within 1% above that range. For lower temperatures, and especially below the critical point, the data are extremely sparse or nonexistent. We anticipate that the theory, with this potential function, will extrapolate well, but we increase our error estimate to 3% for temperatures from the triple point to 270 K.

There are also several sources for the viscosity of methane at elevated pressures. The total viscosity is correlated by the sum of contributions from Eqs. (10) and (15). In addition to the 267 primary data of Diller[9] (above 18 mol dm^{-3} only), Giddings *et al.*,[64] Haynes,[65] and Carmichael *et al.*,[66] we have included comparisons with data from Refs. 82–86. Table 15 summarizes these data and comparisons for the 532 points. Figure 19(a) illustrates the deviations for the primary data, and Fig. 19(b) shows the deviations for the remainder of the points in Table 15. References to additional methane viscosity measurements can be found in the cited papers and in the compilation of Stephan and Lucas.[87] For the selected primary data the AAD-% is 0.559%, while for the entirety of the data of Table 15 this quantity is 1.710%. These statistics, as well as those in the table and the appearances of Figs. 19(a) and 19(b), indicate substantial dispersion and disagreement among the data, so that some discussion is warranted.

For the vapor phase, below the critical temperature, we are aware of no accurate data. We have examined, however, the low-density data along some supercritical isotherms and the uncertainty of the zero-density result in the subcritical region. From this, we estimate that the error can exceed 5% as the saturated vapor line is approached. For the liquid below the critical temperature, the data of Haynes[65] and Boon *et al.*[83] indicate an accuracy of about 3% at the phase boundary. For some points, the disagreement between these references is somewhat higher, and larger deviations for Ref. 83 can be seen in Fig. 19(b). This same accuracy of 3%, based on the data of Diller,[9] Hellemans *et al.*,[85] and Huang *et al.*,[86] probably describes the correlation for the compressed liquid at pressures to 30 MPa. At temperatures above 145 K, there are substantial differences between the data of Ref. 85 and other sources (with deviations to 45%). These are easily

TABLE 15

SOURCES OF VISCOSITY DATA AT ELEVATED PRESSURES

FIRST AUTHOR	REF.	NO.PTS.	TEMPERATURE RANGE, K	PRESSURE RANGE,MPa	VISCOSITY DEVIATIONS AAD-%	BIAS-%	RMS-%
Barua	82	39	223-423	1-18	1.696	1.684	1.026
Boon[a]	83	8	91-114	0.01-0.1	2.456	2.213	1.689
Carmichael[b]	66	67	278-478	0.1-36	0.764	-0.503	0.905
Diller[b]	9	141	100-300	0.6-31	1.101	-0.089	1.598
Giddings[b]	64	100	283-411	0.1-55	0.281	-0.055	0.386
Gonzalez	84	53	311-444	1.4-55	1.658	-1.658	0.768
Haynes[a,b]	65	20	95-190	0.02-4.5	0.766	0.193	1.081
Hellemans	85	56	97-187	0.04-10	7.074	4.317	11.118
Huang	86	48	103-173	0.05-34	1.873	-1.225	1.885

[a] These data were along the saturated liquid boundary.

[b] Primary data were selected from this reference.

discerned in the figures. The isotherm at 173.15 K, the highest temperature reported in Ref. 86, shows deviations near -5%.

There are substantial quantities of data above the critical temperature. In the temperature range T_c to 270 K, the low-density data of Diller[9] and Barua *et al.*[82] indicate an accuracy of about 5% for densities up to 10 mol dm^{-3}. The 200 and 212 K data of Ref. 9 stand out in Fig. 19(b) in the low-density region. In the same temperature range, but for higher densities and for pressures up to about 30 MPa, the viscosity increases and the estimated error drops to about 2%. For the low-density region, to 10 mol dm^{-3}, we estimate that the error associated with the correlation is 1% in the higher temperature range, to 450 K. For pressures up to 55 MPa, and temperatures to 450 K, the error is about 2%. Again, these error estimates are based on the quality and quoted accuracy of the experimental data as well as on the agreement between the correlation and these data. The correlation of Eq. (15) attempts to describe the rapidly rising excess viscosity as the melting line is approached. It has a zero in the denominator, corresponding to a singularity in the correlation within the fluid region; this occurs well outside the range of any data. In addition to the usual warnings concerning extrapolation beyond the range of the correlating equation, any user is cautioned about this singularity, which can be a problem only at pressures exceeding 200 MPa.

4.3.2. Thermal Conductivity

For the dilute methane gas, the correlation of Eq. (13), using Eq. (14) for the factor f_{int}, describes the thermal conductivity, and Fig. 20 illustrates the deviations of experimental data from this correlation. In addition to the primary data of Roder[8] and Le Neindre *et al.*,[67] the figure includes points from Refs. 88-94. Other experimental work is cited in these references. In all cases, we have used either the tabulated zero-density extrapolations of the authors or we have subtracted a small value for the excess thermal conductivity as calculated from the correlation of Eqs. (17)–(18) at the experimental conditions. For the primary data, comprising 21 points spanning the temperature range 133–621 K, the AAD-% is 0.839%. Overall, for the 68 experimental points included in the figure, the AAD-%, BIAS-%, and rms-% are 1.076%, −0.449%, and 1.456%, respectively.

The agreement among the sources of data as well as the quality of the present dilute gas correlation are worse than those seen in the dilute gas viscosity correlation. This last point is perhaps not surprising, since the theory for f_{int} is not completely rigorous and the form we have chosen for this

factor may be overly simplified. In the range 130–625 K, we estimate that the accuracy of the correlation is about 2.5%, comparable to the estimated accuracy of the data. However, extrapolation beyond the range of the primary data leads to greatly increased error, as indicated in the figure. At the lowest temperatures, between the triple point and 130 K, where the transfer of energy between kinetic and internal degrees of freedom is expected to be most inhibited, the correlation seems to exaggerate this effect, and the calculated values of f_{int} and, hence, the thermal conductivity are too small. The correlation of Hanley *et al.*[14,19] based on an experimental determination of the rate of interchange of energy between rotational and translational modes (through rotational collision numbers), is also illustrated in Fig. 20; evidently it gives even worse results at low temperatures. Additional, modern dilute gas thermal conductivity measurements at the lowest temperatures could help to improve the correlation, and a more elaborate expression for f_{int} might then be justified. For temperatures below 130 K, where the vapor pressure is about 0.37 MPa, the current correlation could give errors in excess of 10% for the thermal conductivity of dilute methane.

For higher pressures, the thermal conductivity has contributions from its dilute limit, Eq. (13), and the critical enhancement, Eq. (18), as well as from the excess function of Eq. (17). The deviations of experimental measurements from the total conductivity are shown in Figs. 21(a), 21(b) and 21(c), and Table 16 gives additional information about the experimental data from Refs. 8,67,68,88,89, and 92–96. There are additional sources of thermal conductivity data for methane listed within these references. The AAD-% for the 920 primary data of Roder[8] and of Mardolcar and de Castro,[68] which were used to establish the total thermal conductivity correlation, is 0.518%; these data are shown in Fig. 21(a). For the 1892 points listed in the table, the AAD-% is 2.89%. The large deviations indicated by these statistics and illustrated in the figures again warrant some discussion.

The major deviations between the correlation and data occur near the critical point and along the phase boundary. For the primary data of Roder,[8] these deviations approach 7.5% along the 198 K isotherm at densities near 8 mol dm^{-3}, just below ρ_c, and 3.5% as the saturated vapor boundary is approached near 184 K. Outliers from Mardolcar and de Castro,[68] at 180 K near the liquid phase boundary and near −3%, are also evident in Fig. 21(a). There does seem to be a systematic residual error in the correlation, with the critical enhancement overestimated for densities below ρ_c and underestimated above ρ_c. Other than these regions, however, typical deviations for the primary data of Refs. 8 and 68 are well under 2%.

Much of the secondary thermal conductivity data is illustrated in Fig. 21(b). However, the extensive measure-

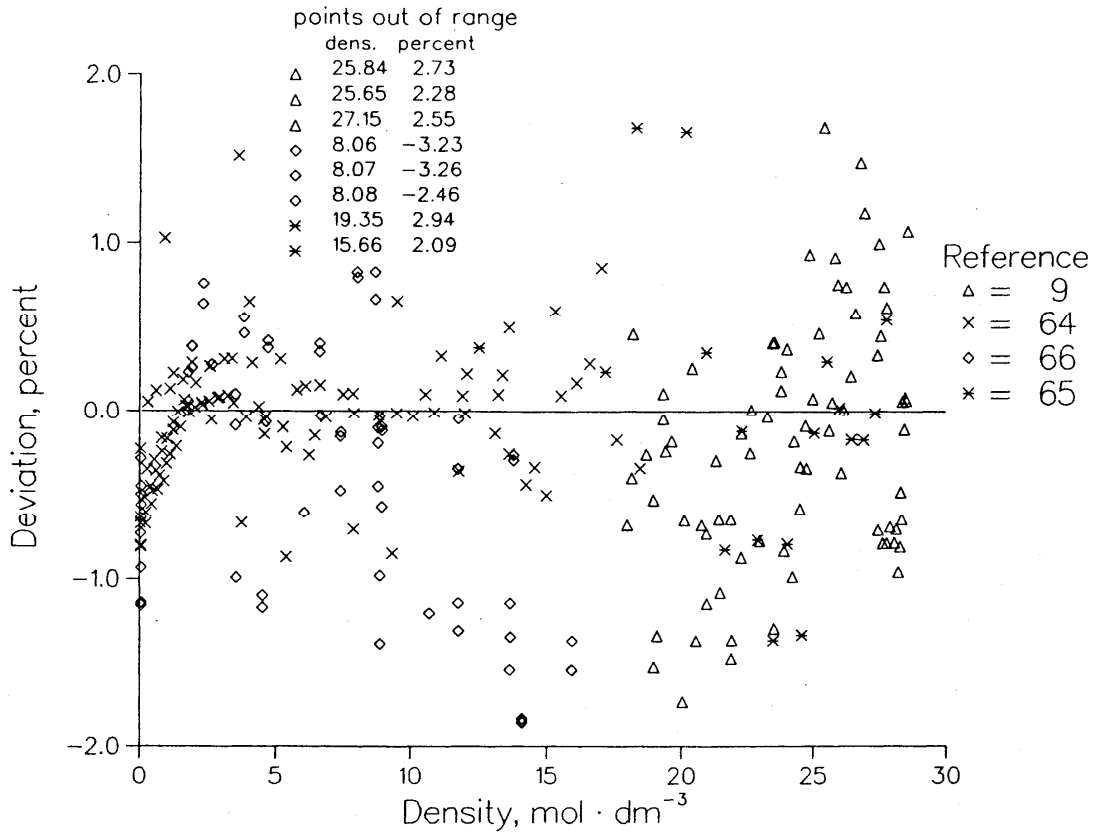

FIG. 19(a). Total viscosity deviations versus density for the primary data used. Abbreviated references are 9, Diller (1980); 64, Giddings (1966); 66, Carmichael (1965); and 65, Haynes (1973).

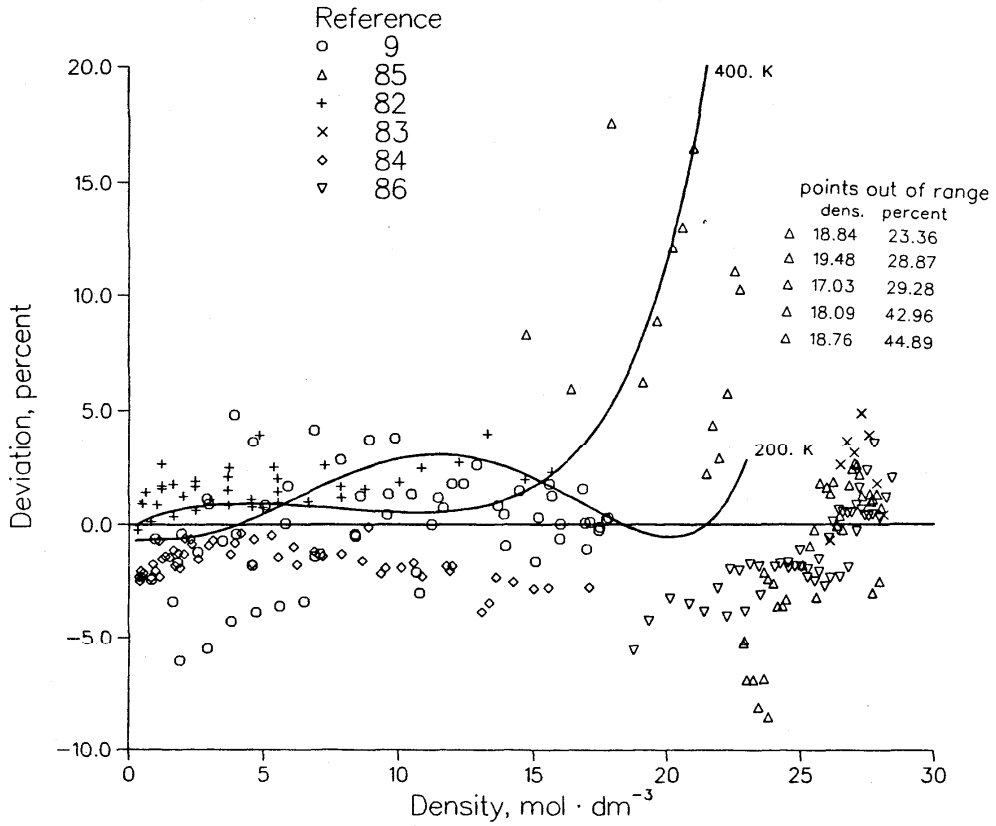

FIG. 19(b). Total viscosity deviations versus density for the secondary data. The solid lines are the correlation of Younglove and Ely (Ref. 13) at 200 and 400 K. Data from Ref. 9 appear in both Figs. 19(a) and 19(b) because only those data at densities greater than 18 mol dm^{-3} were weighted. Abbreviated references are 9, Diller (1980); 85, Hellemans (1970); 82, Barua (1964); 83, Boon (1967); 84, Gonzalez (1967); and 86, Huang (1966).

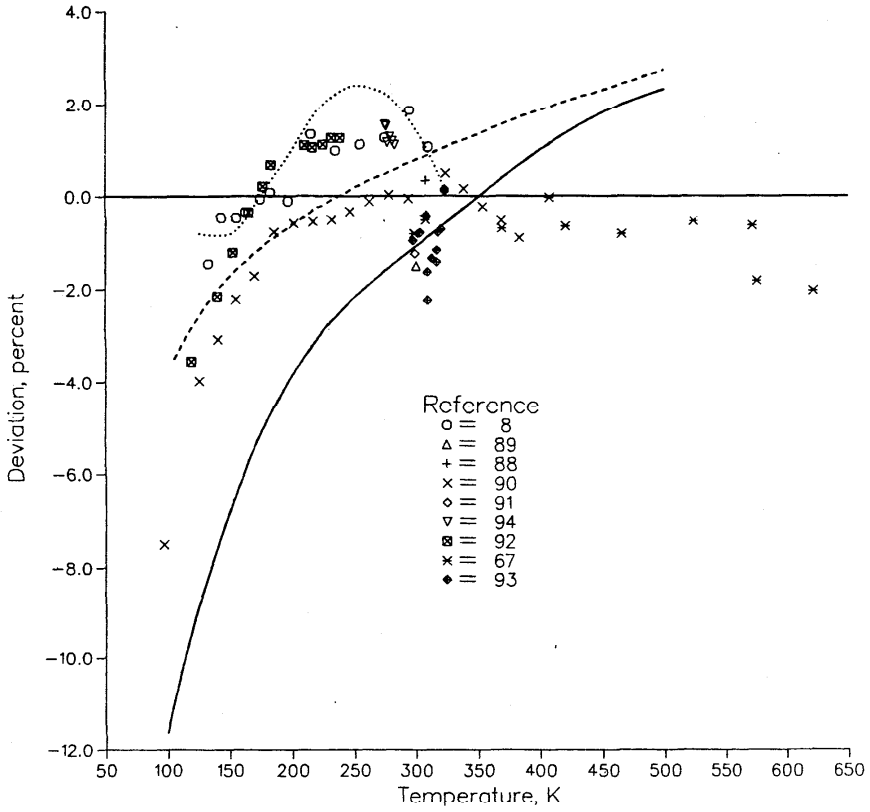

FIG. 20. Dilute gas thermal conductivity coefficient deviations versus temperature. Solid line is the correlation from Hanley *et al.* (Ref. 19,14); dotted line is the correlation from Roder (Ref. 8); and dashed line is correlation from Younglove and Ely (Ref. 13). Abbreviated references are: 8, Roder (1984); 89, Clifford (1979); 88, Assael (1981); 90, Johnston (1946); 92, Sokolova (1967); 67, Le Neindre (1969); and 93, Yorizane (1983); 91, Mamn (1931); 94, Zheng (1984).

ments of Sokolova and Golubev[92] concentrate heavily in the problematic regions and indicate a much larger critical enhancement over a broader range in both temperature and density than that observed by Roder[8] and reflected in the current correlation. These data are shown separately in Fig. 21(c) because a different scale was required. Deviations up to nearly 60% are found for the points closest to the critical point, and these data contribute substantially to the poor statistical agreement between the correlation and experimental data. The few alternate critical-region data, for example the points in Table III of Prasad *et al.*[96] which are on the periphery of the critical region, seem to substantiate the current correlation, as the AAD-% for these 8 points is 2%. Although care was apparently taken by the authors of Ref. 92 to avoid contributions to the heat flux through convective rather than conductive mechanisms, we think that convective heat flow may explain the discrepancy for this older experimental data. In regions of overlapping experimental conditions, the data of Ref. 8 are more consistent with other sources than are the data of Ref. 92. For the supercritical isotherms, the agreement between the data of Ref. 92 and the correlation is about 4% outside the density range 3–16 mol dm^{-3}. Below 185 K, large deviations (in the 10%–20% range) are seen for points near the two-phase boundary. Additional careful measurements near the critical region and phase boundary would be useful to further explain these large disagreements and improve the correlation in this region. If the data from Ref. 92 are excluded, the AAD-% for the remaining 1447 data is 0.81%.

Among the other substantial disagreements between the thermal conductivity correlation and experimental data, notable in Fig. 21(b), are single outliers from Yorizane *et al.*,[93] Prasad *et al.*,[96] and Ikenberry and Rice[95] near −5% at 303, 220, and 200 K, respectively. In addition, the lowest temperature liquid data, at 99 K, from Ref. 95, indicate conductivities substantially higher (18% at the highest pressure, 40 MPa) than those determined from the correlation. All of the high-density data of Ref. 95, at 99, 125, and 150 K, lie above the correlation and the comparable data of Roder.[8] The lowest density measurements of Ref. 96, especially at 300 K, differ substantially (to 9%) from the correlation and from measurements in the other references. The high-density points from this reference are also systematically below the correlation, but typically within 2%. Finally, the high temperature results of Le Neindre,[67] well above the range of the input data for the correlation, agree quite well with our equations; all deviations on the 726 K isotherm (with 8 pressures between 1 and 89 MPa) are $< 1.5\%$. On the basis of these comparisons and again considering the experimental technique and the error estimates of the researchers, we believe that the accuracy of the correlation is about 2% for most of the range between 110 K and 725 K and for pressures to 70 MPa (or densities to about 29 mol dm^{-3}). The exceptions occur around the critical point and near both saturation boundaries, where 5% errors are typical; greater errors could occur in the asymptotically critical region (that is for temperatures between 185 and 196 K with densities between 7.6 and 12.7 mol dm^{-3}). For the vapor at lower temperatures and the dense liquid near the triple point, errors of near 10% are also possible.

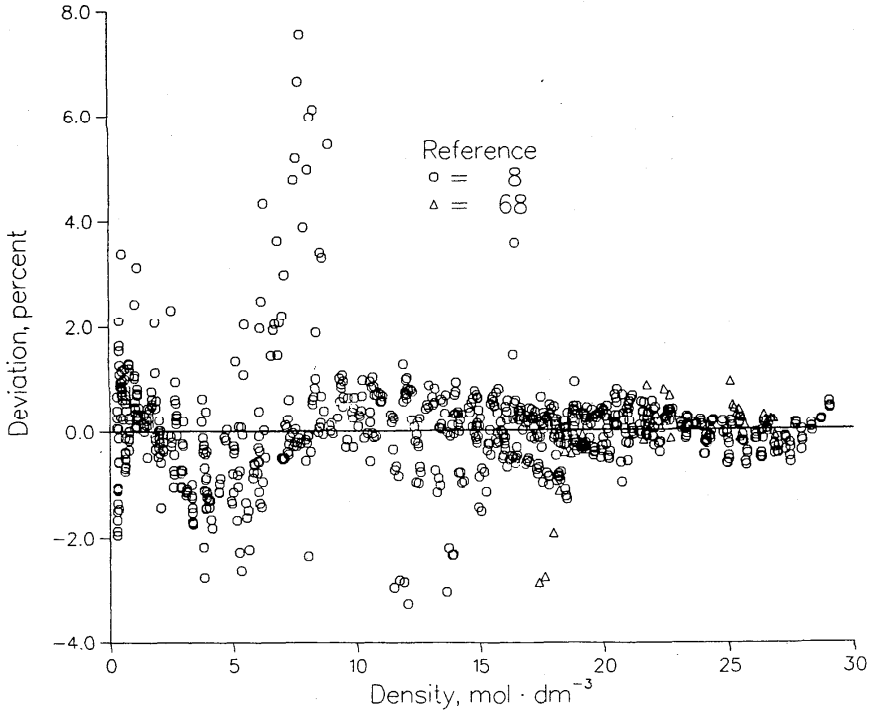

FIG. 21(a). Total thermal conductivity deviations versus density for the primary data used. Abbreviated references are: 8, Roder (1984); and 68, Mardolcar (1987).

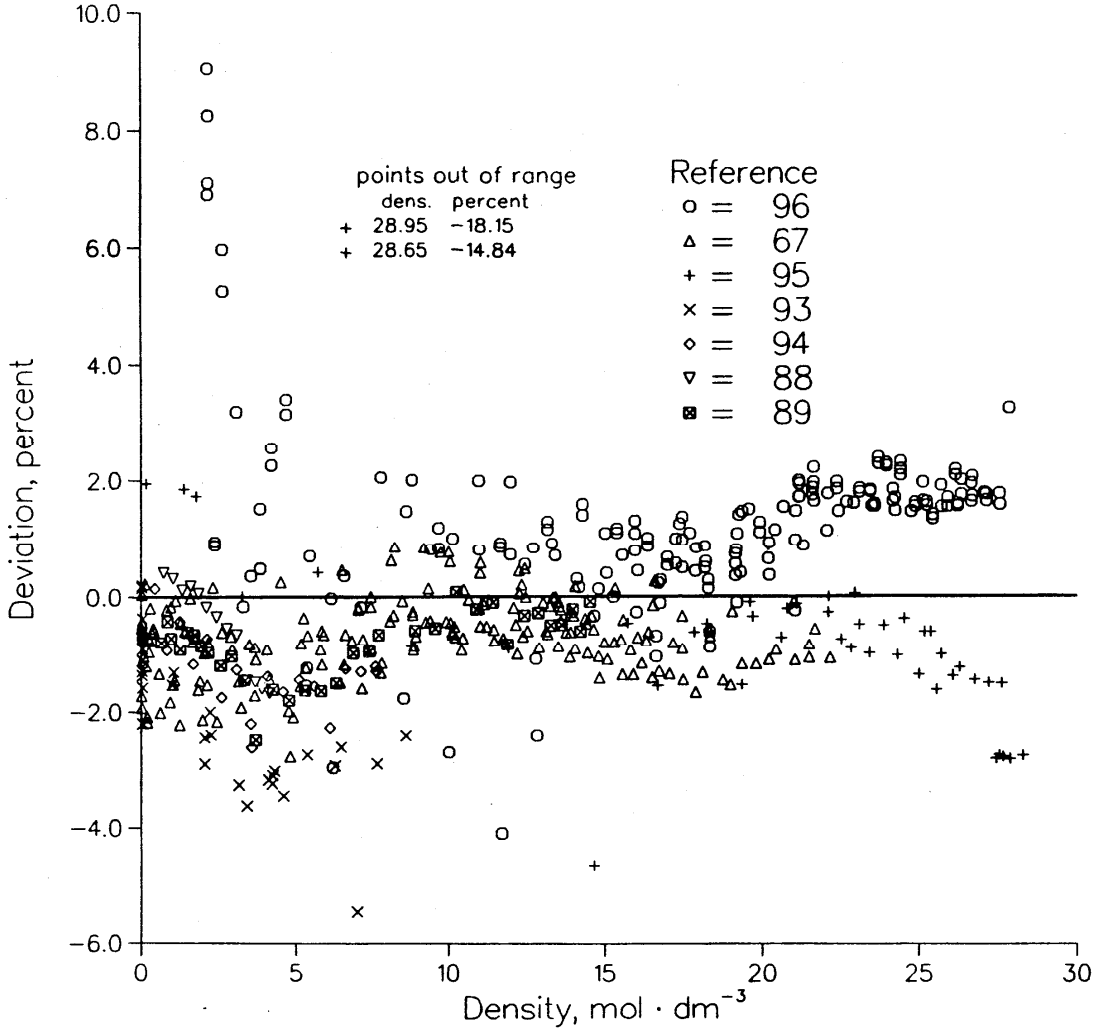

FIG. 21(b). Total thermal conductivity deviations versus density for the secondary data. Abbreviated references are: 67, Le Neindre (1969); 89, Clifford (1979); 88, Assael (1981); 94, Zheng (1984); 93, Yorizane (1983); 96, Prasad (1984); and 95 Ikenberry (1963).

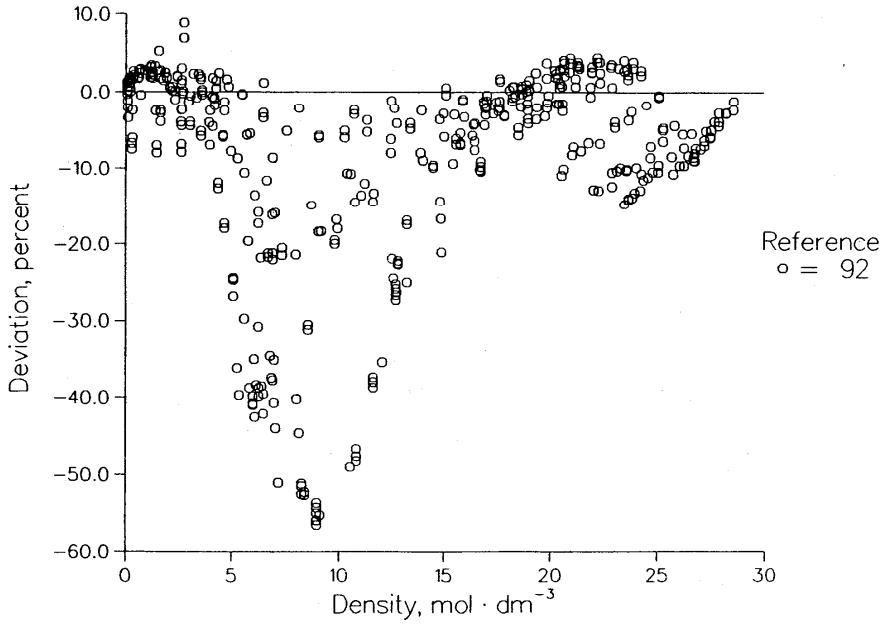

FIG. 21(c). Total thermal conductivity deviations versus density for the data of Sokolova and Golubev (Ref. 92).

TABLE 16

SOURCES OF THERMAL CONDUCTIVITY DATA AT ELEVATED PRESSURES

FIRST AUTHOR	REF.	NO.PTS.	TEMPERATURE RANGE, K	PRESSURE RANGE,MPa	THERMAL CONDUCTIVITY DEVIATIONS AAD,%	BIAS,%	RMS,%
Assael[a]	88	13	307	1.8-9.3	0.630	-0.428	0.706
Clifford[a]	89	33	300	1.6-35	0.777	-0.771	0.531
Ikenberry	95	45	99-235	0.2-51	1.847	-1.585	3.472
Le Neindre[a]	67	193	298-726	0.1-125	0.778	-0.677	0.664
Mardolcar[b]	68	37	111-180	0.2-8.6	0.485	-0.045	0.763
Prasad	96	180	120-400	2.6-70	1.525	1.280	1.547
Roder[a,b]	8	895	111-310	0.3-70	0.577	0.069	0.942
Sokolova[a]	92	445	109-240	0.1-50	9.654	-8.376	13.781
Yorizane[a]	93	32	298-323	0.1-20	2.024	-2.009	1.182
Zheng[a]	94	19	299	0.1-16	1.265	-1.253	0.586

[a] Includes low density data illustrated in Fig.20.

[b] Primary data were selected from this reference.

5. Conclusions

The correlations we have presented represent our best efforts toward empirical algebraic representations of the thermodynamic surface and transport properties over a broad range of the fluid states of methane. The abundance of data for this important and relatively simple molecule has enabled us to determine these correlating equations and to establish reasonable limits on their accuracy. Unfortunately, there continues to be some disagreement among experimental measurements, to the extent that data are too often inconsistent when we consider the error bounds reported by the experimenters. We have used careful judgment when deciding on the relative weights of inconsistent data, and we think that our conservative error estimates of Sec. 4 reflect the true uncertainties of the correlations. In certain instances, it is a sparsity of data or a problem with the correlating function itself which causes an increase in the uncertainty of predictions based on the correlation. These problems have been discussed in Sec. 4.

Additional measurements on fluid methane, especially in some of the problem regions and for some of the specific properties mentioned above, can further refine future correlations. For instance, more *PVT* data in the highly compressed liquid, derivative and transport data in the critical region, low temperature gas-phase viscosity measurements, and also measurements near and on both liquid–vapor phase boundaries would be extremely useful. Such measurements should adhere strictly to appropriate guidelines concerning the acquisition of primary data. Samples should be well characterized and of very high purity; absolute determination of all experimental quantities, traceable to relevant standards is preferred; and the tabulation of original, unsmoothed data, with all experimental correction factors fully discussed or referenced is imperative. Theoretical advances, including improved treatment of the critical region, calculation and incorporation of precise intermolecular potential functions, and a rigorous theory of energy transfer problems for the thermal conductivity and initial density dependences for both transport properties, will also assist in the development of future correlations.

In conclusion, we hope that these correlations will serve

well their intended purposes. Within the specified ranges and tolerances, they will allow the user to calculate the important thermodynamic and transport properties of the methane fluid. We hope that they will also be useful for additional studies, such as for generalized corresponding states models and mixture calculations. Finally, we intend to publish additional correlations for other fluids, using correlating functions similar to those used in this work.

6. Acknowledgments

We thank R. D. McCarty for helpful discussions and Prof. W. Wagner for providing a copy of his experimental tables prior to publication. We also thank Prof. R. T. Jacobsen and Dr. M. W. Chase for their careful reviews of parts of this manuscript.

7. References

[1]D. G. Friend, J. F. Ely, and H. Ingham, National Institute of Standards and Technology, U. S., Technical Note No. 1325, 1989.
[2]S. Angus, B. Armstrong, and K. M. de Reuck, *International Thermodynamic Tables of the Fluid State, Methane*, (Pergamon, Oxford, 1978), Vol. 5.
[3]R. Kleinrahm and W. Wagner, J. Chem. Thermody. **18**, 739 (1986).
[4]N. J. Trappeniers, T. Wassenaar, and J. C. Abels, Physica A **98**, 289 (1979).
[5]J. Mollerup, J. Chem. Thermod **17**, 489 (1985).
[6]V. G. Baidakov, A. M. Kaverin, and V. P. Skripov, J. Chem. Thermody. **14**, 1003 (1982).
[7]E. C. Morris, Int. J. Thermophys. **5**, 281 (1984).
[8]H. M. Roder, Int. J. Thermophys. **6**, 119 (1984); and National Institute of Standards and Technology, U. S., Interagency Report NBSIR 84-3006, 1984.
[9]D. E. Diller, Physica A **104**, 417 (1980); and National Institute of Standards and Technology (Private communication).
[10]J. V. Sengers and J. M. H. Levelt Sengers, Ann. Rev. Phys. Chem. **37**, 189 (1986).
[11]J. V. Sengers, R. S. Basu, and J. M. H. Levelt Sengers, National Aeronautics and Space Administration, U.S., NASA Contractor Report No. 3424, 1981.
[12]R. Schmidt and W. Wagner, Fluid Phase Equil. **19**, 175 (1985).
[13]B. A. Younglove and J. F. Ely, J. Phys. Chem. Ref. Data **16**, 577 (1987).
[14]H. J. M. Hanley, W. M. Haynes, and R. D. McCarty, J. Phys. Chem. Ref. Data **6**, 597 (1977).
[15]J. O. Hirschfelder, C. F. Curtiss, and R. B. Bird, *Molecular Theory of Gases and Liquids* (Wiley, New York, 1967).
[16]M. Klein, H. J. M. Hanley, F. J. Smith, and P. Holland, Natl. Bur. Stand. (U.S.) Monogr **47**, 1 (1974).
[17]R. D. Goodwin, National Institute of Standards and Technology, U.S., Technical Note No. 653, (1974).
[18]R. D. McCarty, Cryogenics **14**, 276 (1974).
[18a]V. V. Sychev, A. A. Vasserman, V. A. Zagoruchenko, A. D. Kozlov, G. A. Spiridonov, and V. A. Tsymarny, *Thermodynamic Properties of Methane* (Hemisphere, Washington, 1987), edited by T. B. Selover Jr., English Language Edition.
[19]H. J. M. Hanley, R. D. McCarty, and W. M. Haynes, Cryogenics **15**, 413 (1974).
[20]R. C. Reid, J. M. Prausnitz, and T. K. Sherwood, *The Properties of Gases and Liquids 3rd ed.* (McGraw-Hill, New York, 1977).
[21]W. Wagner, Cryogenics **13**, 470 (1973); Corrigenda Cryogenics **14**, 63 (1974).
[22]O. B. Verbeke, Cryogenics **10**, 486 (1970).
[23]J. M. H. Levelt Sengers, W. L. Greer, and J. V. Sengers, J. Phys. Chem. Ref. Data **5**, 1 (1976).
[24]J. C. Rainwater and M. R. Moldover, in *Chemical Engineering at Supercritical Fluid Conditions*, edited by M. E. Paulaitis, J. M. L. Penninger, R. D. Gray Jr., and P. Davidson (Arbor Science, Ann Arbor, Mich., 1983), p.199.
[25]R. D. Goodwin, J. Res. Nat. Bur. Stand. Sec. A **75**, 15 (1971).
[26]R. S. McDowell and F. H. Kruse, J. Chem. Eng. Data **8**, 547 (1963).
[27]H J. M. Hanley and M. Klein, National Institute of Standards and Technology, U.S., Technical Note No. 628 (1972).
[28]See Ref.20, Equation 10-3.2.
[29]Alternatively, the denominator of Eq. (15) could be written as $1 + g_{10a}(\delta/\delta_{cL}) + g_{11a}(\delta/\delta_{cL})\tau$ with $g_{10a} = -1.077\,008\,9$ and $g_{11a} = 0.098\,095\,691$.
[30]Committee on Data for Science and Technology, (CODATA) Newsletter No.38 (Oct. 1986).
[30a]M. Vicentini-Missoni, J. M. H. Levelt Sengers, and M. S. Green, J. Res. Nat. Bur. Stand. Sec. A **73**, 563 (1969); and Phys. Rev. Lett. **22**, 389 (1969).
[31]E. R. Cohen and B. N. Taylor, J. Res. Nat. Bur. Stand. **92**, 85 (1987).
[32]IUPAC Commission on Atomic Weights and Isotopic Abundances, Pure Appl. Chem. **58**, 1677 (1986).
[33]R. E. Bedford, G. Bonnier, H. Maas, and F. Pavese, Metrologia **20**, 145 (1984).
[34]F. Pavese, Metrologia **17**, 35 (1981).
[35]G. C. Maitland, R. D. Trengove, and W. A. Wakeham, Int. J. Thermo. Phys. **7**, 553 (1986).
[36]D. D. Wagman, W. H. Evans, V. B. Parker, R. H. Schumm, I. Halow, S. M. Bailey, K. L. Churney, and R. L. Nuttall, J. Phys. Chem Ref. Data **11**, Sup. 2 (1982).
[37]D. R. Douslin, R. H. Harrison, R. T. Moore, and J. P. McCullough, J. Chem. Eng. Data **9**, 358 (1964).
[38]A. E. Hoover, I. Nagata, T. W. Leland, Jr., and R. Kobayashi, J. Chem. Phys. **48**, 2633 (1968).
[39]M. A. Byrne, M. R. Jones, and L. A. K. Staveley, Trans. Faraday Soc. **64**, 1747 (1968).
[40]G. A. Pope, Ph.D. Thesis, Rice University, 1971.
[41]J. M. H. Levelt Sengers, M. Klein, and J. S. Gallagher, in *Amer. Inst. Phys. Handbook*, 3rd ed., (McGraw-Hill N.Y. 1972), pp. 4–204.
[42]H. J. Achtermann T. K. Bose, H. Rögener, and J. M. St-Arnaud, Int. J. Thermophys. **7**, 709 (1986).
[42a]H. J. Achtermann, F. Klobasa, and H. Rögener, Brennst.-Waerme-Kraft **34**, 266 and 311 (1982).
[43]V. M. Cheng, Ph.D. Thesis, Princeton University, 1972.
[44]B. E. Gammon and D. R. Douslin, J. Chem. Phys. **64**, 203 (1976).
[45]R. D. Goodwin, Ref. 17; data appears in Table 4, pp 69–78, some data also published in R. D. Goodwin and R. Prydz, J. Research Nat. Bur. Stand. Sec. A **76**, 81 (1972).
[46]See Ref.17, Table 4, p. 53.
[47]H. M. Kvalnes and V. L. Gaddy, J. Am. Chem. Soc. **53**, 394 (1931).
[48]S. L. Robertson and S. E. Babb, Jr., J. Chem. Phys. **51**, 1357 (1969).
[49]A. Sivaraman and B. E. Gammon, "*Speed-of-Sound Measurements in Natural Gas Fluids*", Gas Research Institute Report No. 86-0043, 1986.
[50]A. Van Itterbeek, O. Verbeke, and K. Staes, Physica **29**, 742 (1963).
[51]A. J. Vennix, Ph.D. Thesis, Rice University, 1966; and A. J. Vennix, T. W. Leland, Jr., and R. Kobayashi, J. Chem. Eng. Data **15**, 238 (1970).
[52]R. Kleinrahm, W. Duschek, and W. Wagner, J. Chem. Thermody. **18**, 1103 (1986).
[53]B. A. Younglove, J. Res. Nat. Bur. Stand. Sec. A **78**, 401 (1974).
[54]H. M. Roder, J. Res. Nat.Bur.Stand. Sec. A **80**, 739 (1976).
[55]M. L. Jones Jr., D. T. Mage, R. C. Faulkner Jr., and D. L. Katz, Chem. Eng. Prog. Symp. Ser. **59**, 52 (1963).
[56]Y. P. Blagoi, A. E. Butko, S. A. Mikhailenko, and V. V. Yakuba, Zh. Fiz. Khim. **41**, 1699 (1967).
[57]G. C. Straty, Cryogenics **14**, 367 (1974).
[58]W. Van Dael, A. Van Itterbeek, J. Thoen, and A. Cops, Physica **31**, 1643 (1965).
[59]A. Van Itterbeek, J. Thoen, A. Cops, and W. Van Dael, Physica **35**, 162 (1967).
[60]R. Prydz and R. D. Goodwin, J. Chem. Thermody. **4**, 127 (1972); R. D. Goodwin and R. Prydz, J. Research Nat. Bur. Stand. Sec. A **76**, 81 (1972).
[61]W. M. Haynes National Institute of Standards and Technology (private communication).
[62]W. M. Haynes and M. J. Hiza, J. Chem. Thermody. **9**, 179 (1977).
[63]J. M. Hellemans, J. Kestin, and S.T. Ro, Physica **65**, 376 (1973).
[64]J. C. Giddings, J. T. Kao, and R. Kobayashi, J. Chem. Phys. **45**, 578 (1966).
[65]W. M. Haynes, Physica **70**, 410 (1973).
[66]L. T. Carmichael, V. Berry, and B. H. Sage, J. Chem. Eng. Data **10**, 57 (1965).
[67]B. Le Neindre, R. Tufeu, P. Bury, P. Johannin, and B. Vodar, in *Proceedings of the Eighth Conference on Thermal Conductivity*, edited by C. Y. Ho and R .E. Taylor (Plenum, N.Y., 1969), p.229.

and R .E. Taylor (Plenum, N.Y., 1969), p.229.
[68]U. V. Mardolcar and C. A. Nieto de Castro, Ber. Bunsenges. Phys. Chem. **91**, 152 (1987).
[69]H. J. M. Hanley, R. D. McCarty, and J. V. Sengers, National Aeronautics and Space Administration, U.S., NASA Contractor Report No. 2440, 1974.
[70]J. E. Orrit and J. M. Laupretre, Adv. Cry. Eng. **23**, 573 (1978).
[71]C. R. McClune, Cryogenics **16**, 289 (1976).
[72]G. A. Olchowy and J. V. Sengers (to be published).
[73]P. H. G. Van Kasteren and H. Zeldenrust, Ind. Eng. Chem. Fundam. **18**, 333 (1979).
[74]Y. Abe, J. Kestin, H. E. Khalifa, and W. A. Wakeham, Physica A **93**, 155 (1978).
[75]A. G. Clarke and E. B. Smith, J. Chem. Phys. **51**, 4156 (1969).
[76]R. A. Dawe, G. C. Maitland, M. Rigby, and E. B. Smith, Trans. Faraday Soc. **66**, 1955 (1970).
[77]A. G. De Rocco and J. O. Halford, J. Chem. Phys. **28**, 1152 (1958).
[78]J. Kestin, S. T. Ro, and W. A. Wakeham, Trans. Faraday Soc. **67**, 2308 (1971).
[79]J. Kestin and J. Yata, J. Chem Phys. **49**, 4780 (1968).
[80]G. C. Maitland and E. B. Smith, J. Chem. Soc. Faraday Trans. 1 **70**, 1191 (1973).
[81]D. L. Timrot, M. A. Serednitskaya, and M. S. Bespalov, Sov. Phys. Dokl. **20**, 107 (1975).
[82]A. K. Barua, M. Afzal, G. P. Flynn, and J. Ross, J. Chem. Phys. **41**, 374 (1964).
[83]J. P. Boon, J. C. Legros, and G. Thomaes, Physica **33**, 547 (1967).
[84]M. H. Gonzalez, R. F. Bukacek, and A. L. Lee, Soc. Petr. Eng. J. **7**, 75 (1967).
[85]J. Hellemans, H. Zink, and O. Van Paemel, Physica **46**, 395 (1970).
[86]E. T. Huang, G. W. Swift and F. Kurata, AIChE J. **12**, 932 (1966).
[87]K. Stephan and K. Lucas, *Viscosity of Dense Fluids*, (Plenum, N.Y., 1979).
[88]M. J. Assael and W. A. Wakeham, J. Chem. Soc. Faraday Trans. 1 **77**, 697 (1981).
[89]A. A. Clifford, J. Kestin, and W. A. Wakeham, Physica A **97**, 287 (1979).
[90]H. L. Johnston and E. R. Grilly, J. Chem. Phys. **14**, 233 (1946).
[91]W. B. Mann and B. G. Dickins, Proc. R. Soc. A **134**, 77 (1931).
[92]V. P. Sokolova and I. F. Golubev, Teploenergetika **14**, 91 (1967).
[93]M. Yorizane, S. Yoshimura, H. Masuoka, and H. Yoshida, Ind. Eng. Chem. Fundam. **22**, 454 (1983).
[94]X. Y. Zheng, S. Yamamota, H. Yosida, H. Masuoka, and M. Yorizane, J. Chem. Eng. Japan **17**, 237 (1984).
[95]L. D. Ikenberry and S. A. Rice, J. Chem. Phys. **39**, 1561 (1963).
[96]R. C. Prasad, N. Mani, and J. E. S. Venart, Int. J. Thermophys. **5**, 265 (1984).

8. Appendix

TABLE A1. Properties of ideal gas at 0.1 MPa and dilute gas transport properties

T K	A^{id} kJ·mol^{-1}	H^{id} kJ·mol^{-1}	S^{id} J·mol^{-1}·K^{-1}	C_p^{id} J·mol^{-1}·K^{-1}	η_0 μPa·s	λ_0 mW·m^{-1}·K^{-1}
100.	-12.479	3.311	149.58	33.277	3.95	9.83
110.	-14.074	3.644	152.76	33.277	4.33	11.00
120.	-15.699	3.977	155.65	33.279	4.71	12.18
130.	-17.352	4.309	158.31	33.283	5.09	13.36
140.	-19.031	4.642	160.78	33.290	5.48	14.55
150.	-20.734	4.975	163.08	33.302	5.86	15.73
160.	-22.459	5.308	165.23	33.320	6.24	16.92
170.	-24.204	5.642	167.25	33.348	6.62	18.10
180.	-25.969	5.975	169.16	33.388	6.99	19.28
190.	-27.753	6.309	170.96	33.443	7.36	20.46
200.	-29.555	6.644	172.68	33.518	7.73	21.64
210.	-31.373	6.980	174.32	33.614	8.10	22.83
220.	-33.207	7.317	175.88	33.735	8.46	24.03
230.	-35.057	7.655	177.39	33.883	8.81	25.24
240.	-36.921	7.994	178.83	34.061	9.16	26.46
250.	-38.799	8.336	180.23	34.268	9.51	27.71
260.	-40.692	8.680	181.58	34.507	9.85	28.97
270.	-42.597	9.026	182.88	34.778	10.19	30.27
280.	-44.515	9.376	184.15	35.079	10.53	31.59
290.	-46.446	9.728	185.39	35.411	10.86	32.94
300.	-48.389	10.084	186.60	35.773	11.18	34.32
310.	-50.344	10.443	187.78	36.162	11.50	35.73
320.	-52.311	10.807	188.93	36.578	11.82	37.18
330.	-54.289	11.175	190.06	37.018	12.13	38.66
340.	-56.279	11.548	191.17	37.481	12.44	40.18
350.	-58.279	11.925	192.27	37.964	12.75	41.73
360.	-60.290	12.307	193.34	38.466	13.05	43.31
370.	-62.312	12.694	194.41	38.984	13.35	44.93
380.	-64.344	13.087	195.45	39.515	13.65	46.57
390.	-66.387	13.485	196.49	40.059	13.94	48.25
400.	-68.440	13.888	197.51	40.613	14.23	49.96

The ideal gas values of the Helmholtz energy, enthalpy, entropy, and isobaric heat capacity are evaluated from Eq. (7). The conversion from atmospheric pressure to 0.1 MPa affects the values of A^{id} and S^{id}. The dilute gas viscosity is from Eq. (10a) and the dilute gas thermal conductivity is from Eq.(13a).

TABLE A2. Properties along saturation boundary

T K	P_σ MPa	$\rho_{\sigma L}$ mol·dm^{-3}	$\rho_{\sigma V}$ mol·dm^{-3}	$C_{\sigma L}$ J·mol^{-1}·K^{-1}	$W_{\sigma L}$ m·s^{-1}	$\eta_{\sigma L}$ μPa·s	$\lambda_{\sigma L}$ mW·m^{-1}·K^{-1}
92.	0.014	28.04	0.018	53.37	1532.7	194.89	209.7
94.	0.018	27.87	0.023	53.85	1509.0	184.39	207.2
96.	0.022	27.70	0.028	54.24	1486.6	174.60	204.7
98.	0.028	27.52	0.035	54.54	1465.1	165.47	202.1
100.	0.034	27.35	0.042	54.80	1444.3	156.97	199.5
102.	0.042	27.18	0.051	55.02	1424.0	149.04	196.8
104.	0.051	27.00	0.061	55.21	1403.9	141.66	194.2
106.	0.062	26.83	0.072	55.39	1384.1	134.79	191.4
108.	0.074	26.65	0.085	55.56	1364.4	128.37	188.7
110.	0.088	26.47	0.100	55.72	1344.7	122.39	186.0
112.	0.104	26.29	0.116	55.89	1325.0	116.80	183.2
114.	0.122	26.11	0.135	56.07	1305.2	111.59	180.4
116.	0.143	25.92	0.155	56.26	1285.4	106.71	177.6
118.	0.166	25.74	0.178	56.46	1265.4	102.14	174.8
120.	0.192	25.55	0.204	56.68	1245.3	97.85	172.0
122.	0.220	25.36	0.231	56.91	1225.1	93.83	169.2
124.	0.252	25.16	0.262	57.16	1204.7	90.05	166.3
126.	0.287	24.97	0.296	57.43	1184.0	86.49	163.5
128.	0.325	24.77	0.333	57.73	1163.2	83.14	160.7
130.	0.368	24.56	0.373	58.05	1142.2	79.97	157.8
132.	0.414	24.36	0.417	58.39	1120.9	76.97	155.0
134.	0.464	24.15	0.464	58.76	1099.4	74.13	152.1
136.	0.519	23.93	0.516	59.16	1077.7	71.43	149.3
138.	0.578	23.72	0.572	59.59	1055.6	68.86	146.4
140.	0.642	23.50	0.633	60.05	1033.3	66.42	143.6
142.	0.711	23.27	0.699	60.55	1010.7	64.08	140.7
144.	0.785	23.04	0.770	61.09	987.8	61.85	137.9
146.	0.864	22.80	0.846	61.67	964.6	59.70	135.0
148.	0.950	22.56	0.929	62.30	941.1	57.65	132.2
150.	1.041	22.31	1.018	62.98	917.2	55.67	129.3
152.	1.138	22.06	1.115	63.72	892.9	53.76	126.5
154.	1.242	21.80	1.219	64.52	868.2	51.91	123.6
156.	1.352	21.53	1.331	65.40	843.1	50.13	120.8
158.	1.469	21.25	1.452	66.36	817.6	48.39	117.9
160.	1.593	20.96	1.584	67.42	791.5	46.70	115.0
162.	1.724	20.66	1.726	68.60	765.0	45.05	112.1
164.	1.864	20.36	1.880	69.92	738.0	43.44	109.3
166.	2.011	20.03	2.048	71.40	710.3	41.86	106.4
168.	2.166	19.70	2.232	73.10	682.1	40.30	103.4
170.	2.329	19.35	2.432	75.04	653.2	38.76	100.5
172.	2.502	18.97	2.653	77.33	623.6	37.23	97.5
174.	2.683	18.58	2.897	80.05	593.2	35.70	94.6
176.	2.874	18.16	3.170	83.36	562.0	34.16	91.6
178.	3.075	17.70	3.477	87.53	529.8	32.61	88.5
180.	3.287	17.21	3.827	92.96	496.4	31.01	85.5
182.	3.509	16.65	4.236	100.42	461.3	29.36	82.5
184.	3.742	16.02	4.726	111.46	423.8	27.60	79.7
186.	3.988	15.26	5.344	129.94	382.2	25.65	77.3
188.	4.247	14.27	6.200	169.79	332.7	23.33	76.9
190.	4.521	12.50	7.827	389.90	264.3	19.75	100.3

Values of the pressure, density of the saturated liquid, density of the saturated vapor, heat capacity, sound speed, viscosity, and thermal conductivity along the two-phase liquid–vapor coexistence curve. The quantities P_σ, $\rho_{\sigma L}$, and $\rho_{\sigma V}$ are from the ancillary equations, Eqs. (3)–(5). The heat capacity along the saturated boundary is from the equation in Table 7; the sound speed is also taken from Table 7 but the density argument is for the saturated liquid and is taken from column 3 of this table. The viscosity and thermal conductivity at saturation are from Eqs. (8) and (9) [with the terms evaluated from Eqs. (10)–(25)]; again the density input is from column 3 of this table.

TABLE A3. Properties of methane in the single-phase region

T K	P MPa	ρ mol·dm^{-3}	H kJ·mol^{-1}	S J·mol^{-1}·K^{-1}	C_v J·mol^{-1}·K^{-1}	C_p J·mol^{-1}·K^{-1}	W m·s^{-1}	η μPa·s	λ mW·m^{-1}·K^{-1}
100.	0.1	27.37	-5.242	73.05	34.08	54.64	1446.8	157.48	199.8
100.	0.5	27.38	-5.232	73.00	34.10	54.59	1450.3	158.19	200.2
100.	1.0	27.41	-5.219	72.95	34.11	54.53	1454.5	159.09	200.7
100.	2.0	27.45	-5.194	72.83	34.14	54.41	1463.0	160.88	201.6
100.	5.0	27.59	-5.118	72.50	34.25	54.08	1487.3	166.34	204.5
100.	10.0	27.81	-4.989	71.98	34.42	53.61	1525.0	175.69	209.1
100.	20.0	28.20	-4.729	71.01	34.79	52.85	1592.3	195.61	217.9
100.	30.0	28.56	-4.465	70.13	35.17	52.29	1651.5	217.69	226.1
100.	40.0	28.88	-4.198	69.32	35.53	51.85	1704.9	242.62	234.0
100.	50.0	29.18	-3.929	68.56	35.88	51.50	1753.9	271.34	241.5
110.	0.1	26.49	-4.689	78.32	33.49	55.84	1347.4	122.80	186.3
110.	0.5	26.51	-4.679	78.26	33.50	55.77	1351.4	123.40	186.7
110.	1.0	26.54	-4.668	78.20	33.52	55.68	1356.3	124.15	187.2
110.	2.0	26.59	-4.644	78.07	33.56	55.51	1365.9	125.65	188.3
110.	5.0	26.75	-4.572	77.71	33.66	55.05	1393.5	130.21	191.5
110.	10.0	27.01	-4.449	77.13	33.86	54.39	1435.8	137.99	196.6
110.	20.0	27.46	-4.197	76.08	34.26	53.40	1510.1	154.46	206.2
110.	30.0	27.86	-3.940	75.14	34.67	52.67	1574.6	172.67	215.1
110.	40.0	28.23	-3.678	74.28	35.06	52.13	1632.3	193.30	223.5
110.	50.0	28.56	-3.413	73.49	35.44	51.72	1684.7	217.19	231.5
120.	0.1	0.10	3.890	155.17	25.68	35.03	282.7	4.73	12.4
120.	0.5	25.58	-4.116	83.17	32.66	56.96	1251.0	98.49	172.6
120.	1.0	25.62	-4.105	83.09	32.67	56.83	1256.8	99.13	173.2
120.	2.0	25.68	-4.084	82.95	32.71	56.59	1268.0	100.43	174.4
120.	5.0	25.88	-4.017	82.53	32.83	55.92	1299.8	104.33	178.0
120.	10.0	26.18	-3.902	81.89	33.04	55.02	1347.9	110.90	183.6
120.	20.0	26.70	-3.662	80.74	33.49	53.70	1430.5	124.63	194.0
120.	30.0	27.16	-3.412	79.73	33.93	52.79	1501.0	139.62	203.5
120.	40.0	27.57	-3.156	78.82	34.35	52.12	1563.2	156.46	212.5
120.	50.0	27.94	-2.896	77.99	34.75	51.62	1619.5	175.88	221.0
130.	0.1	0.09	4.237	157.95	25.39	34.48	295.5	5.12	13.5
130.	0.5	24.58	-3.539	87.79	31.87	58.64	1145.3	80.22	158.1
130.	1.0	24.63	-3.529	87.70	31.88	58.44	1152.2	80.81	158.8
130.	2.0	24.71	-3.511	87.53	31.92	58.07	1165.6	81.97	160.2
130.	5.0	24.95	-3.452	87.05	32.04	57.09	1203.2	85.44	164.2
130.	10.0	25.31	-3.348	86.32	32.27	55.81	1258.7	91.19	170.4
130.	20.0	25.93	-3.123	85.05	32.74	54.05	1351.6	102.92	181.7
130.	30.0	26.45	-2.884	83.96	33.21	52.90	1428.9	115.44	191.9
130.	40.0	26.91	-2.635	82.99	33.65	52.09	1496.4	129.30	201.3
130.	50.0	27.32	-2.380	82.11	34.06	51.49	1556.8	145.09	210.3
140.	0.1	0.09	4.580	160.49	25.28	34.20	307.5	5.50	14.7
140.	0.5	0.48	4.309	145.80	26.55	38.82	292.3	5.61	15.7
140.	1.0	23.54	-2.934	92.12	31.23	60.90	1040.0	66.84	144.2
140.	2.0	23.65	-2.920	91.91	31.26	60.29	1056.7	67.96	145.8
140.	5.0	23.95	-2.874	91.34	31.37	58.76	1102.5	71.20	150.4
140.	10.0	24.40	-2.785	90.50	31.60	56.91	1167.8	76.45	157.3
140.	20.0	25.13	-2.580	89.08	32.09	54.55	1273.1	86.80	169.5
140.	30.0	25.73	-2.354	87.88	32.57	53.10	1358.4	97.54	180.3
140.	40.0	26.24	-2.114	86.85	33.03	52.11	1431.5	109.18	190.3
140.	50.0	26.69	-1.866	85.92	33.44	51.40	1496.4	122.21	199.6

TABLE A3. Properties of methane in the single-phase region — Continued

T K	P MPa	ρ mol·dm^{-3}	H kJ·mol^{-1}	S J·mol^{-1}·K^{-1}	C_v J·mol^{-1}·K^{-1}	C_p J·mol^{-1}·K^{-1}	W m·s^{-1}	η μPa·s	λ mW·m^{-1}·K^{-1}
150.	0.1	0.08	4.921	162.84	25.21	34.01	319.0	5.88	15.9
150.	0.5	0.44	4.689	148.42	26.15	37.45	306.6	5.99	16.6
150.	1.0	0.97	4.342	141.02	28.16	45.57	287.7	6.16	18.3
150.	2.0	22.46	-2.301	96.18	30.77	63.83	938.2	56.76	131.2
150.	5.0	22.86	-2.274	95.48	30.84	61.25	996.2	60.01	136.5
150.	10.0	23.42	-2.209	94.47	31.03	58.42	1074.8	65.03	144.3
150.	20.0	24.30	-2.032	92.86	31.52	55.21	1195.3	74.51	157.7
150.	30.0	24.99	-1.822	91.56	32.01	53.39	1289.5	83.99	169.2
150.	40.0	25.57	-1.593	90.45	32.47	52.20	1368.8	94.01	179.6
150.	50.0	26.07	-1.352	89.47	32.89	51.36	1438.4	105.00	189.3
160.	0.1	0.08	5.261	165.03	25.18	33.89	330.0	6.26	17.1
160.	0.5	0.40	5.059	150.81	25.91	36.58	319.6	6.36	17.7
160.	1.0	0.87	4.773	143.80	26.95	41.43	305.0	6.52	18.9
160.	2.0	21.05	-1.634	100.48	30.52	70.18	804.0	47.23	116.0
160.	5.0	21.64	-1.644	99.54	30.46	65.11	882.0	50.75	122.6
160.	10.0	22.37	-1.615	98.31	30.58	60.52	979.4	55.84	131.7
160.	20.0	23.44	-1.476	96.45	31.03	56.05	1118.5	64.84	146.2
160.	30.0	24.23	-1.286	95.01	31.52	53.76	1222.6	73.46	158.5
160.	40.0	24.88	-1.070	93.82	31.98	52.33	1308.5	82.31	169.3
160.	50.0	25.44	-0.839	92.78	32.40	51.36	1382.8	91.80	179.3
170.	0.1	0.07	5.599	167.09	25.16	33.81	340.5	6.64	18.2
170.	0.5	0.37	5.422	153.01	25.73	35.95	331.8	6.74	18.8
170.	1.0	0.80	5.177	146.25	26.51	39.51	320.0	6.88	19.7
170.	2.0	1.90	4.548	137.78	29.24	55.59	290.3	7.35	23.1
170.	5.0	20.19	-0.963	103.67	30.30	71.82	755.4	42.64	108.4
170.	10.0	21.22	-0.995	102.06	30.24	63.46	881.0	48.16	119.3
170.	20.0	22.54	-0.910	99.88	30.62	57.08	1043.0	57.03	135.4
170.	30.0	23.46	-0.746	98.29	31.10	54.21	1157.9	65.06	148.3
170.	40.0	24.20	-0.546	97.00	31.55	52.51	1250.5	73.05	159.6
170.	50.0	24.81	-0.325	95.90	31.97	51.39	1329.7	81.43	169.9
180.	0.1	0.07	5.937	169.02	25.18	33.77	350.7	7.01	19.4
180.	0.5	0.35	5.779	155.05	25.61	35.51	343.3	7.11	20.0
180.	1.0	0.74	5.565	148.47	26.22	38.25	333.5	7.24	20.8
180.	2.0	1.68	5.057	140.70	27.78	47.53	311.1	7.64	23.2
180.	5.0	18.32	-0.182	108.13	30.58	86.75	606.4	34.82	93.3
180.	10.0	19.92	-0.341	105.80	30.04	67.74	779.0	41.48	107.2
180.	20.0	21.60	-0.333	103.17	30.28	58.31	969.1	50.54	125.1
180.	30.0	22.68	-0.202	101.40	30.73	54.71	1095.7	58.20	138.7
180.	40.0	23.50	-0.020	100.00	31.18	52.73	1195.2	65.58	150.4
180.	50.0	24.18	0.189	98.84	31.58	51.45	1279.2	73.13	160.9
190.	0.1	0.06	6.275	170.84	25.21	33.77	360.5	7.39	20.6
190.	0.5	0.33	6.133	156.96	25.55	35.20	354.2	7.47	21.2
190.	1.0	0.69	5.943	150.52	26.02	37.38	346.0	7.60	21.9
190.	2.0	1.52	5.512	143.16	27.15	43.83	328.1	7.95	24.0
190.	5.0	14.99	0.939	114.17	32.57	172.39	396.8	25.12	78.2
190.	10.0	18.42	0.367	109.62	30.01	74.30	673.4	35.43	95.8
190.	20.0	20.61	0.257	106.36	30.00	59.74	897.5	45.05	115.5
190.	30.0	21.87	0.348	104.37	30.42	55.27	1036.2	52.49	129.8
190.	40.0	22.80	0.509	102.86	30.85	52.96	1142.6	59.41	141.9
190.	50.0	23.54	0.704	101.62	31.25	51.52	1231.3	66.33	152.6

TABLE A3. Properties of methane in the single-phase region — Continued

T K	P MPa	ρ mol·dm^{-3}	H kJ·mol^{-1}	S J·mol^{-1}·K^{-1}	C_v J·mol^{-1}·K^{-1}	C_p J·mol^{-1}·K^{-1}	W m·s^{-1}	η μPa·s	λ mW·m^{-1}·K^{-1}
200.	0.1	0.06	6.613	172.58	25.27	33.80	370.0	7.75	21.8
200.	0.5	0.31	6.483	158.76	25.54	35.00	364.6	7.84	22.2
200.	1.0	0.64	6.313	152.42	25.91	36.77	357.6	7.96	22.9
200.	2.0	1.40	5.939	145.34	26.77	41.60	343.0	8.28	24.5
200.	5.0	5.46	4.144	130.69	32.02	116.34	292.0	10.90	40.4
200.	10.0	16.59	1.159	113.68	30.21	84.94	566.0	29.72	84.1
200.	20.0	19.57	0.862	109.47	29.79	61.34	829.1	40.32	106.5
200.	30.0	21.05	0.904	107.22	30.16	55.85	979.9	47.67	121.5
200.	40.0	22.09	1.039	105.58	30.57	53.20	1092.8	54.26	133.9
200.	50.0	22.91	1.220	104.26	30.96	51.60	1185.9	60.68	144.8
210.	0.1	0.06	6.951	174.23	25.35	33.85	379.1	8.12	23.0
210.	0.5	0.29	6.833	160.46	25.58	34.88	374.5	8.20	23.4
210.	1.0	0.61	6.679	154.20	25.87	36.35	368.6	8.32	23.9
210.	2.0	1.30	6.347	147.34	26.53	40.13	356.4	8.61	25.3
210.	5.0	4.34	5.015	134.94	29.53	70.53	319.8	10.40	34.3
210.	10.0	14.31	2.083	118.19	30.62	100.26	467.0	24.22	73.1
210.	20.0	18.49	1.484	112.50	29.65	63.03	764.9	36.21	98.2
210.	30.0	20.22	1.465	109.96	29.95	56.42	927.0	43.55	113.9
210.	40.0	21.38	1.573	108.18	30.35	53.43	1046.1	49.88	126.6
210.	50.0	22.28	1.736	106.78	30.72	51.68	1143.2	55.92	137.7
220.	0.1	0.05	7.290	175.80	25.47	33.94	388.0	8.48	24.1
220.	0.5	0.28	7.181	162.09	25.65	34.83	384.0	8.56	24.5
220.	1.0	0.57	7.041	155.89	25.89	36.08	378.9	8.67	25.1
220.	2.0	1.22	6.743	149.18	26.42	39.13	368.8	8.94	26.3
220.	5.0	3.77	5.647	137.88	28.52	57.62	340.3	10.38	32.9
220.	10.0	11.70	3.144	123.12	30.89	108.93	401.9	19.47	63.5
220.	20.0	17.36	2.123	115.47	29.56	64.68	706.4	32.64	90.8
220.	30.0	19.38	2.032	112.60	29.80	56.96	878.1	40.00	107.0
220.	40.0	20.67	2.108	110.68	30.17	53.65	1002.4	46.14	119.9
220.	50.0	21.65	2.254	109.19	30.53	51.76	1103.2	51.87	131.1
230.	0.1	0.05	7.630	177.31	25.61	34.07	396.6	8.83	25.3
230.	0.5	0.27	7.530	163.63	25.76	34.85	393.1	8.91	25.7
230.	1.0	0.55	7.401	157.49	25.96	35.91	388.8	9.02	26.2
230.	2.0	1.14	7.130	150.90	26.39	38.45	380.2	9.27	27.3
230.	5.0	3.39	6.189	140.29	27.96	51.39	357.5	10.51	32.7
230.	10.0	9.46	4.177	127.72	30.42	94.96	381.1	16.46	55.3
230.	20.0	16.20	2.776	118.38	29.52	65.99	655.4	29.54	84.3
230.	30.0	18.53	2.604	115.14	29.69	57.42	833.5	36.94	100.9
230.	40.0	19.97	2.645	113.06	30.04	53.84	962.1	42.91	113.9
230.	50.0	21.02	2.772	111.49	30.39	51.84	1065.9	48.38	125.1
240.	0.1	0.05	7.971	178.77	25.78	34.22	404.9	9.18	26.6
240.	0.5	0.26	7.878	165.12	25.91	34.91	401.9	9.26	26.9
240.	1.0	0.52	7.760	159.01	26.08	35.84	398.2	9.36	27.4
240.	2.0	1.08	7.512	152.53	26.43	37.98	390.9	9.60	28.4
240.	5.0	3.10	6.683	142.40	27.66	47.76	372.5	10.69	33.0
240.	10.0	7.98	5.036	131.38	29.72	77.75	383.4	14.99	49.8
240.	20.0	15.04	3.440	121.20	29.50	66.66	613.2	26.92	78.7
240.	30.0	17.68	3.180	117.59	29.63	57.75	793.5	34.29	95.4
240.	40.0	19.26	3.185	115.36	29.96	53.99	925.1	40.11	108.5
240.	50.0	20.41	3.290	113.70	30.29	51.90	1031.2	45.36	119.7

TABLE A3. Properties of methane in the single-phase region — Continued

T K	P MPa	ρ mol·dm^{-3}	H kJ·mol^{-1}	S J·mol^{-1}·K^{-1}	C_v J·mol^{-1}·K^{-1}	C_p J·mol^{-1}·K^{-1}	W m·s^{-1}	η μPa·s	λ mW·m^{-1}·K^{-1}
250.	0.1	0.05	8.315	180.17	25.98	34.42	413.0	9.53	27.8
250.	0.5	0.24	8.228	166.55	26.09	35.03	410.4	9.60	28.1
250.	1.0	0.50	8.118	160.48	26.24	35.84	407.1	9.70	28.6
250.	2.0	1.03	7.891	154.07	26.54	37.69	400.9	9.93	29.5
250.	5.0	2.88	7.148	144.30	27.53	45.43	385.9	10.91	33.5
250.	10.0	6.99	5.753	134.31	29.19	66.52	392.4	14.28	46.6
250.	20.0	13.92	4.107	123.92	29.50	66.46	580.5	24.74	74.0
250.	30.0	16.85	3.759	119.95	29.62	57.91	758.4	32.00	90.7
250.	40.0	18.57	3.725	117.57	29.93	54.08	891.5	37.68	103.7
250.	50.0	19.80	3.809	115.82	30.25	51.95	999.3	42.74	114.8
260.	0.1	0.05	8.660	181.52	26.22	34.64	420.8	9.87	29.1
260.	0.5	0.23	8.579	167.92	26.32	35.19	418.5	9.94	29.4
260.	1.0	0.48	8.477	161.88	26.44	35.91	415.7	10.04	29.8
260.	2.0	0.98	8.267	155.55	26.70	37.52	410.5	10.25	30.7
260.	5.0	2.69	7.594	146.05	27.52	43.86	398.2	11.16	34.3
260.	10.0	6.29	6.380	136.77	28.86	59.48	403.2	13.94	45.0
260.	20.0	12.87	4.766	126.51	29.50	65.33	556.7	22.98	70.2
260.	30.0	16.04	4.338	122.22	29.64	57.88	728.2	30.04	86.6
260.	40.0	17.89	4.266	119.69	29.94	54.12	861.3	35.58	99.4
260.	50.0	19.20	4.329	117.86	30.25	51.98	970.0	40.45	110.4
270.	0.1	0.04	9.008	182.83	26.48	34.90	428.3	10.21	30.3
270.	0.5	0.23	8.932	169.25	26.57	35.39	426.4	10.28	30.6
270.	1.0	0.46	8.836	163.24	26.68	36.04	424.0	10.37	31.0
270.	2.0	0.94	8.641	156.96	26.90	37.46	419.5	10.58	31.9
270.	5.0	2.54	8.027	147.68	27.60	42.78	409.5	11.41	35.1
270.	10.0	5.75	6.951	138.92	28.71	54.89	414.1	13.80	44.2
270.	20.0	11.91	5.411	128.94	29.51	63.45	540.8	21.61	67.2
270.	30.0	15.25	4.915	124.40	29.71	57.64	702.8	28.37	83.1
270.	40.0	17.23	4.807	121.73	30.00	54.08	834.5	33.74	95.8
270.	50.0	18.61	4.849	119.82	30.30	51.99	943.3	38.45	106.6
280.	0.1	0.04	9.358	184.11	26.78	35.19	435.7	10.54	31.7
280.	0.5	0.22	9.287	170.55	26.86	35.64	434.0	10.61	32.0
280.	1.0	0.44	9.198	164.55	26.96	36.22	432.0	10.70	32.3
280.	2.0	0.90	9.016	158.32	27.15	37.48	428.2	10.90	33.1
280.	5.0	2.40	8.451	149.22	27.75	42.04	420.0	11.68	36.1
280.	10.0	5.33	7.483	140.86	28.70	51.76	424.7	13.78	44.0
280.	20.0	11.06	6.034	131.21	29.56	61.20	531.1	20.57	64.7
280.	30.0	14.50	5.490	126.49	29.82	57.21	681.9	26.96	80.3
280.	40.0	16.58	5.348	123.69	30.10	53.99	810.9	32.15	92.6
280.	50.0	18.04	5.369	121.71	30.39	51.98	919.2	36.70	103.2
290.	0.1	0.04	9.711	185.35	27.11	35.51	442.8	10.87	33.0
290.	0.5	0.21	9.645	171.80	27.18	35.92	441.4	10.94	33.3
290.	1.0	0.42	9.561	165.83	27.27	36.45	439.6	11.02	33.6
290.	2.0	0.86	9.391	159.64	27.44	37.58	436.4	11.22	34.4
290.	5.0	2.29	8.868	150.69	27.97	41.54	429.8	11.95	37.2
290.	10.0	4.98	7.989	142.63	28.78	49.58	434.9	13.83	44.1
290.	20.0	10.32	6.635	133.32	29.65	58.92	526.0	19.79	62.9
290.	30.0	13.80	6.059	128.49	29.96	56.62	665.0	25.78	77.9
290.	40.0	15.96	5.887	125.59	30.25	53.83	790.3	30.78	89.9
290.	50.0	17.49	5.888	123.53	30.53	51.96	897.5	35.16	100.3

TABLE A3. Properties of methane in the single-phase region — Continued

T K	P MPa	ρ mol·dm^{-3}	H kJ·mol^{-1}	S J·mol^{-1}·K^{-1}	C_v J·mol^{-1}·K^{-1}	C_p J·mol^{-1}·K^{-1}	W m·s^{-1}	η μPa·s	λ mW·m^{-1}·K^{-1}
300.	0.1	0.04	10.068	186.56	27.47	35.86	449.7	11.20	34.4
300.	0.5	0.20	10.006	173.02	27.54	36.24	448.5	11.26	34.7
300.	1.0	0.41	9.927	167.07	27.61	36.72	447.0	11.35	35.0
300.	2.0	0.83	9.768	160.92	27.77	37.74	444.3	11.53	35.7
300.	5.0	2.18	9.282	152.09	28.24	41.23	439.1	12.22	38.3
300.	10.0	4.69	8.477	144.28	28.95	48.02	444.6	13.93	44.6
300.	20.0	9.67	7.213	135.28	29.79	56.84	524.3	19.22	61.5
300.	30.0	13.14	6.622	130.40	30.14	55.93	651.8	24.80	76.0
300.	40.0	15.37	6.424	127.41	30.43	53.63	772.6	29.59	87.6
300.	50.0	16.95	6.408	125.30	30.71	51.92	878.0	33.81	97.8
310.	0.1	0.04	10.429	187.74	27.86	36.25	456.5	11.52	35.8
310.	0.5	0.20	10.370	174.22	27.92	36.59	455.4	11.58	36.1
310.	1.0	0.39	10.296	168.28	27.99	37.03	454.2	11.66	36.4
310.	2.0	0.80	10.146	162.16	28.13	37.96	452.0	11.84	37.1
310.	5.0	2.09	9.693	153.44	28.55	41.06	447.9	12.50	39.5
310.	10.0	4.44	8.951	145.84	29.18	46.90	453.8	14.07	45.2
310.	20.0	9.11	7.772	137.11	29.99	55.04	524.8	18.81	60.6
310.	30.0	12.53	7.177	132.22	30.36	55.19	641.7	23.99	74.5
310.	40.0	14.81	6.959	129.16	30.66	53.39	757.5	28.56	85.8
310.	50.0	16.44	6.927	127.00	30.93	51.87	860.8	32.63	95.6
320.	0.1	0.04	10.793	188.90	28.28	36.66	463.1	11.84	37.2
320.	0.5	0.19	10.737	175.39	28.33	36.97	462.2	11.90	37.5
320.	1.0	0.38	10.668	169.46	28.39	37.38	461.1	11.98	37.8
320.	2.0	0.77	10.527	163.37	28.52	38.22	459.3	12.15	38.5
320.	5.0	2.00	10.104	154.74	28.90	41.00	456.3	12.77	40.8
320.	10.0	4.22	9.416	147.32	29.47	46.10	462.7	14.23	46.0
320.	20.0	8.61	8.315	138.84	30.23	53.54	526.8	18.52	60.1
320.	30.0	11.96	7.726	133.96	30.62	54.45	634.2	23.32	73.3
320.	40.0	14.27	7.492	130.85	30.92	53.14	744.8	27.69	84.2
320.	50.0	15.94	7.445	128.64	31.18	51.82	845.5	31.60	93.8
330.	0.1	0.04	11.162	190.03	28.72	37.09	469.5	12.15	38.7
330.	0.5	0.18	11.109	176.53	28.76	37.38	468.7	12.21	39.0
330.	1.0	0.37	11.043	170.62	28.82	37.76	467.9	12.29	39.3
330.	2.0	0.75	10.911	164.55	28.94	38.53	466.4	12.45	39.9
330.	5.0	1.93	10.514	156.00	29.29	41.04	464.3	13.05	42.1
330.	10.0	4.02	9.874	148.73	29.80	45.54	471.1	14.41	46.9
330.	20.0	8.18	8.844	140.47	30.52	52.32	529.9	18.33	59.9
330.	30.0	11.44	8.267	135.63	30.92	53.74	628.9	22.79	72.4
330.	40.0	13.76	8.022	132.49	31.22	52.88	734.3	26.94	83.0
330.	50.0	15.46	7.963	130.24	31.47	51.77	832.2	30.70	92.3
340.	0.1	0.04	11.535	191.15	29.18	37.55	475.7	12.46	40.2
340.	0.5	0.18	11.485	177.65	29.22	37.82	475.1	12.52	40.5
340.	1.0	0.36	11.423	171.75	29.28	38.17	474.4	12.59	40.8
340.	2.0	0.72	11.298	165.70	29.39	38.88	473.3	12.75	41.4
340.	5.0	1.86	10.925	157.23	29.70	41.16	472.0	13.33	43.5
340.	10.0	3.85	10.327	150.08	30.17	45.18	479.2	14.60	48.0
340.	20.0	7.79	9.362	142.01	30.85	51.35	533.7	18.20	59.9
340.	30.0	10.97	8.801	137.22	31.25	53.11	625.4	22.35	71.9
340.	40.0	13.28	8.549	134.06	31.54	52.62	725.6	26.30	82.1
340.	50.0	15.00	8.481	131.78	31.79	51.73	820.5	29.91	91.1

TABLE A3. Properties of methane in the single-phase region — Continued

T K	P MPa	ρ mol·dm^{-3}	H kJ·mol^{-1}	S J·mol^{-1}·K^{-1}	C_v J·mol^{-1}·K^{-1}	C_p J·mol^{-1}·K^{-1}	W m·s^{-1}	η μPa·s	λ mW·m^{-1}·K^{-1}
350.	0.1	0.03	11.913	192.24	29.66	38.03	481.8	12.76	41.8
350.	0.5	0.17	11.866	178.76	29.70	38.28	481.3	12.82	42.0
350.	1.0	0.35	11.807	172.86	29.75	38.60	480.8	12.89	42.3
350.	2.0	0.70	11.689	166.83	29.85	39.26	479.9	13.05	42.9
350.	5.0	1.79	11.337	158.43	30.14	41.35	479.4	13.60	44.9
350.	10.0	3.70	10.778	151.39	30.58	44.96	487.0	14.80	49.1
350.	20.0	7.44	9.872	143.49	31.21	50.60	538.0	18.14	60.2
350.	30.0	10.53	9.329	138.75	31.61	52.55	623.4	22.01	71.5
350.	40.0	12.83	9.074	135.58	31.90	52.39	718.5	25.75	81.4
350.	50.0	14.57	8.998	133.28	32.14	51.69	810.5	29.22	90.2
360.	0.1	0.03	12.296	193.32	30.16	38.52	487.8	13.07	43.4
360.	0.5	0.17	12.251	179.84	30.20	38.76	487.4	13.12	43.6
360.	1.0	0.34	12.195	173.95	30.25	39.06	487.0	13.19	43.9
360.	2.0	0.68	12.083	167.95	30.34	39.67	486.4	13.35	44.4
360.	5.0	1.73	11.752	159.59	30.61	41.59	486.5	13.88	46.3
360.	10.0	3.56	11.227	152.65	31.01	44.86	494.5	15.01	50.3
360.	20.0	7.13	10.375	144.91	31.61	50.02	542.7	18.12	60.7
360.	30.0	10.12	9.852	140.23	32.00	52.09	622.5	21.74	71.4
360.	40.0	12.41	9.597	137.06	32.28	52.19	713.0	25.30	81.0
360.	50.0	14.15	9.515	134.74	32.52	51.68	801.8	28.62	89.5
370.	0.1	0.03	12.684	194.38	30.68	39.04	493.6	13.37	45.0
370.	0.5	0.16	12.641	180.91	30.71	39.26	493.4	13.42	45.2
370.	1.0	0.33	12.588	175.03	30.76	39.54	493.1	13.49	45.5
370.	2.0	0.66	12.482	169.04	30.84	40.11	492.7	13.64	46.0
370.	5.0	1.68	12.169	160.74	31.10	41.87	493.4	14.15	47.8
370.	10.0	3.43	11.675	153.88	31.47	44.85	501.7	15.23	51.6
370.	20.0	6.85	10.873	146.27	32.04	49.61	547.5	18.14	61.3
370.	30.0	9.75	10.371	141.65	32.41	51.71	622.5	21.54	71.5
370.	40.0	12.01	10.118	138.48	32.69	52.03	708.7	24.91	80.8
370.	50.0	13.76	10.031	136.15	32.92	51.68	794.5	28.10	89.0
380.	0.1	0.03	13.077	195.43	31.21	39.57	499.4	13.66	46.6
380.	0.5	0.16	13.036	181.96	31.24	39.77	499.2	13.71	46.8
380.	1.0	0.32	12.986	176.09	31.28	40.03	499.0	13.78	47.1
380.	2.0	0.64	12.885	170.11	31.37	40.56	498.9	13.93	47.6
380.	5.0	1.63	12.589	161.86	31.60	42.20	500.1	14.42	49.4
380.	10.0	3.31	12.124	155.08	31.95	44.93	508.7	15.45	53.0
380.	20.0	6.60	11.367	147.59	32.49	49.32	552.6	18.18	62.0
380.	30.0	9.41	10.887	143.02	32.85	51.42	623.3	21.38	71.8
380.	40.0	11.63	10.638	139.87	33.12	51.90	705.4	24.59	80.7
380.	50.0	13.38	10.548	137.53	33.35	51.70	788.3	27.65	88.7
390.	0.1	0.03	13.475	196.46	31.75	40.11	505.0	13.95	48.3
390.	0.5	0.15	13.437	183.00	31.78	40.30	504.9	14.00	48.5
390.	1.0	0.31	13.389	177.14	31.82	40.55	504.8	14.07	48.7
390.	2.0	0.62	13.293	171.17	31.90	41.04	504.9	14.21	49.3
390.	5.0	1.58	13.013	162.96	32.12	42.56	506.6	14.69	51.0
390.	10.0	3.20	12.574	156.24	32.45	45.07	515.5	15.67	54.4
390.	20.0	6.36	11.859	148.87	32.96	49.14	557.7	18.26	62.9
390.	30.0	9.09	11.400	144.36	33.31	51.22	624.8	21.27	72.2
390.	40.0	11.28	11.157	141.22	33.57	51.82	703.2	24.33	80.8
390.	50.0	13.02	11.066	138.87	33.79	51.75	783.2	27.26	88.6

TABLE A3. Properties of methane in the single-phase region — Continued

T K	P MPa	ρ mol·dm^{-3}	H kJ·mol^{-1}	S J·mol^{-1}·K^{-1}	C_v J·mol^{-1}·K^{-1}	C_p J·mol^{-1}·K^{-1}	W m·s^{-1}	η μPa·s	λ mW·m^{-1}·K^{-1}
400.	0.1	0.03	13.879	197.49	32.31	40.66	510.5	14.24	50.0
400.	0.5	0.15	13.842	184.03	32.34	40.84	510.5	14.29	50.2
400.	1.0	0.30	13.797	178.17	32.37	41.07	510.5	14.36	50.4
400.	2.0	0.61	13.706	172.22	32.44	41.53	510.8	14.49	50.9
400.	5.0	1.53	13.441	164.04	32.65	42.95	512.9	14.96	52.6
400.	10.0	3.10	13.026	157.39	32.96	45.27	522.1	15.90	55.8
400.	20.0	6.15	12.350	150.11	33.44	49.05	562.8	18.35	63.9
400.	30.0	8.80	11.911	145.65	33.78	51.08	626.7	21.20	72.8
400.	40.0	10.95	11.675	142.53	34.04	51.79	701.7	24.11	81.1
400.	50.0	12.68	11.583	140.19	34.25	51.82	778.9	26.93	88.7

Values of the density, enthalpy, entropy, isochoric and isobaric heat capacities, speed of sound, viscosity, and thermal conductivity in the single-phase region of the methane fluid. The independent variables were chosen to be temperature and pressure. The density was evaluated by inverting the pressure equation in Table 7; the quantities H, S, C_V, C_P, and W were then evaluated directly from the expressions in Table 7. The viscosity and thermal conductivity are from Eqs. (8) and (9) [with the terms evaluated from Eqs. (10)–(25)]; the density input is from column 3 of this table.